Charles University

Faculty of Science

Study programme: Biology

Branch of study: Cellular and Developmental Biology

Bc. Iuliia Efimova

Structural composition and functional properties of mitochondrial FoF1 ATP synthase on models of specific subunits deficiencies

Analýza podjednotkového složení a funkce mitochondriální FoF1 ATP syntázy u modelů deficience strukturních podjednotek

Diploma thesis

Supervisor: RNDr. Tomáš Mráček, Ph.D.

Prague, 2018

Prohlášení:

Prohlašuji, že jsem závěrečnou práci zpracovala samostatně a že jsem uvedla všechny použité informační zdroje a literaturu. Tato práce ani její podstatná část nebyla předložena k získání jiného nebo stejného akademického titulu.

V Praze, 13.08.2018 Podpis

Acknowledgements

I would like to express gratitude to my supervisor, RNDr. Tomáš Mráček, Ph.D. for his valuable guidance and all of the opportunities I was given to conduct this work.

My special thanks belong to Mgr. Hana Nůsková, Ph.D. and RNDr. Marek Vrbacký, Ph.D. for their help during my experimental part of the work and to Ing. Andrea Brazdová, Ph.D. for her support, help and confidence placed into myself. I would like to thank to the entire team of Department of Bioenergetics, Institute of Physiology of the Czech Academy of Sciences for friendly atmosphere and the stimulating scientific environment You created.

This work was supported by the Czech Ministry of Health (16-33018A).

Abstrakt

Mitochondriální ATP syntáza je posledním z komplexů oxidačně fosforylačního (OXPHOS) systému lokalizovaného na vnitřní mitochondriální membráně. Její hlavní funkcí je využití mitochondriálního membránového potenciálu ($\Delta\psi_m$) vytvořeného komplexy elektron transportního řetězce (ETC) k produkci energie ve formě ATP. Savčí ATP syntáza je sestavená ze 17 různých podjednotek, které jsou organizovány do membránové F_o a do matrix směřující F_1 domény. Defekty komplexu V a jejich projevy na úrovni mitochondrií, buněk, tkání i celého organizmu byly zkoumány na různých modelech, včetně lidských buněčných linií odvozených z tkání pacientů. V mnoha případech vykazují mitochondriální onemocnění tzv. prahový efekt (efekt thresholdu), při kterém se defekt na úrovni genu fenotypově projeví pouze v případě poklesu enzymové aktivity a/nebo obsahu konkrétního komplexu pod určitou prahovou hodnotu.

Tato práce byla zaměřená na objasnění funkčních dopadů deficience ATP syntázy u HEK293 buněčných linií s potlačenou expresí γ, δ nebo ε podjednotek centrálního stonku ATP syntázy. Analyzovali jsme řadu klonů s utišenou expresí uvedených podjednotek a ukázali na proměnlivé snížení obsahu sestavené ATP syntázy, kterému odpovídalo i snížení obsahu jednotlivých podjednotek tohoto enzymu. Jedinou výjimkou byla podjednotka F_o-c, jejíž obsah se nesnižoval spolu s ostatními podjednotkami a u některých z klonů byl dokonce zvýšen. Deficience ATP syntázy měla za následek snížení viability buněk za podmínek limitace živinami, které se projevilo jako threshold v knockdown klonech (KD) se zbytkovým obsahem ATP syntázy nižším než 50 %. Snížená funkční kapacita ATP syntázy byla následně charakterizována u nejvíce postíženého klonu, kdy jsme pozorovali pokles respiračních kontrolních indexů. Zatímco obsah ATP syntázy u studovaných klonů byl snížen v rozmezí 90-15 % v porovnání s kontrolou, ostatní OXPHOS komplexy vykazovaly variabilně zvýšenou expresi, pravděpodobně v důsledku kompenzace.

Dále jsme zavedli techniku afinitní purifikace ATP syntázy pomocí vazby IF_1 inhibičního proteinu. Připravili jsme dostatečné množství rekombinantního IF_1 proteinu, který vykazoval schopnost vázat se na ATP syntázu a v praxi ověřili použitelnost metodiky pro izolaci ATP syntázy z mitochondrií potkanních jater. Izolovaná ATP syntáza nebyla kontaminována ostatními OXPHOS komplexy. Daná metoda bude použitelná k budoucí charakterizaci modelů s deficiencí ATP syntázy, jako například i modelů utišění podjednotek centrálního stonku.

Klíčová slova: mitochondrie, ATP syntáza, deficience, prahový efekt, biogeneze, afinitní purifikace

Abstract

Mitochondrial ATP synthase represents the final complex of oxidative phosphorylation (OXPHOS) system located in the inner mitochondrial membrane. Its primary role is to utilize mitochondrial membrane potential ($\Delta\psi_m$) generated by respiratory chain complexes to produce energy in the form of ATP. Mammalian ATP synthase comprises of 17 different subunits organized into membranous F_o and matrix-oriented F_1 domains. Defects of complex V and their manifestation have been studied on mitochondrial, cellular, tissue and organism levels using different models, including human cell lines and cell lines derived from patient tissues. In many cases mitochondrial diseases display threshold behaviour, when genetic defect is phenotypically manifested only bellow certain threshold in particular enzyme complex activity and/or content.

This work was aimed at elucidation of functional consequences of ATP synthase deficiency in HEK293 cell lines with suppressed gene expression of γ, δ or ε subunits of ATP synthase central stalk. We have analysed range of clones with respective subunits knockdown and found varying decrease in assembled ATP synthase content, which was mirrored by the decrease in individual ATP synthase subunits. The only exception was subunit F_o-c, whose levels remained unchanged or even increased. ATP synthase deficiency translated into limitation of cell viability, which was manifested under nutrient limiting conditions as a threshold in knockdown clones (KD) harbouring less than 50 % of residual ATP synthase content. Decreased functional capacity of ATP synthase was further characterized in the most severely affected clone, where we observed decrease in respiratory control indexes. While ATP synthase content showed decrease in the range of 90-15 % compared to controls, other OXPHOS complexes displayed variable compensatory upregulation.

Next, we adapted the technique of ATP synthase affinity purification through the IF_1 inhibitory protein. We prepared sufficient quantities of recombinant IF_1 protein construct, verified its ability to bind ATP synthase and performed proof-of-concept isolation of ATP synthase from rat liver mitochondria. Isolated ATP synthase was devoud of contamination by other OXPHOS complexes. This approach will be available for future characterisation of ATP synthase dysfunction models, such as knockdowns of the central stalk.

Key words: mitochondria, ATP synthase, deficiency, threshold effect, biogenesis, affinity purification

Content

List of abbreviations

AA	amino acid
ADP	adenosine diphosphate
ANT	adenine nucleotide translocator
ATP	adenosine triphosphate
β_{DP}	β subunit with ADP molecule bound
β_{E}	empty β subunit, no ATP or ADPbound
β_{TP}	β subunit with ATP molecule bound
BN-PAGE	blue native polyacrylamide gel electrophoresis
bp	base pair
CNE-PAGE	clear native polyacrylamide gel electrophoresis
Core2	subunit of complex III
Cox3 and Cox4	subunits of complex IV
DAPIT	diabetes-associated protein in insulin-sensitive tissues
ETC	electron transport chain
FAD/$FADH_2$	flavin adenine dinucleotide (oxidized/reduced)
Fe/S	iron/sulfur centre
FMN	flavin mononucleotide
FPLC	fast protein liquid chromatography
GPDH	glycerol-3-phosphate dehydrogenase
GST	glutathione-S-transferase
H^+	proton ion
HAP1	abbreviation for near haploid cell line
HEK293	human embryonic kidney cell line
hrCNE-PAGE	high resolution clear native polyacrylamide gel electrophoresis
IF_1	inhibitor of F_1F_o ATPase
IMM	inner mitochondrial membrane
IMS	intermembrane space
kDa	kilodaltons
KD	knockdown
KO	knockout
MELAS	syndrome of mitochondrial encephalopathy, lactic acidosis and stroke-like episodes
MD	megadaltons
MLQ	another name for 6.8 kDa protein, named after first three aminoacids (methionine, leucine,
MS	mass spectometry
mt-DNA	mitochondrial deoxyribonucleic acid
NAD^+/NADH	nicotinamide adenine dinucleotide (oxidized/reduced)
NARP	neuropathy, ataxia, and retinitis pigmentosa
nc-DNA	nuclear deoxyribonucleic acid

NDUFA9	subunit of complex I
OMM	outer mitochondrial membrane
OSCP	oligomycin sensitivity conferral protein
OXPHOS	oxidative phosphorylation
P_i	phosphate anion
PIC	protease inhibitor cocktail
POS	polarographic oxygen sensor
PCR	polymerase chain reaction
Δp	proton motive force
ΔpH	pH gradient
$\Delta\psi_m$	mitochondrial membrane potential
Q cycle	pathway of electrons in complex III
Q_p/Q_m	biding sites for ubiquinone/ubiquinol
RC	respiratory chain
RCI	respiration control index
RE	restriction enzyme
RNA	ribonucleic acid
rRNA	ribosomal ribonucleic acid
ROS	reactive oxygen species
SDHA, SDHC, SDHD	subunits of complex II
SEM	standard error of the mean
SHR	
TCA	tricarboxylic acid
TIM	translocase of the inner membrane
TOM	translocase of the outer membrane
tRNA	transfer ribonucleic acid
UCR	uncoupling control ratio
UQ/UQH_2	ubiquinone/ubiquinol
ΔV	voltage gradient
VDAC	voltage-dependent anion channel

1 Introduction

1.1 Mitochondria

Mitochondrion is an essential organelle for the eukaryotic organisms. This cellular compartment is mistress of multitasking: TriCarboxylic Acid (TCA) cycle, β-oxidation of fatty acids, oxidative phosphorylation, Ca^{2+} storage, heme biosynthesis, assembly of iron-sulfur clusters, role in programmed cell death – not this is not yet the complete list of mitochondrial functions. Mitochondrial morphology may vary among spices and also in different tissues of one organism. First references to intracellular structures which were later described as mitochondria appeared in nineteenth century, specifically in 1840s in the works of Richard Altmann (Ernster and Schatz, 1981).

The origin of mitochondria is explained in the endosymbiotic theory (Sagan, 1967). Ofa free-living organism, e.g. α-proteobacteria (*Rickettsia*) (Andersson *et al.*, 1998), engulfed by the archaeal ancestor (reviewed in Martin et al. 2015).

Mitochondria present two-membranous compartment. The outer membrane (OMM) is semi-permeable and it accommodates porins, β-barrel proteins, including translocases (TOM family), ion channels (e.g. VDAC), through which ions and molecules smaller than 5 kDa are transported to the inter-membrane space (IMS).

The inner mitochondrial membrane separates the IMS from the inner space of mitochondria, named matrix. Phospholipid bilayer of the inner mitochondrial membrane is rich in cardiolipin, making the IMM highly selective and impermeable to ions. The IMM is convoluted and its surface is highly increased by formation of folds termed cristae (Alberts et al. 2015) as depicted in figure 1, where majority of enzymatic complexes of the oxidative phosphorylation (OXPHOS) apparatus is located (Gilkerson, Selker and Capaldi, 2003; Wilkens, Kohl and Busch, 2013).

Matrix of mitochondria is a place, where many of the important biochemical processes occur: TCA or Krebs cycle, β-oxidation of fatty acids, first steps of the urea cycle.

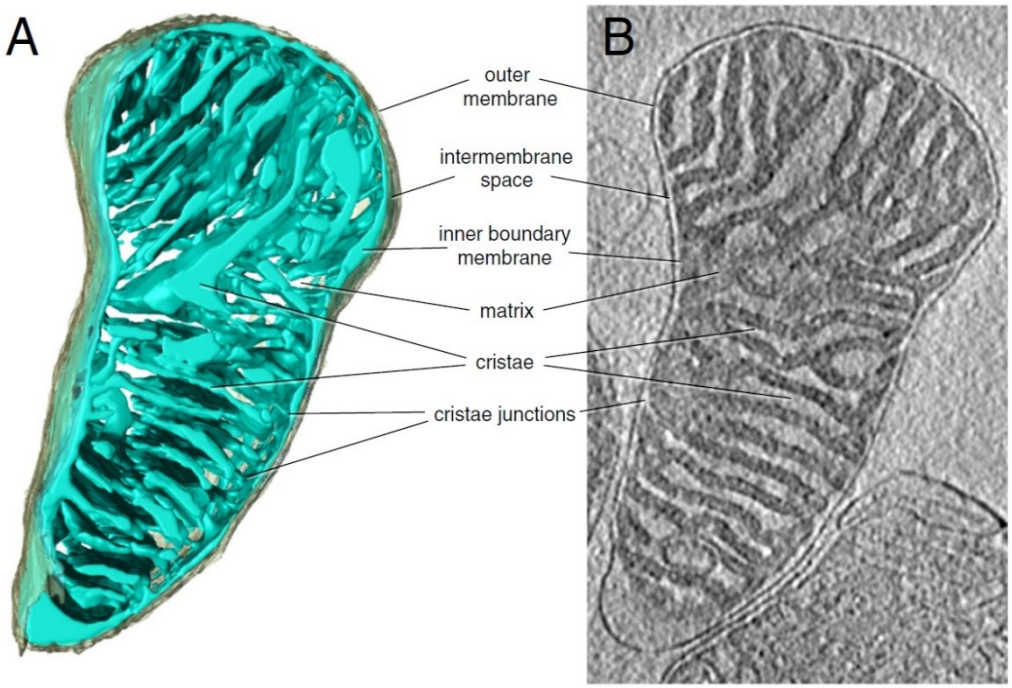

Figure 1. Images of mitochondrion from mouse heart.

Three-dimensional image of mitochondrion resolved by cryo-ET (A) and one of the tomographic slices (B). Cristae junctions represent sites of cristae membrane joining the inner boundary membrane. Adapted and modified from Kühlbrandt, 2015.

Mitochondria (as well as chloroplasts) are considered as semiautonomic organelles as they still possess their own genome and proteosynthetic apparatus, both located in matrix. Mitochondrial DNA (mt-DNA) has been decreasing in size during the evolution, as most of the genes encoded by prokaryotic ancestor had been transferred to the nucleus. Unlike the nuclear DNA, the mitochondrial DNA is present in many (10-10 000) copies per cell and is usually circular, albeit with some exceptions (e.g. *Tetrahymena* or *Chlamidomonas*) (Alberts et al. 2015). Human mt-DNA with its size of 16 569 bp (Anderson *et al.*, 1981; Andrews *et al.*, 1999) contains 37 genes which encode 13 proteins for the enzymes of oxidative phosphorylation apparatus, 22 transfer RNAs (tRNAs) and 2 ribosomal RNAs (rRNAs) (reviewed in Ladoukakis and Zouros, 2017).

1.2 Energy and oxidative phosphorylation

One of the primary roles of mitochondria as “the powerhouse of the cell” is production of energy. This organelle generates approximately 90 % of cellular ATP via the process of oxidative phosphorylation. OXPHOS apparatus is comprised of five complexes: NADH-dehydrogenase (complex I), succinate-dehydrogenase (complex II), cytochrome c reductase (complex III), cytochrome c oxidase (complex IV) and ATP synthase (complex V). The system is localized on the IMM and, besides abovementioned complexes I-V, includes mobile electron carriers (coenzyme Q, or ubiquinone UQ, and

cytochrome c) (figure 2). Oxidative phosphorylation couples respiration with ATP production through the mechanism described by the chemiosmotic theory postulated by D. Mitchell (Mitchell 1961).

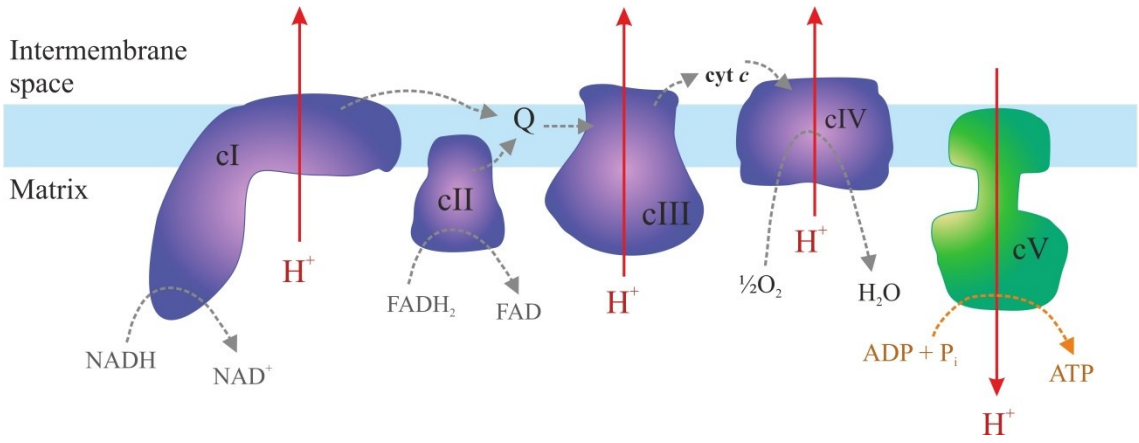

Figure 2. Oxidative phosphorylation apparatus.

cI - cV are the complexes of OXPHOS, H^+ - direction of proton translocation across the inner membrane. Q and cyt c depict the pool of coenzyme Q and cytochrome c respectively.

First four complexes of OXPHOS are part of the respiratory chain (RC), where respiration occurs together with build-up of proton gradient. Reduced coenzymes, $FADH_2$ and NADH, from the TCA cycle and β-oxidation of fatty acids, are reoxidized to FAD and NAD^+ through complexes I and II, respectively. The oxidation donates electrons that flow in the direction of ascending redox potential to the terminal electron acceptor, oxygen, in the complex IV, where they are reduced to water. The energy released from that process is stored as an electrochemical proton gradient. Protons are pumped across the IMM into the IMS, which leads to the following outcomes: generation of pH, or chemical, gradient (ΔpH) and voltage gradient (ΔV). Both these gradients contribute to the overall mitochondrial membrane potential ($\Delta\psi_m$). The electrochemical gradient forms the proton-motive force (Δp), which drives protons back into the matrix and maintains a balance of proton ion (H^+) concentrations. Complex V, or ATP synthase, dissipates the $\Delta\psi_m$ and synthesizes the ATP from ADP and inorganic phosphate, P_i, at the expanse of Δp (Nicholls *et al.*, 2013a).

1.3 Oxidative phosphorylation apparatus:

1.3.1 NADH-dehydrogenase

Complex I or NADH-dehydrogenase (NADH:coenzyme Q oxidoreductase) is the largest OXPHOS multi-subunit complexes (table 1). Its size prevented for the long time determination of its crystal structure and thus it remained the least well understood. Mammalian NADH-dehydrogenase possess 45 nc- and mt-DNA encoded subunits with

the total molecular weight of approximately 1 MDa (Carroll *et al.*, 2006; Zhu, Vinothkumar and Hirst, 2016). 14 central subunits form catalytic core and are conserved from bacteria to humans, whereas other 31 accessory subunits do not participate in energy conversion. Three classes of complex I (class 1, 2 and 3), according to different functional states of enzyme, were described (Zhu, Vinothkumar and Hirst, 2016; Blaza, Vinothkumar and Hirst, 2018). Thanks toL-shape, complex I has hydrophobic arm located in the IMM and hydrophilic arm protruding into the matrix. The electrons from the NADH are accepted by the flavin mononucleotide (FMN) at the matrix arm and are transferred through 8 iron-sulfur clusters (Fe/S centers) to the coenzyme Q along with proton translocation across the IMM with the $4H^+/2e^-$ stoichiometry (Wikström, 1984; Galkin, Dröse and Brandt, 2006), and the transport of electrons and protons is separated (reviewed in Sazanov, 2015; Wirth, Brandt and Hunte, 2016).

Table 1.The key features of respiration complexes.

	Complex I	*Complex II*	*Complex III*	*Complex IV*
	NADH dehydrogenase	Succinate dehydrogenase	Cytochrome c reductase	Cytochrome c oxidase
Catalytic function	NADH: ubiquinone oxidoreductase	succinate: ubiquinone oxidoreductase	ubiquinol: ferricytochrome c oxidoreductase	ferrocytochrome c: oxygen oxidoreductase
Molecular weight [kDa]	~1000	124	240(dimer - 480)	204(dimer - 408)
Number of subunits (mt-DNA encoded)	45(7)	4(0)	11(1)	13(3)

1.3.2 Succinate dehydrogenase

Complex II or Succinate dehydrogenase (Succinate:coenzyme Q oxidoreductase) is the second and the smallest of OXPHOS complexes. It comprises of only 4 subunits encoded by in the nucleus and has a molecular weight of 124 kDa (Sun *et al.*, 2005). Succinate dehydrogenase is at the crossroads between the TCA and OXPHOS. Oxidation of succinate to fumarate on matrix side donates electrons to covalently bound FAD, electrons then pass through three Fe/S clusters into the IMM region, where they are accepted by UQ. Membranous SDHC and SDHD subunits coordinate heme b, the role of which remains unclarified (reviewed in Bezawork-Geleta *et al.*, 2017). Unlike the

other three complexes of RC, complex II does not couple electron translocation to H^+ pumping.

1.3.3 Cytochrome c reductase

Complex III or Cytochrome c reductase (cytochrome bc_1 complex or coenzyme Q:cytochrome c oxidoreductase) catalyzes the transfer of electrons from UQ to cytochrome c during/in a Q-cycle. Mammalian monomer of the enzyme consists of 11 subunits (Schägger *et al.*, 1986; Iwata *et al.*, 1998), one of which is encoded by mitochondrial genome (cyt b). The redox/prosthetic groups include Reiske protein with 2Fe/2S cluster, cytochrome b containing two hemes b, cytochrome c_1 heme. Symmetric dimer of the enzyme presents functionally active complex III, with molecular weight of approximately 480 kDa. The Q-cycle starts with oxidation of UQH_2 at the Q_p site. First electron passes through the Reiske iron-sulfur center to cyt c_1 and then to mobile cyt c, the second electron is transferred through the two cyt b hemes to the Q_n site with bound oxidized UQ and reduce UQ to the radical semiquinone. In the following part of the cycle, a second molecule of UQH_2 binds to the Q_p site and the cycle repeats to reduce the semiquinone to UQH_2 at the Q_n site. This electron transfer is coupled to the H^+ translocation across the IMM. The process of Q-cycle at the molecular level is still not fully understood (reviewed in Fernández-Vizarra, Tiranti and Zeviani, 2009; Meunier *et al.*, 2013).

1.3.4 Cytochrome c oxidase

The last enzyme of RC is complex IV or Cytochrome c oxidase (COX). Mammalian Mitochondrial Complex IV consists of 13 subunits (Tsukihara *et al.*, 1996), three of which are encoded by the mt-DNA (subunits I, II and III). Subunits I and II form catalytic core, where the release of electrons from the cyt c occurs together with proton translocation and reduction of oxygen to water. The cyt c donates e^- to Cu_A at IMS site; the electrons then pass though the a- and a_3-heme groups to Cu_B site. Reduction of oxygen happens at the a_3/Cu_B center and include several stages, in the end of the process one molecule of O_2 is reduced to 2 molecules of H_2O, which require 4 electrons (Nicholls *et al.*, 2013b). The proton pumping in cytochrome c oxidase is not fully clarified yet, with several possible models describing it. Two H^+-channels, K and D, in subunit I have been determined in both bacteria and mammals, whereas the third H-channel was identified only in bovine heart (reviewed in Kadenbach and Hüttemann, 2015).

1.4 F_1F_o-ATP synthase

1.4.1 Description and structure

Mitochondrial F_1F_o-ATP synthase or complex V is the final enzyme in OXPHOSthat produces the energy in form of ATP at the expense of proton-motive force. Mammalian ATP synthase consist of at least 17 different subunits with total molecular weight of 650 kDa (figure 3 and table 2). Majority of the subunits are encoded in the nucleus and only two of them: a and A6L are encoded by mt-DNA (Anderson *et al.*, 1981; Fearnley and Walker, 1986). Complex V possesses two large domains: F_1 (α3β3 hexamer) matrix-oriented hydrophilic domain and F_o (subunits a, c, A6L, e, f, g, 6.8 kDa proteolipid and DAPIT) membranous highly hydrophobic domain. These two major domains are attached to each other by the central (γ, ε, δ subunits) and peripheral (subunits b, d, F_6, OSCP) stalks. Subunits of the central stalk together with oligomer of c subunits (c-ring) form a rotor of the enzyme. Rotation drives conformational changes in α3β3 hexamer, the catalytic core of the ATP synthase. The peripheral stalk works as a stator, that fixes the catalytic core in rigid position preventing its rotation (reviewed in Walker, 2013).

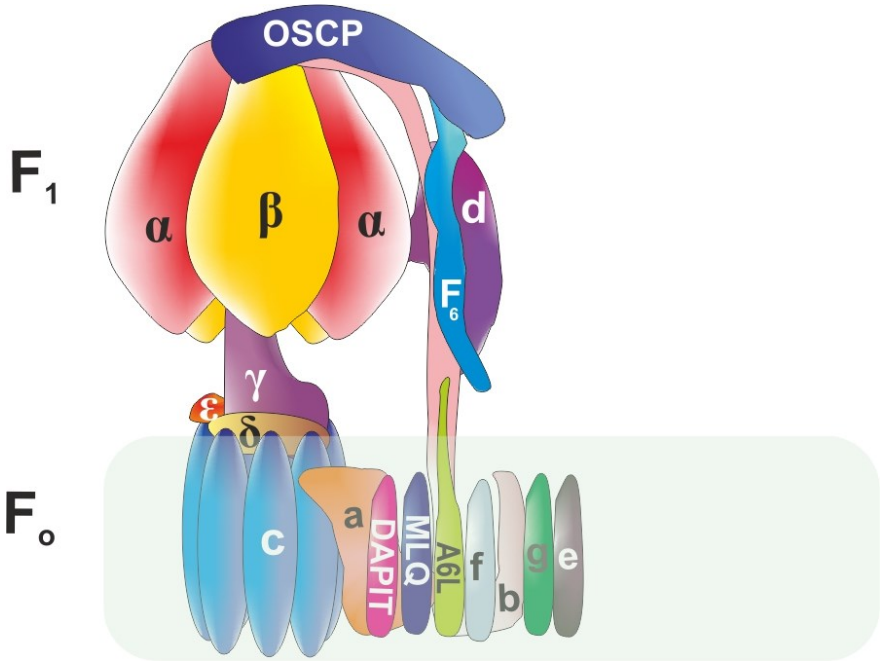

Figure 3. Structure of mammalian F_1F_o ATP synthase.

Rectangle in light green represents inner mitochondrial membrane.

To study F_1F_o ATP synthase structure, wide spectrum of techniques has been utilized. This varies from electrophoretic approaches (SDS-, BN-, CNE-, hr-CNE- PAGE) (Wittig and Schägger, 2005; Wittig, Braun and Schägger, 2006; Wittig, Karas and

Schägger, 2007) to crystallographic studies (Abrahams *et al.*, 1994) and recently electron cryo-tomography (Davies *et al.*, 2012).

Table 2. Nomenclature of ATP synthase subunits.

		gene name		
	S. Cerevisiae	*S. Cerevisiae*	Mammals	gene name mammals
F_1	α	ATP1	α	ATP5A1
	β	ATP2	β	ATP5B
	γ	ATP3	γ	ATP5C1
	δ	ATP16	δ	ATP5D
	ε	ATP15	ε	ATP5E
F_o	OSCP	ATP5	OSCP	ATP5O
	6	ATP6	a	MT-ATP6
	4	ATP4	b	ATP5F1
	9	ATP9	c	ATP5G2;ATP5G1;ATP5G3
Associated	8	ATP8	A6L	MT-ATP8
	d	ATP7	d	ATP5H
	f	ATP17	f	ATP5J2
	h	ATP14	F6	ATP5J
	g	ATP20	g	ATP5L
	e	ATP21	e	ATP5I
	i or i/j	ATP18	-	
	k	ATP19	-	
	IF_1		IF_1	ATPIF1
	Stf1p		-	
	Stf2p		-	
	-		AGP, DAPIT	USMG5
	-		MLQ	c14orf2, MP68, PLPM
	-		s, coupling factor b	ATP5S
	-		s-like	ATP5SL

1.4.2 Function of F_1F_o ATP synthase/ATP synthesis: molecular mechanism

ATP synthesis by Complex V is coupled with the proton translocation across the IMM. Molecular mechanism of coupling was described/proposed by W. Junge (Junge, Lill and Engelbrecht, 1997). F_o-part of the enzyme provides the transport of hydrogen ions in the direction of H^+ gradient: from the IMS into the matrix. Protons at near proximity to subunit F_o-a enter the channel and bound on aspartate or glutamate of the c subunit. The negative charge is protonated which leads to the loss of interaction between the c subunit and positively charged arginine on F_o-a subunit. This event propagates rotation of c-ring by one monomer/unit in a clockwise direction (a view from the membranous F_o part to the F_1 part). The subunit F_o-a has also a second matrix-oriented channel, which interacts with another c-subunit of the c-ring. During the rotation, protonated c-subunit replaces charged one adjacent the second channel and the proton released on the site of IMS (D Stock, Leslie and Walker, 1999; Allegretti *et al.*, 2015). When ATP synthase works in a reverse mode, the hydrolysis of ATP occurs leading to rotation of the c-ring in a counterclockwise direction.

Rotation of the c-ring drives γ, ε and δ subunits of the central stalk to spin. The asymmetrical γ subunit introduces conformational changes at α/β subunits interfaces of α3β3 hexamer, where each β subunit possesses a catalytic site. Three catalytic states have different conformation depending on their affinity to ATP/ADP nucleotides during the catalytic cycle. Binding of ADP with Mg^{2+} and P_i occurs in “loose” position, β_{DP}. Then, the γ subunit performs a 120° turn, “loose” conformation switches to “tight”, β_{TP}, and the synthesis of ATP occurs. The next 120° rotary step converts β_{TP} to β_E, “empty” position, when the molecule of ATP is released and the cycle repeats. During one cycle γ subunit makes a complete 360° turn with three molecules of ATP synthesized (summarized in Walker, 2013). The first evidence of physical rotation of central stalk induced by the hydrolysis of ATP was observed on bacterial α3β3γ complex (Noji *et al.*, 1997).

1.4.3 Regulation of ATP synthase

1.4.3.1 C_x ring

Number of H^+ ions required for the 360° complete cycle and production of 1 molecule of ATP depends on the number of c subunits in the c-ring. In vertebrates, c-ring is usually assembled with 8-10 c subunits, the outer c-ring forms gaps and the inner ring then interact with cardiolipin, a phospholipid of the IMM, through the trimethylated Lys-43 residue (Watt *et al.*, 2010). Other organisms as prokaryotes, fungi and chloroplasts, possess 10-15 c subunits in a ring. Their c-rings are assembled by tightly packed α-helixes of outer ring with no interaction occurring between the inner ring and

the lipid bilayer. (Daniela Stock, Leslie and Walker, 1999; Matthies *et al.*, 2009; Vollmar *et al.*, 2009).

The less monomers form the c-ring, the less protons are required for a full rotation of the ring and thus the less protons are needed for one molecule of ATP synthesized (three molecules per full rotation). Vertebrate c-ring is assembled by eight monomers and thus represents the most efficient form of ATP synthase among organisms. The synthesis of one ATP molecule in vertebrates requires 2.7 H^+ (Watt *et al.*, 2010), whereas organisms with c_{10}-c_{15} subunits require 3.3-5 H^+ (summarized in Ferguson, 2000).

1.4.3.2 Coupling factor B

One of the regulators of ATP synthase activity is coupling factor B or, as designated earlier, ATP synthase subunit s (Lam, Warshaw and Sanadi, 1967). Mature form of human factor B has molecular weight of ~21 kDa but can also be present as shorter forms due to alternative splicing. It has been demonstrated that factor B plays role in energy transduction activity of complex V; removing of factor B results in inability to develop and maintain the mitochondrial membrane potential (Belogrudov and Hatefi, 2002).

This protein was a subject of discussion for being a component of the ATP synthase. While Sanadi D.R. and coworkers isolated factor B from bovine heart mitochondria, including fraction of H^+-ATPase (Lam, Warshaw and Sanadi, 1967; Joshi *et al.*, 1979, 1985; Rao Sanadi, 1982), others did not observe factor B to be presented in preparations of bovine heart complex V (Walker *et al.*, 1991; Collinson *et al.*, 1994). Crystal structure of bovine factor B (Lee, Belogrudov and Stroud, 2008) revealed the amphipathic N-terminal α-helix that was suggested to anchor factor B to the matrix side of mitochondrial inner membrane. Factor B was indicated to interact with ADP/ATP carrier (Belogrudov, 2008). It was proposed that factor B shelters a second proton-translocating pathway formed by Complex V supernumerary subunits together with the carrier. Factor B would block proton translocation through this pathway and maintain the coupling activity of ATP synthase (reviewed in Belogrudov, 2009).

1.4.3.3 Cristae and dimers of complex V

The distribution of OXPHOS complexes on the inner membrane is not random; complexes were reported to be localized rather on the cristae membrane than on the inner boundary membrane (Scorrano *et al.*, 2002; Gilkerson, Selker and Capaldi, 2003; Wilkens, Kohl and Busch, 2013).

Complex V was observed not only in form of monomers, but also dimers and higher oligomers (reviewed in Wittig and Schägger, 2009). Dimers of complex V are considered to contribute to cristae membrane curvature, shaping the tips and edges of cristae (Strauss *et al.*, 2008; Davies *et al.*, 2011). It has been proposed that subunits g and e of the membranous F_o part contribute to dimer formation (Paumard *et al.*, 2002; Davies *et al.*, 2012; Habersetzer *et al.*, 2013). In mammalian ATP synthase, IF_1 protein (inhibitor of F_1F_o ATPase) has also been suggested to contribute to dimerization of ATP synthase (García *et al.*, 2006; Campanella *et al.*, 2008). Recent studies have indicated that ATP synthase monomers can bend the lipid bilayers and thus promote association of Complex V into dimers and formation of dimer rows (Baker *et al.*, 2012; Jiko *et al.*, 2015).

Organization of ATP synthases into dimers and higher oligomers stabilizes the stator of the enzyme (Buzhynskyy *et al.*, 2007). While the rotor rotates clockwise during the synthesis of ATP the stator, being in a fluid membrane and not fortified by anything that can hold the enzyme, would rotate counterclockwise. As a result, entire complex V is moving in the membrane that leads to energy dissipation. Oligomeric form prevents the movement, because the torque force of every stator is compensated and only rotors move. Oligomeric assembly stabilizes the F_o boundary of rotor-stator and thus, ensure the integrity of ATP synthase enzyme structure.

It has been reported that the distribution of protons along the IMS of inner membrane is not uniform and that the local pH gradient is higher in areas of membrane with higher curvature (Strauss *et al.*, 2008). Therefore, higher proton gradient contributes to higher proton-motive force, Δp. ATP synthase presented at the apex of cristae thus appears to be in optimal position for the enzyme to utilize Δp and produce ATP.

1.4.4 Hydrolysis of ATP by Complex V

Under the physiological conditions Complex V dissipates the mitochondrial membrane potential, $\Delta\psi_m$, and generates energy via synthesis of ATP. When the matrix pH is lowered and the $\Delta\psi_m$ is decreased due to improper functioning of RC either by physiological (lack of substrates, oxygen deprivation during hypoxia) or pathological (ischemia) conditions, ATP synthase switches to reverse mode. To maintain the $\Delta\psi_m$ Complex V hydrolyses ATP to ADP and transfers protons back to IMS. By commencing this step, ATP synthase preserves the $\Delta\psi_m$ that is crucial for the mitochondrial protein import (Martin, Mahlke and Pfanner, 1991). However, the hydrolytic activity of Complex V decreases the ATP pool in the cell which may limit its proper functioning and induce cell death (Campanella *et al.*, 2008). Wasting of energy is prevented by the IF_1 inhibitory

protein, that binds to ATP synthase and acts as specific unidirectional inhibitor (Pullman and Monroy, 1963).

1.4.4.1 Inhibitory IF_1 protein

The IF_1 protein is encoded by the nuclear *ATPIF1* gene, which can be translated into three different isoforms. Approximal molecular weight of the IF_1 protein is 10 kDa. The protein is localised in matrix, although it can be present also in cytosol or on plasma membrane and in some cases even in the extracellular space (rewieved in Faccenda and Campanella, 2012; García-Bermúdez and Cuezva, 2016). Active form of IF_1 is a dimer, which dimerizes through antiparallel α-helical coiled-coil in the C-terminal region, while the N-terminal domain interacts with F_1 domain of ATP synthases with the ratio 1:1. The protein is activated by the matrix change in pH: when the pH is lower than 7.0 the IF_1 dimer binds into the catalytic interface between α and β subunits. In the inhibitory active state, the N-terminus of IF_1 forms strong interaction with α_{DP}-β_{DP} interface of F_1-ATPase and blocks the rotation. When the pH is increased to 8.0 or higher, the Complex V switches back to ATP synthesis. This mode leads to disruption of the interaction between the α_{DP}-β_{DP} and IF_1 (Bason *et al.*, 2011, 2014). The IF_1 then forms tetramers (dimers of the dimers) and higher oligomers, where the N-terminal inhibitory domain is hidden and thus unable to interact with ATP synthase (Cabezon *et al.*, 2000; Cabezón *et al.*, 2001) (figure 4).

IF_1 has been reported to inhibit also the synthetic activity of ATP synthase (summarized in García-Bermúdez and Cuezva, 2016). Earlier work on bovine heart sub-mitochondrial particles showed the correlation between presence of IF_1 and ATP synthase hydrolytic and synthetic capacities. When the vesicles had generated Δp, it led to release of the IF_1 and further increase in ATP synthase hydrolytic and synthetic activities (Lippe, Sorgato and Harris, 1988). Later studies confirmed the inhibition of synthetic activity by IF_1 (Sánchez-Cenizo *et al.*, 2010; Formentini *et al.*, 2014; Santacatterina *et al.*, 2016). Inhibition activity of IF_1 was shown to be dependent on phosphorylation state as dephosphorylated IF_1 does inhibit both activities of ATP synthase (García-Bermúdez *et al.*, 2015).

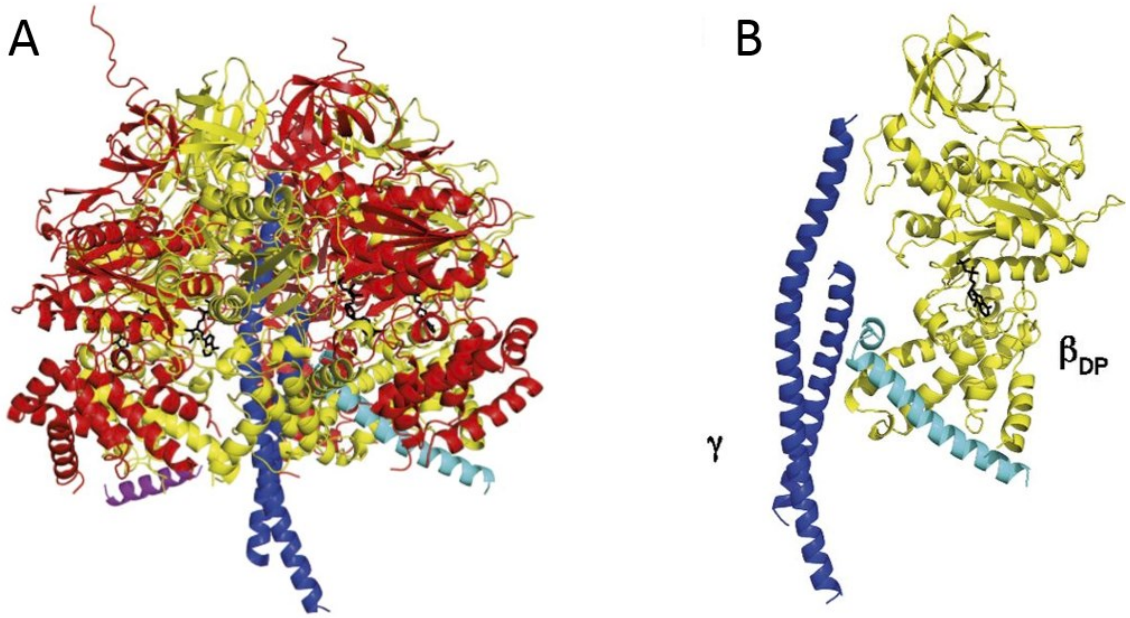

Figure 4. The IF_1 protein bound to the F_1-ATPase.

(A) Structure of the F_1-(I1-60His aa residue)$_2$ complex. α, β and γ subunits are depicted in red, yellow and dark blue, respectively. Nucleotides are in black and the I1-60His aa residue of IF_1 is in purple (position β_E) and light blue (position β_{DP}). (B) The view on the I1-60His aa residue bound at β_{DP} and interacting with γ subunit. The designation of colors is the same as for (A). Adapted from Bason et al., 2014.

The IF_1 could also serve as oncogenic marker. It has been shown that increased expression of the IF_1 in some cancer types leads to mitochondrial hyperpolarization, increased ROS production and activation of aerobic glycolysis, *i.e.* Warburg effect (Sánchez-Cenizo *et al.*, 2010; Formentini *et al.*, 2012; Sánchez-Aragó *et al.*, 2013; Hardonnière *et al.*, 2017). The IF_1 contributes to proliferation of cancer cells (Yin *et al.*, 2015), while its silencing lead to inhibition of tumour cell growth (Wei *et al.*, 2015). However, the function of IF_1 in tumours may vary in different cancer types.

1.4.5 Biogenesis of F_1F_o ATP synthase

ATP synthase biogenesis is a complicated process occurring in several stages. Most of the studies were performed on yeast *Saccharomyces cerevisiae*, where the modular model has been proposed. According to that, assembly begins with formation of smaller domains or modules that are later attached to each other to form fully assembled and functional holoenzyme (Rak, Gokova and Tzagoloff, 2011). In yeasts, following stages are found: c-ring, followed by binding of F_1 sector, Atp8p (A6L in mammals), stator arm, Atp6p (F_o-a in mammals).

In contrast to yeasts, mammalian mt-DNA does not encode subunit c, which may preclude differences in the assembly process. Notably, in ρ^0 cells lacking mt-DNA and

thus subunits a and A6L, assembled and hydrolytically active ATP synthase contained all subunits except for accessory subunits MLQ and DAPIT and possibly subunit ε (Wittig *et al.*, 2010). These subunits are very small, ε subunit was not detected even in control cells, which is also the case of small accessory subunits that sometimes are not detected by MS. c-ring was present in both monomer and F_1-c subcomplex.

Another example of exception from the proposed modular model is the case of mt-DNA 9205ΔTA microdeletion that alters the *ATP6* gene stop codon and cleavage site of mRNAs for cV subunit F_o-a and cIV subunit Cox3. ATP synthase isolated from the patient fibroblasts showed decreased (< 20% of control) content of subunit F_o-a. Assembled monomer of Complex V lacking the F_o-a was present, yet in low amount, 7 % among all detected (sub)complexes. Assembled monomer was hydrolytically active and showed no proton leak, however it was uncapable of ATP synthesis (Jesina *et al.*, 2004; Hejzlarová *et al.*, 2015). The overall profile of subassemblies was similar to the ATP synthase in ρ^0 cells.

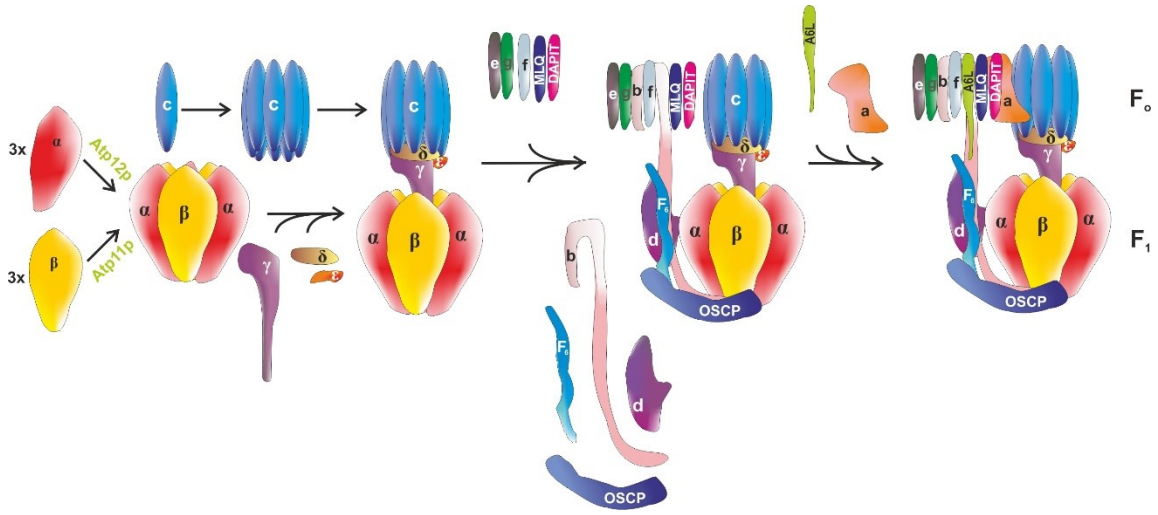

Figure 5. Schematic representation of mammalian ATP synthase biogenesis.

The following sequence of events during the assembly of the mammalian complex V was suggested (figure 5). The first step in the process is assembly of c-subunit oligomer of the F_o domain and α3β3 hexamer of F_1 domain, which proceeds independently. Subunits of the central stalk are then connected to the α3β3 hexamer with subsequent attachment to the c-ring. The peripheral stalk and subunits of F_o domain are joined in the final stages. ATP synthase formation is completed with attachment of mt-DNA encoded A6L and F_o-a subunits (figure 5). Nevertheless, later studies on mammalian cells have indicated that models lacking some subunits do not behave according to the proposed scheme.

Disruption of all the three genes encoding for isoforms of subunit c (ATP5G1, 2 and 3) in human HAP1 cell line led to formation of vestigial ATP synthase, which contained F_1-catalytic domain, peripheral stalk and e, f, g supernumerary subunits, but beside c-ring lacked also DAPIT, MLQ, a and A6L subunits (He, Ford, *et al.*, 2017). Therefore, residual monomeric ATP synthase can occur even in the absence of c subunit and c_8-ring is not an obligatory prerequisite for the assembly of F_1 catalytic domain or of the peripheral stalk.

Recent study on knockouts of subunits e, f, g, DAPIT and MLQ indicated further dissimilarities (He *et al.*, 2018). While in KO of subunit e or g assembled ATP synthase lacked all supernumerary subunits and subunits F_o-a and A6L, the situation was different for DAPIT or MLQ knockouts. When MLQ subunit was absent from ATP synthase, the enzyme contained all subunits except for DAPIT, F_o-a and A6L. In case of DAPIT KO only DAPIT subunit was not detected. ATP synthase in knockouts occurred in monomeric form or as subcomplexes with smaller molecular weights depending on subunits the subcomplex lacked. Results of this work demonstrated that not all supernumerary subunits are incorporated into the ATP synthase before subunits F_o-a and A6L would associate with the enzyme to finalize the assembly process. Furthermore, DAPIT, and not F_o-a and A6L, appeared to be the last subunit to associate with the ATP synthase.

1.4.6 Assembly factors of ATP-synthase

Several assembly factors have been elucidated to participate in the process of ATP synthase formation and folding. In general, assembly factors are proteins not presented in the final holo-complex but are necessary for the incorporation and (or) stability of complex subunits and enzyme intermediates. ATP synthase requires specific ancillary factors, some of which are highly conserved among eukaryotes (ATP11 and ATP12), whereas others are present only in yeasts (for example, ATP10, ATP23) or vertebrates (TMEM70). ATP11 and ATP12 are the ancillary factors for F_1 domain assembly, namely for α3β3 hexamer (ATP12 binds subunit α and ATP11 binds β, (Wang and Ackerman, 2000; Wang *et al.*, 2000; Wang, White and Ackerman, 2001)). Yeast specific factors ATP10 and ATP23 participate in the F_o-part assembly through assisting of the subunit F_o-a maturation and incorporation into the membranous domain (Tzagoloff *et al.*, 2004; Osman *et al.*, 2007; Zeng, Neupert and Tzagoloff, 2007). In case of mammals TMEM70 protein, it has been proposed as ATP synthase assembly factor (Cízková *et al.*, 2008; Houštěk, Kmoch and Zeman, 2009). However, there is no evidence for the TMEM70 interaction with Complex V and the function of this protein remains unclear (Kratochvílová *et al.*, 2014).

1.4.7 Subunits of the central stalk

The presence of γ, δ and ε subunits in the ATP synthase and their functionality are crucial for proper activity of the enzyme. The central stalk subunits connect the F_o-domain with α3β3 hexamer and transform rotation of the c-ring and proton pumping into catalytic changes of the β subunits and subsequent synthesis of ATP (table 2 and figure 6).

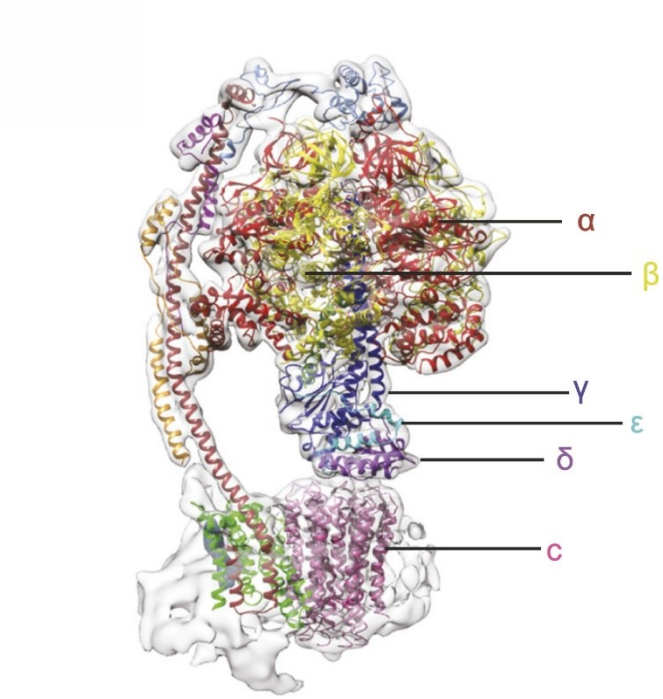

Figure 6. Structure of ATP synthase indicating position of the central stalk subunits.
Adapted and adjusted from Zhou *et al.*, 2015

1.4.7.1 Yeasts

The role of the central stalk subunits in the ATP synthase biogenesis and function was studied mainly in *S. cerevisiae*. In these studies, ATP3, ATP16 or (and) ATP16 genes corresponding to γ, ε and δ, respectively, were disrupted and it has been shown, that γ, ε or δ deficient mutants are unable to grow on non-fermentable source of carbon. They also displayed proton leakage through the F_o-domain and uncoupling of proton transport to ATP synthesis (Guélin *et al.*, 1993; Duvezin-Caubet *et al.*, 2003; Tetaud *et al.*, 2014). Moreover, deletion of γ or δ subunit lead to cytoplasmic petite mutants, ρ^-/ρ^0, i.e. clones with massive deletion or the complete loss of the mt-DNA (Lai-Zhang, Xiao and Mueller, 1999; Xiao, Metzl and Mueller, 2000) and thus, of the subunits a and c encoded by the mt-DNA. The possible explanation for this effect is that elimination of the proton-translocating subunits of the F_o-domain prevents formation of the incomplete ATP

synthase in the Δγ or Δδ and thus dissipation of $\Delta\psi_m$ and subsequent cell lethality (Duvezin-Caubet *et al.*, 2006, reviewed in Mueller, 2000). Unlike the deletion of γ or δ subunits, deletion of subunit ε does not result in 100 % ρ^-/ρ^0 colonies, gaining just 60-70 % of ρ^-/ρ^0 (Guélin *et al.*, 1993; Tetaud *et al.*, 2014). Considering that the ε subunit has no homologue in bacteria and is not an essential subunit for the *S. cerevisiae* ATP synthase (Mueller, 2000b), the less severe phenotype of Δε mutants can be expected. The findings also demonstrated presence of F_o membranous subassemblies in the Δγ, Δε or Δδ mutants, implicating independent assembly of F_1 and F_o regions.

1.4.7.2 Mammals

Structure of the mammalian central stalk has been elucidated (Gibbons *et al.*, 2000). However, no assembly factor specific for the central stalk subunits incorporation into the ATP synthase in mammals has been detected. The ε subunit was demonstrated to appear in heterodimer with δ subunit (Orriss *et al.*, 1996), which could serve as possible intermediate of the F_1-domain. There are only few works focused on the role of mammalian γ, ε and δ subunits in the function of ATP synthase and its biogenesis.

Dysfunction of the ε subunit has been studied on the patient with the missense mutation in *ATP5E* gene (Mayr *et al.*, 2010) and on the knockdown model of the ε subunit (Havlícková *et al.*, 2010). In both cases, the content of ATP synthase and its activity were reduced; the mutated ε subunit was present in the Complex V and its intermediates. nevertheless, in contrary to the yeast models, subunit c accumulation , yet not associated with the Complex V, was observed in mammalian cells. Moreover, no proton leak was documented. These data indicate that the mammalian ε subunit can have a regulatory function in the interaction between the c-oligomer and F_1-domain.

The role of the γ and δ subunits in the mammalian ATP synthase biogenesis and function was studied in our laboratory on the knockdown models of γ and δ subunits in the HEK293 cells (Pecina *et al.*, 2018). Phenotype of these models was very similar to the above-mentioned deficiency of the ε subunit. Studying missense mutations in *ATP5D* gene for δ subunit in patients revealed slightly different results comparing with described deficiencies of central stalk subunits (Oláhová *et al.*, 2018). Notably, content of δ subunit in patients remained unchanged, whereas content of other cV subunits (i.e. α, β, OSCP) was decreased. Fully assembled monomer of complex and its activity were also decreased. According to results, authors suggested that subunit δ can play a role in assembly of ATP synthase.

1.4.8 ATP synthase deficiencies

Dysfunction of the complex V or decreased content of the enzyme are associated with the failure of mitochondrial energy metabolism and lead to severe pathological conditions typical for mitochondrial diseases (reviewed in Houštěk *et al.*, 2006). The age of onset and phenotypic manifestation vary between the pathological states and particular diseases. The most affected tissues and organs are those with higher energetic demand: heart, skeletal muscle and central nervous system. Moreover, mitochondrial defects contribute to the neurodegenerative disorders like Alzheimer, Parkinson or Huntington diseases, but also to cancer and ageing (reviewed in Greaves *et al.*, 2012; Gorman *et al.*, 2016).

ATP synthase deficiencies were described to be divided into two types of isolated defects. One of the groups represents qualitative defects caused by mutations in mt-DNA genes encoding subunits a (Holt *et al.*, 1990; Baracca *et al.*, 2007) and A6L (Jonckheere *et al.*, 2009). The second group includes quantitative defects of complex V biogenesis occurring due to mutations of nuclear origin affecting ATP synthase subunits (subunit ε - Mayr *et al.*, 2010; subunit α - Jonckheere *et al.*, 2013) or assembly factors of the enzyme (ATP12 - De Meirleir *et al.*, 2004; TMEM70 - Cízková *et al.*, 2008).

1.5 Mitochondrial threshold effects

Mitochondrial cytopathies display broad variability in phenotypic manifestation of genetic defects. The variability was indicated in patients with mitochondrial diseases and cell lines carrying different portions of mutations. It was proposed that there is a threshold level for phenotypic presentation of mutation – pathological defect is present only after exceeding of the threshold. Mitochondrial threshold effects were observed at several levels, including biochemical and translational ones (figure 7). Overall sum of individual threshold levels then represents phenotypic threshold effect (reviewed in Rossignol *et al.*, 2003).

1.5.1 mt-DNA mutations

One mitochondrion contains thousands of mt-DNA copies. Occurrence of mutation in the molecule of mt-DNA leads to coexistence/mixture of normal, wild-type, and mutated mt-DNA copies. Ratio of mutant to normal mt-DNA indicates the portion of the heteroplasmy. Variability of this parameter between cells or tissues within a patient and among different patients can partly explain miscellaneous phenotypic manifestations of the same genetic defect in different individuals. Nevertheless, heteroplasmy does not apply to all mitochondrial diseases (reviewed in Rossignol *et al.*, 2003; DiMauro, 2013). Numerous cases with no direct dependence of clinical manifestation on percentage of

hetroplasmy were indicated (for example Vernham *et al.*, 1994; Zhou *et al.*, 1997; Chinnery *et al.*, 2001).

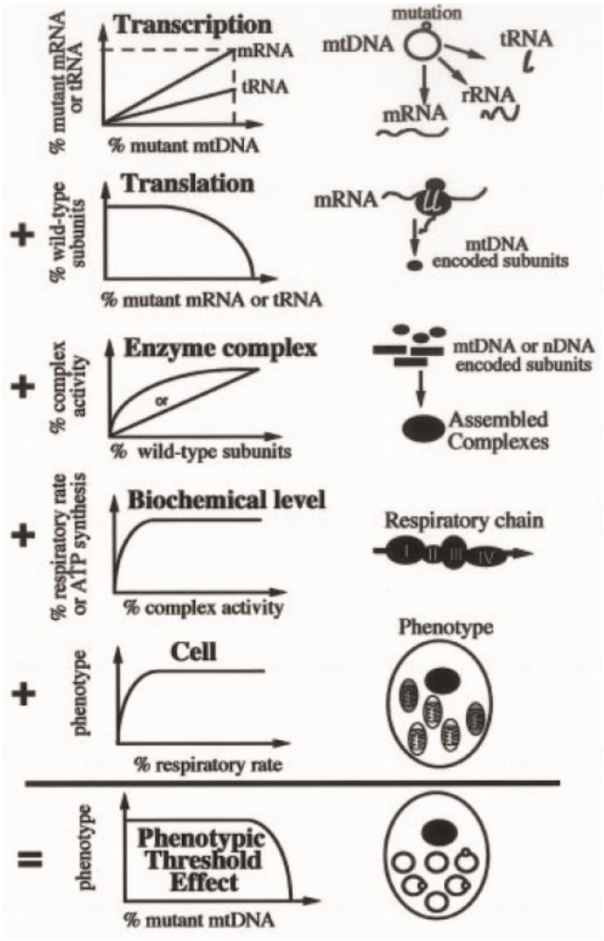

Figure 7. Mitochondrial threshold effects.

Detrimental impact of genetic defect occurs at six various levels: transcription, translation, enzyme activity, oxidative phosphorylation or respiration flux (biochemical level), cellular activity and, final, phenotypic effect. Adapted from Rossignol et al., 2003.

Several mitochondrial diseases have been reported to exhibit threshold level: mutation load that alters the phenotype. As example, threshold for the presentation of A3243G mt-DNA mutation (substitution in gene coding the $tRNA^{Leu}$) known as MELAS syndrome (mitochondrial encephalopathy, lactic acidosis and stroke-like episodes) is more than 60% in affected skeletal muscle. Exceeding this threshold affected the activities of ETC enzymes (Miyabayashi *et al.*, 1992). Another example is above-mentioned mt-DNA 9205ΔTA microdeletion (section 1.4.5), where the biochemical consequences occurred only when heteroplasmy load ≥90% was achieved (Jesina *et al.*, 2004; Hejzlarová *et al.*, 2015).

1.5.2 Reserve capacities

Occurrence of mt-DNA mutation leads to presence of mixture of wild-type and mutated RNAs, deficient proteins, including subunits of OXPHOS, and impaired OXPHOS complexes. Presented wild-type molecules can supply mitochondrion to maintain physiologic activities until their content is limited to significant threshold, when they cannot longer compensate for the genetic defect caused by mutation. It has been proposed that mitochondria possess excess of RNAs and OXPHOS subunits, that are sufficient to support/provide normal OXPHOS enzymes activities and functional respiration and oxidative phosphorylation and keep reserve capacities in case of increased energy demand or OXPHOS deficiency (example of reserve capacities on biochemical level Rossignol *et al.*, 1999; reviewed in Rossignol *et al.*, 2003).

2 Aims of the study

The general aim of this work was to develop tools for studying assembly of mitochondrial F1Fo ATP synthase and to study biological consequences of the absence of central stalk subunits, achieved by the silencing of the expression of ATP synthase subunits γ, δ, or ε in HEK293 cell line. These goals were achieved through focuss on several specific aims outlining individual parts of the study:

- Quantify content of ATP synthase as well as other respiratory chain complexes in individual knockdown (KD) clones using electrophoretic and immunodetection methods
- Describe the impact of varying range of ATP synthase deficiencies on cellular respiration, oxidative phosphorylation and cell viability
- Adapt the technique of ATP synthase affinity purification through recombinant IF_1 inhibitory protein to isolate ATP synthase for future characterization of ATP synthase subassemblies

3 Methods and materials

3.1 Materials

3.1.1 List of chemicals:

6-aminocaproic acid	Merck Millipore (USA)
ADP	Merck Millipore (USA)
Agarose	Merck Millipore (USA)
Acrylamide	SERVA (Germany)
Ascorbate	Merck Millipore (USA)
Bis-acrylamide	SERVA (Germany)
Ampicillin	Merck Millipore (USA)
Aurovertin	Merck Millipore (USA)
Bradford reagent	Bio-Rad, USA
Bis-Tris	Merck Millipore (USA)
BSA (Bovine Serum Albumin)	Merck Millipore (USA)
Digitonin	Merck Millipore (USA)
DMM (n-Dodecyl β-n-Maltoside)	Merck Millipore (USA)
DMSO (DiMethyl SulfOxide)	Merck Millipore (USA)
DMEM + GlutaMax™	Thermo Fisher Scientific (USA)
(Dulbecco's Modified Eagle Medium + L-alanyl-L-glutamine)	
EDTA (EthyleneDiamineTetraacetic Acid)	Merck Millipore (USA)
Ethanol	Penta (Czech Republic)
FBS (Fetal Bovine Serum)	Thermo Fisher Scientific (USA)
FCCP	Merck Millipore (USA)
(Carbonyl Cyanide-4-(triFluoromethoxy)Phenylhydrazone)	
Galactose	Merck Millipore (USA)
Glucose	Merck Millipore (USA)
Monosodium glutamate	Merck Millipore (USA)
Glycerol	Merck Millipore (USA)
HEPES	Merck Millipore (USA)
(4-(2-HydroxyEthyl)-1-Piperazine-1-EthaneSulfonic acid)	
Chloroform	Merck Millipore (USA)
Imidazole	Merck Millipore (USA)
IPTG	Merck Millipore (USA)
(isopropyl β-D-1-thiogalactopyranoside)	
Isopropanol	Merck Millipore (USA)

Kanamycin	Merck Millipore (USA)
KCN (Potassium cyanide)	Merck Millipore (USA)
Sodium malate	Merck Millipore (USA)
Malonate	Merck Millipore (USA)
2-Merkaptoethanol	Merck Millipore (USA)
Methanol	Penta (Czech Republic)
NativeMark Unstained Protein Standard	Themo Fisher Scientific (USA)
Laktino powdered milk	ARTIFEX Instant (Czech Republic)
LB Agar (Lysogeny Broth Agar)	Thermo Fisher Scientific (USA)
Oligomycin	Merck Millipore (USA)
PageRuler^{TM} Prestained Protein Ladder	Thermo Fisher Scientific (USA)
Penicillin/Streptomycin	Merck Millipore (USA)
Ammonium persulfate	Bio-Rad, USA
Proteinase K	Roche (Switzerland)
Sodium Pyruvate	Merck Millipore (USA)
Rotenone	Merck Millipore (USA)
SDS (Sodium Dodecyl Sulfate)	SERVA (Germany)
Serva Blue G (Coomassie Brilliant Blue G-250)	SERVA (Germany)
Sodium succinate	Merck Millipore (USA)
TEMED (Tetramethylethylenediamine)	SERVA (Germany)
TMPD (*N,N,N′,N′*-tetramethyl-*p*-phenylenediamine)	Merck Millipore (USA)
Tris (Trizma baze) (tris(hydroxymethyl)aminomethane)	Merck Millipore (USA)
Tricin (N-[Tris(hydroxymethyl)methyl]glycine)	Merck Millipore (USA)
Trypsin	Merck Millipore (USA)
Tween-20 (Polyoxyethylenesorbitan monolaurate)	Merck Millipore (USA)

3.1.2 List of kits:

CellTiter-Blue® assay kit	Promega (USA)
NucleoBond Xtra kit	Macherey-Nagel (Germany)
QIAuick gel extraction kit	QIAGEN (USA)
QIAquick PCR Purification kit	QIAGEN (USA)

3.2 Methods

3.2.1 Functional characterization of the central stalk subunits (ε, γ, δ) knockdown

3.2.1.1 Cultivation of cell lines

HEK293 control cell lines and HEK293 cell lines with downregulated subunits of the mitochondrial ATP-synthase: γ, δ, and ε - were cultivated under the standard conditions.

The cells were cultivated in the DMEM medium (Dulbecco's Modified Eagles Medium) + GlutaMax™ with glucose concentration of 4.5 g/L, supplemented with 10% (v/v) FBS, 20 mM HEPES and antibiotics (penicillin (10 U/mL) and streptomycin (10 µg/mL)) in the tissue culture incubator at 37°C temperature and 5% CO_2 atmosphere.

Splitting of the cells were performed at 80-100 % confluency in a sterile laminar box. PBS (phosphate buffer, 140 mM NaCl, 5 mM KCl, 8 mM Na_2HPO_4, 1.5 mM KH_2PO_4, pH 7.2 – 7.3), cultivation medium and T+E (0.05% trypsin + 0.02% EDTA in PBS) were preheated in a water bath to 37°C. Medium in a cultivation dish was sacked and HEK293 cells on the dish were washed with PBS. 1,5 mL of T+E were added to the cells with following incubation for 3-5 min during which the cells were releasing from the bottom. Following addition of 5 mL medium inhibited trypsinisation. Cell suspension was then diluted in cultivation medium to appropriate ratio and resuspended.

Harvesting of the cells was performed on ice. Medium from the cultivation dish was poured into the glass flask for the later use. Cells on cultivation dish were washed with 5 mL of PBS, 1,5 mL of T+E were added with following incubation for 3-5 min, the mixture was then replenished with cultivation medium to the final volume of 10 mL. After resuspension the mixture was transferred to sterile 15 mL tubes with the following centrifugation at 4°C for 5 min and 3000 *g* in Sigma 3-K18 (Sigma Laborzentrifugen GmbH, Germany) centrifuge. The supernatant was then removed and the pellet was resuspended with the small volume of prechilled PBS and, again, replenished with the PBS to the final volume of 10 mL. In the next step, there was a second round of centrifugation and resuspension in PBS under the identical conditions. After the final centrifugation, the pellet was stored in -80°C for the following electrophoretic analysis or resuspended in 150-300 µL of PBS for the measurement of respiration on OXYGRAPH.

3.2.1.2 Estimation of protein concentration via Bradford assay

Samples were diluted in distilled H_2O (dH_2O) to final ratio 1:10, vortexed and sonicated with microsond K72 for 20 seconds at 20 % intensity in the ultrasonic

homogenizer BANDELIN SONOPULS (BANDELIN electronic GmbH, Germany). In the next step 10 µL of sonicated sample were placed in a new tube and mixed with 990 µL of dH_2O on vortex with additional step of sonication. 250 µL of Bradford reagent (Bio-Rad, USA) were added to each tube, vortexed and incubated at room temperature for 2 min. The content of tube was transferred into the plastic polystyrene cuvette with 1 cm width. Afterwards, absorbance of each sample was measured at 595 mm wavelength on spectrophotometer BioPhotometer (Eppendorf, Germany). Calibration standards (0, 4, 8, 12, 16, 20 µg) were prepared from BSA (ε= 43.824M^{-1} cm^{-1}).

3.2.1.3 Electrophoretic analysis

3.2.1.3.1 Tricine SDS-PAGE

Tricine SDS-PAGE has been performed (Schägger, 2006). Samples for SDS-PAGE were prepared from the pellets of harvested cells (for the details, see section 3.2.1.1). In order to degrade the DNA and RNA in the protein samples, endonuclease Benzonase® (Merck Millipore, USA) was added to the samples (1200x diluted in PBS, 4U), with following incubation at 37°C for 10 min. In the next step, cells in the pellets were lysed with sample lysis buffer (SLB) containing 2% (v/v) 2-merkaptoethanol, 4% (w/v) SDS, 50 mM Tris (pH 7.0), 10% (v/v) glycerol, 0.02% Coomassie Brilliant Blue R-250. The final protein concentration in the sample was in the range of 2-5 mg protein/mL. The samples were then incubated at 65°C for 15 min in Techno Dri-Block DB-2D (Cole-Parmer, UK). Prepared samples were stored at -80 °C until assayed.

Stacking and separating gels solutions for SDS-PAGE were prepared on ice according to the table 3 . After the vertical electrophoretic apparatus was assembled (Mini-Protean®/Criterion® system, Bio-Rad, USA), 4.3–4.5 mL of separating gel solution was pipetted (1 mm thickness gel) and overlaid with water. After 40-50 min, when separating gel solution was polymerised, the water layer was removed and 2.3-2.5 mL of Stacking gel solution were pipetted with following insertion of a comb. After 40-50 min the comb was removed and polymerised gel was washed with distilled water.

Table 3. Stacking and Separating gel solutions for Tricine SDS-PAGE

	Stacking gel 4% [mL]	***Separating gel 10% [mL]***
	2.5 mL	*10 mL*
AB[1]	0.20	2
3×GB[2]	0.60	3.30
Glycerol 99%	0	1

dH_2O	1.68	3.64
APS[3]	20 µL	50 µL
TEMED[4]	2 µL	6 µL

[1]AB - 48% (wt.) acrylamide, 1.5% (wt.) *N,N'*-methylenebis(acrylamide)

[2]3xGB – gel buffer – 3M Tris HCL, 0.3% SDS, pH 8.45

[3]APS – 10% (wt.) ammonium persulfate

[4]TEMED - *N,N,N',N'*-tetramethylethylenediamine

When the gel was prepared for sample loading, 3 µL of size protein standard PageRuler™ Prestained Protein Ladder (Thermo Fisher Scientific, USA) was pipetted. The samples were pipetted in the volume corresponding to 25-50 µg of protein per well (precise amount is always indicated in a legend to particular image). In the next step, chamber for the vertical electrophoresis was assembled, anode buffer (100 mM Tris-HCl; pH 8.9) was poured into the chamber and cathode buffer (100 mM Tris-HCl, 100 mM Tricine, 0.1% (w/v) SDS; pH 8.25) was poured into the space between the electrophoretic glasses. Initial voltage for the electrophoresis was 45 V, that was increased to 100 V after the samples had stacked and migrated the barrier between the stacking and separating gels.

3.2.1.3.2 Western Blot - electrophoretic transfer onto the PVDF membrane:

When the process of electrophoresis was finished, the electrophoretic transfer of proteins onto the Hydrophobic Polyvinylidene Fluoride (PVDF) membrane (Immobilon-FL 0.45 µm, Millipore, USA) was performed by semi-dry electroblotting Immediately after the electrophoresis, gels were incubated in blotting buffer III (38 mM Tris, 10% (v/v) methanol, 10 mM glycine; pH 8.5). PVDF membrane (7x9 cm for one gel, 9.5x13 cm for 2 gels) was activated in 100% methanol for 15 sec, washed with dH_2O for 2 min and equilibrated in blotting buffer II (25 mM Tris, 10% (v/v) methanol; pH 9.0) for 5 min. The solutions for the blotting buffers are also presented in the table 4.

In the next step, it was proceeded with the preparation of Transblot SD apparatus (Bio-rad Laboratories, USA)On the wet surface of the anode 6 filter papers (3MM, Whatman, UK) with the same size of the PVDF membrane soaked with blotting buffer I (0.3 M Tris, 10% (v/v) methanol; pH 10.4) were placed, then 3 filter papers soaked with blotting buffer II, PVDF membrane soaked with blotting buffer II, the gel incubated in blotting buffer III and 6 filter papers soaked with blotting buffer III. This layer was then covered with cathode, the duration of the electrophoretic transfer was 60 min with constant amperage 0.8 mA/cm^2.

When the transfer was finished, the membrane was washed with TBS (150 mM Tris-HCl, 10 mM NaCl; pH 7.5) for 5 min and incubated with 5% (w/v) dried fat-free milk diluted in TBS for 60 min. The step of incubation with milk, or blocking, is important to prevent primary and secondary antibodies from unspecific binding. After the blocking the membrane was washed in TBST (0.1% (v/v) detergent Tween-20 in TBS) twice for 10 min. The membrane was prepared for the immunodetection with antibodies.

Table 4. Solutions for Western Blot technique.

	Solution
Blotting buffer I	0.3 M Tris, 10% (v/v) methanol; pH 10.4
Blotting buffer II	25 mM Tris, 10% (v/v) methanol; pH 9.0
Blotting buffer III	38 mM Tris, 10% (v/v) methanol, 10 mM glycine; pH 8.5
TBS	150 mM Tris-HCl, 10 mM NaCl; pH 7.5
TBST	0.1% (v/v) detergent Tween-20 in TBS

Table 5. List of primary and secondary antibodies.
Mo – mouse, Rb – rabbit, M – monoclonal, P – polyclonal

Protein specificity	***Dilution***	***Type***	***Catalogue number***	***Provider***
		Primary antibodies		
F_1-α	1:1000	Mo/P	-	Moradi-Ameli and Godinot, 1983
F_1-γ	1:1000	Rb/P	GTX114275	GeneTex (USA)
F_1-δ	1:1000	Rb/P	GTX101503	GeneTex (USA)
F_1-ε	1:1000	Mo/M	H00000514-M01	Abnova (Taiwan)
F_o-c	1:1000	Rb/P	ab180919	Abcam (UK)
actin	1:60000	Mo/M	MAB1501	Merck Millipore (USA)
NDUFA9	1:1000	Mo/M	Ab14713	Abcam (UK)
SDHA	1:10000	Mo/M	ab14715	Abcam (UK)
core2	1:1000	Mo/M	Ab14745	Abcam (UK)

COX4	1:1000	Rb/P	11463-1-AP	Proteintech Group (USA)
IF_1	1:1000	Mo/M	ab110277	Abcam (UK)
6xHis-tag	1:500	Mo/M	MA1-135	Thermo Fisher Scientific (USA)
GST-tag	1:1000	Mo/M	MA4-004	Thermo Fisher Scientific (USA)

Secondary antibodies

	Dilution	***Detection wavelenght***	***Provider***
Alexa Fluor 680: donkey anti-mouse, donkey anti-rabbit IgG	1:3000	700 nm	Thermo Fisher Scientific (USA)
IRDye 800CW: donkey anti-rabbit, anti-mouse IgG	1:15000	800 nm	LI-COR (USA)

3.2.1.3.3 Native electrophoresis

The pellets of isolated mitochondria were resuspended in solubilization buffer A (50mM NaCl, 50mM imidazole/HCl, 2 mM 6-aminocaproic acid, 1mM EDTA; pH 7.0) to the final protein concentration of 8 mg/mL. Appropriate volume of 20% n-dodecyl-β-maltoside (DDM) (Merck Millipore, USA) or was added to the samples to final concentration of 2 mg of DDM per 1 mg of protein for solubilization for 15 min on ice. After solubilization, the samples were centrifugated for 20 min at 30 000 g, 4 ºC. The pellets were removed and the supernatants were transferred into new sterile tube. The volume of the supernatant and its protein concentration was measured. The 50% (v/v) glycerol in the volume of 5 µL was added to the samples. Sample buffer containing CBB (5% w/v of CBB in 5 mM 6-aminocaproic acid) was added to the samples so that the final ratio of the DDM and CBB in the samples was 1:8.

The gradient of the gel used for BN-PAGE was 4-8% (Mini-PROTEAN III, Bio-Rad Laboratories, USA). The gel was prepared\the mixing of gels was performed via peristaltic pump (Cole-Parmer Instruments, USA) (table 6). After the pumping, the gel was overlaid with water. The water was removed, when the gel was polymerized and solidified, and 3.5% Stacking gel was loaded with following insertion of a comb.

Table 6. Stacking and Separating gel solutions for BN-PAGE.

	Stacking gel 3.5% [mL]	***Separating gel 4% [mL]***	***Separating gel 13% [mL]***
	5 mL	*5 mL*	*5 mL*
AB[1]	0.37	0.42	1.3
3×GB[2]	1.67	1.67	1.67
Glycerol 99%	0	0	1
dH_2O	2.83	2.89	1
APS[3]	41.7 µL	27 µL	25 µL
TEMED[4]	4.17 µL	2.7 µL	2.5 µL

[1]AB - 48% (wt.) acrylamide, 1.5% (wt.) *N,N'*-methylenebis(acrylamide)

[2]3xGB – gel buffer – 75 mM imidazole, 1.5 mM 6-aminocaproic acid, pH 7.0

[3]APS – 10% (wt.) ammonium persulfate

[4]TEMED - *N,N,N',N'*-tetramethylethylenediamine

Electrophoresis was performed at 4 ºC under the constant voltage of 45 V until the samples migrated across the boundary between the stacking and the gradient gels. After that the voltage was increased up to 120 V. Anode buffer (25 mM imidazole; pH 7.0) for BN-PAGE was poured into the chamber and cathode buffer B (50 mM Tricine, 7.5 mM imidazole, 0.02% (w/v) CBB; pH 7.0) was poured into the space between glasses. When the samples crossed the boundary of the gels, the cathode buffer B was replaced with cathode buffer B/10 (50 mM Tricine, 7.5 mM imidazole, 0.002% (w/v) CBB; pH 7.0). The NativeMark Unstained Protein Standard (Thermo Fisher Scientific, USA) was used as size protein standard.

3.2.1.4 Cellular respiration

We can choose between two key types of measurements, depending on the respiration we would like to study. Respiration of the intact cells or *in vivo* respiration corresponds to the physiological state of routine cellular activity, when cells respire on endogenous substrates. Respiration of the permeabilized cells allows analysis of of OXPHOS pathway. After the cytoplasmic membrane permeabilization, all endogenous substrates are dissolved in the medium inside the chamber. Composition of the assay medium (80 mM KCl, 10 mM Tris-HCl, 3 mM MgCl2, 1 mM EDTA, 5 mM KH2PO4, pH 7.3) simulates physiological conditions of intracellular environment. To modulate and study respiratory capacities of the electron transport chain or the individual complexes with the mentioned adjustment, the system is supplemented with saturating concentrations of substrates and inhibitors (Gnaiger, 2014).

The combination of substrates was used to saturate the OXPHOS and determine the capacities of enzymatic complexes,. Maximal flux (and thus, ETC capacity) was gained under conditions, when the respiration is not limited by the coupled phosphorylation. This effect/status is reached by inhibition of ATP synthase f.e. with oligomycin and the following uncoupling of oxidative phosphorylation via f.e. FCCP uncoupler (carbonilcyanide p-triflouromethoxyphenylhydrazone). The uncoupler is a protonophore, the proton translocator that moves H^+ across the membrane. The series of inhibitors (figure 8) were applied to gradually inhibit the individual complexes of ETC and measure the capacity.

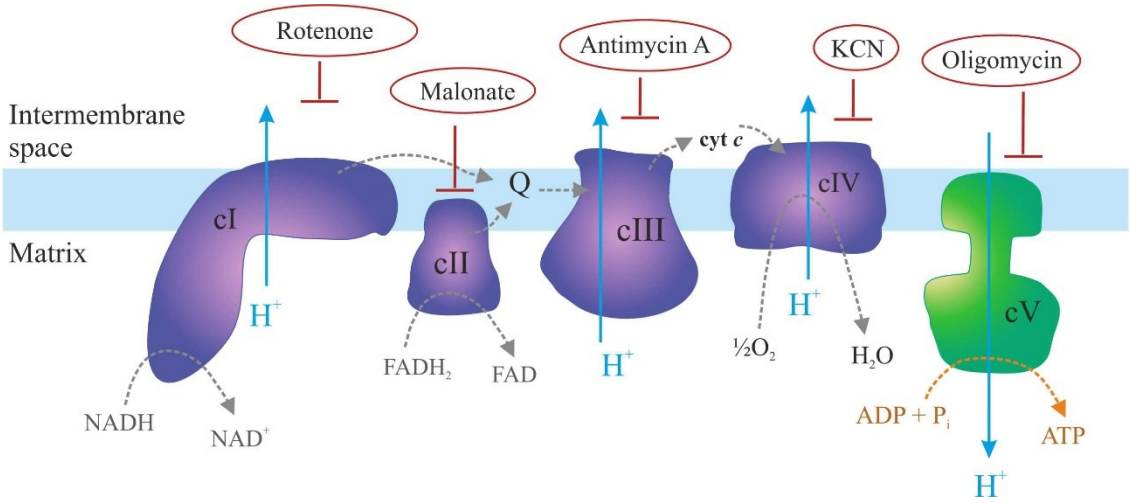

Figure 8. Selected inhibitors of individual complexes of oxidative phosphorylation apparatus.

Each inhibitor is specific to enzymatic complex. Rotenone binds to the binding site for the coenzyme Q and inhibit electron transfer. Malonate is a competitive inhibitor of cII. Antimycin A similar as Rotenone, binds to the binding site for the ubiquinone and blocks e^- transfer in cIII. KCN is a competitive inhibitor of cIV. Oligomycin blocks the proton channel, that is essential for the ATP synthesis.

The substrates and inhibitors were injected via Hamilton syringes (Hamilton, USA), when the signal for respiration was stabilized (during the steady states). For this experiment only two cell lines were used: the HEK293 control cells and HEK293 knock-down clone with the lest ATP-synthase residual content of 15 %. The measurement was performed in glass chambers with the volume of 2 mL at 30 °C under continual stirring at 750 rpm. The cells were harvested as described in the section 3.2.2.1, cultivation of cell lines. The concentration of protein in a sample was calculated and the sample was added into the chamber to the final concentration of 0.4 mg/mL. In the beginning of the experiments, the cells were permeabilized by digitonin (concentration and volumes of substrates and inhibitors are in the table 7).

Respiration is then calculated as time negative derivation of oxygen concentration ("$J_{V,O2}$" [$pmol \cdot s^{-1} \cdot cm^{-3}$]) (Gnaiger 2008). Graphic and numerous data record of the

measurements are saved and analyzed on DatLab5 software (OROBOROS INSTRUMENTS, Innsbruck, Austria).

Table 7. Substrates and inhibitors applied in the measurement of the respiration on Oxygraph.

REAGENT	STOCK CONCENTRATION	ADDED VOLUME	FINAL CONCENTRATION
DIGITONIN	20 mg/mL		0.5 mg/mg protein
PYRUVATE	1 M	20 µL	10 mM
MALATE	1 M	6 µL	3 mM
ADP	0.4 M	7.5 µL	1.5 mM
GLUTAMATE	1 M	20 µL	10 mM
SUCCINATE	1 M	20 µL	10 mM
A-GLYCEROL-3-PHOSPHATE	1 M	20 µL	10 mM
OLIGOMYCIN	1 mM	2 µL	1 µM
FCCP	0.1 mM	2 µL titration	200-300 nM
ROTENONE	1 mM	2 µL	1 µM
MALONATE	1 M	20 µL	10 mM
ANTIMYCIN A	1 mM	1 µL	0.5 µM
ASCORBATE	0.8 M	5 µL	2 mM
TMPD	0.2 M	6 µL	0.6 mM
KCN	0.5 M	2 µL	0.5 mM

3.2.1.5 Cell Viability

Cell Viability of the HEK293 knockdown and control cell lines was performed with CellTiter-Blue® assay kit (Promega, USA). This kit is based on the ability of viable cells to reduce the indicator dye (resazurin to resorufin) (figure 9).

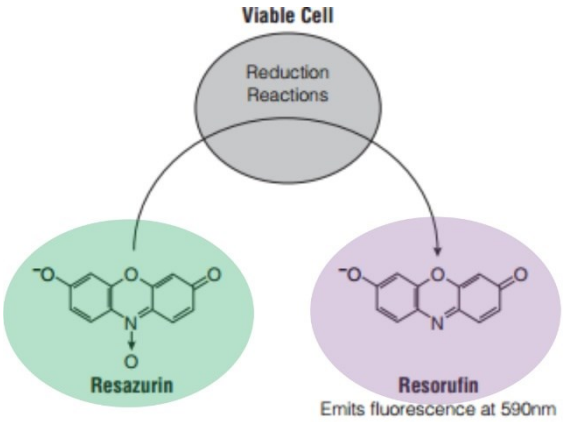

Figure 9. Scheme of CellTiter-Blue assay.

Viable, metabolically active cells converse resazurin to resorufin, as a result fluorescent product is generated. Produced fluorescence is proportional to the number of viable cells. Adapted from CellTiter-Blue assay kit (Promega, USA).

Cells were cultivated in six-well plates under the standard conditions (see cell cultivation paragraph) prior to experiment. At the day of experiment the medium in a cultivation dishes was sacked and cells were washed with PBS. 300 µL of T+E (0.05% trypsin + 0.02% EDTA in PBS) were added to the cells with following incubation for 3-5 min, 1700 µL of medium were then added to stop trypsinisation. The cells were then transferred to 1.5 mL sterile tubes and centrifugated at 4°C for 5 min and 600 *g*, supernatant was removed and pellets were resuspended in 500 µL DMEM medium (Dulbecco's Modified Eagles Medium) without glucose supplemented with 10% (v/v) αFBS (dialysed, filtered FBS, GIBco, Thermo Fisher Scientific, USA), 5 mM Pyruvate, 9 g/100 mL Galactose, 20 mM HEPES and antibiotics (penicillin (10 U/mL) and streptomycin (10 µg/mL). Cells were counted with Scepter (Millipore, USA): 10 µL of cell suspension were diluted in 90 µL PBS and counted according to manufacturer's instruction. After counting, cells in suspension were transferred to 96 well plates in ratio 40 000 cells per well and appropriate volume of the medium with galactose was added to the final 100 µL of suspension Plates were then placed to the tissue culture incubator at 37°C temperature and 5% CO_2 atmosphere and incubated for 2 hours. In the following step, the plates were removed from the incubator and 20 µL of CellTiter-Blue® Reagent were added to the cells, the plates were shacked for 10 sec and placed bake to the thermostat for incubation for 4 hours. The record of the fluorescence on the TECAN plate

reader (TECAN, Switzerland) at 560/590 nm was performed after the 1st, 2nd or 3rd hour of incubation with the CellTiter-Blue® Reagent. The plates were shacked for 10 sec prior to fluorescence recording. Calibration was prepared on the control cell line (0, 5, 10, 20, 40 and 60 $\cdot 10^3$ cells per each well).

3.2.2 Structural composition of ATP synthase.

3.2.2.1 Overexpression of IF_1 inhibitor protein

IF_1 protein possesses inhibitory sector in the N-terminal region of residues 1-60 and, thus, only this sequence was used to prepare the construct. The construct also contains a 14 AA passive linker followed by the C-terminal glutathione-S-transferase (GST) tag and Histidine tag (six histidines in sequence/in a row) (figure 4). Constructs are prepared as GeneStrings (Thermo Fisher Scientific, USA) and cloned into expression plasmid pET28b(+) (Merck Millipore, USA) through the *NcoI* and *XhoI* cloning sites (figure 10 and 11).

Figure 10. Scheme of the IF1 protein construct.

5′ GCTCAGTACCATGGGCTCGGACTCGTCGGAGAGCATGGATTCGGGCGCTGGCTCCA
TCCGAGAAGCTGGTGGGGCCTTCGGGAAACGAGAGAAGGCTGAAGAGGATCGGTACTT
CCGAGAGAAGACTAGAGAGCAGCTGGCTGCCTTGAAGAAGCACCATGAAGATGAGATT
GACCACCATTCGAAGGAGATAATCCGTCCGCGTGCGATCGGTGGTTCTAAACCGCGTG
TTGCGTCCCCTATACTAGGTTATTGGAAAATTAAGGGCCTTGTGCAACCCACTCGACT
TCTTTTGGAATATCTTGAAGAAAAATATGAAGAGCATTTGTATGAGCGCGATGAAGGT
GATAAATGGCGAAACAAAAAGTTTGAATTGGGTTTGGAGTTTCCCAATCTTCCTTATT
ATATTGATGGTGATGTTAAATTAACACAGTCTATGGCCATCATACGTTATATAGCTGA
CAAGCACAACATGTTGGGTGGTTGTCCAAAAGAGCGTGCAGAGATTTCAATGCTTGAA
GGAGCGGTTTTGGATATTAGATACGGTGTTTCGAGAATTGCATATAGTAAAGACTTTG
AAACTCTCAAAGTTGATTTTCTTAGCAAGCTACCTGAAATGCTGAAAATGTTCGAAGA
TCGTTTATGTCATAAAACATATTTAAATGGTGATCATGTAACCCATCCTGACTTCATG
TTGTATGACGCTCTTGATGTTGTTTTATACATGGACCCAATGTGCCTGGATGCGTTCC
CAAAATTAGTTTGTTTTAAAAAACGTATTGAAGCTATCCCACAAATTGATAAGTACTT
GAAATCCAGCAAGTATATAGCATGGCCTTTGCAGGGCTGGCAAGCCACGTTTGGTGGT
GGCGACCATCCTCCAAAATCGGATCTGGTTCCCTCGAGCGGTCACC 3′

Figure 11. The DNA sequence of the rat IF_1 fragment.

GCTCAGTA at the 5'end and CGGTCACC at the 3'prime end are the overhangs (stiffers). CCATGG is the NcoI sequence (including the ATGG sequence of the IF_1) and CTCGAG is the XhoI sequence. The sequence in blue is the IF_1 protein. The 14AA residue in green is the passive linker and the sequence in black is the GST-tag.

3.2.2.2 Molecular cloning

In order to clone the IF_1 DNA fragment into the pET28b(+) plasmid, the bacterial vector for expression of proteins. pET28b(+) contain 6xHis-tag, the IF_1 DNA fragment is cloned through the *NcoI* and *XhoI* cloning sites and is expressed under the T7 promoter (figure 12). The expression is controlled by the T7*lac* promoter (Dubendorf and Studier, 1991). IPTG, Isopropyl β-D-1-thiogalactopyranoside, when added to bacteria, inhibits the Lac repressor and, thus induces expression of the T7 RNA polymerase, which induce the expression of the gene of interest from T7 promoter. pET28b(+) plasmid possesses gene for Kanamycin resistance, which is used as a selection marker of amplified plasmid.

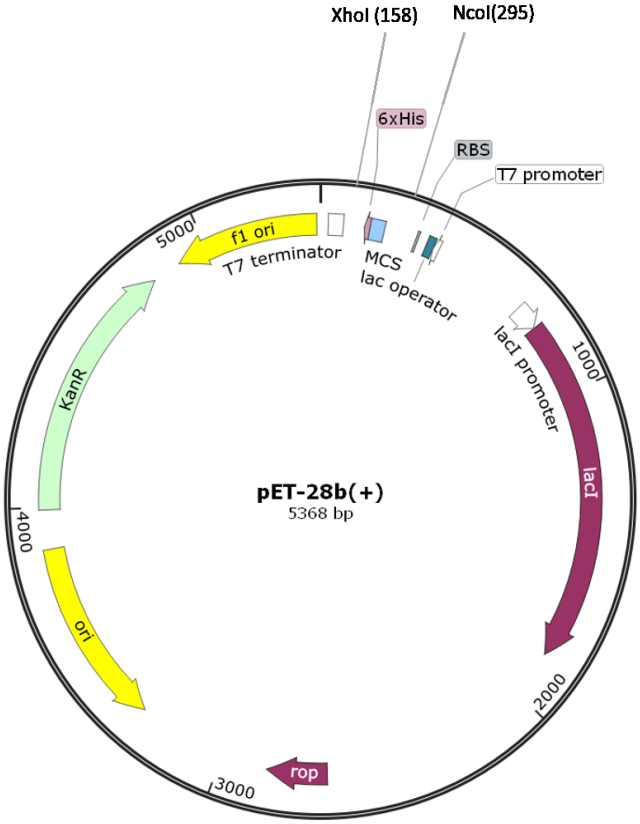

Figure 12. Map of the pET28b(+) plasmid.

Scheme of the chosen features in the pET28b(+) plasmid. The IF_1 fragment is inserted into the plasmid at the NcoI and XhoI sites. KanR anR s. I hoIresistense gene. The figure was produced with SnapGene Viewer.

The IF_1 fragment and pET28b(+) plasmid were firstly subjected to restriction. The procedure is processed by the restriction endonucleases (RE), enzymes that cut the DNA at the specific recognition site (or in its proximity). The RE introduce blunt or sticky ends, the latter creating 5' or 3' nucleotide overhangs The fragment and the vector, should both be treated with two RE to create compatible ends for cloning.

In this work, *NcoI* and *XhoI* RE (New England Biolabs, USA) were chosen for restriction. Double digestion (system with two RE in one mixture, table 8) was performed on both the IF_1 fragment and pET28b(+) plasmid. Concentrations of the DNA sequences were estimated on NanoDrop Spectrophotometer ND-1000 (Thermofisher, USA) as absorbance at 260 and 280 nm. Appropriate amount of the plasmid or fragment was pipetted into the sterile tubes, following by addition of the RE (*NcoI* or *XhoI* or both), NEB3.1 10x buffer (New England Biolabs, USA) and PCR water (free from nucleic acids contamination and exonucleases, Merck Millipore, USA) according to the table 7. The reactions were performed at 37 °C for 1 hour, then reactions were stopped by 20 min incubation at 65 °C. The digest of the plasmid was then subjected to 1% agarose gel electrophoresis and gel extraction (QIAuick gel extraction kit, QIAGEN, USA), whereas the digest of the IF_1 was purified using QIAquick PCR Purification kit (QIAGEN, USA). Concentrations of the obtained DNA were then measured at Nanodrop.

3.2.2.3 Agarose gel electrophoresis

Agarose gel electrophoresis was applied to verify correctness of molecular cloning. Concentration of agarose for gel was 1%, agarose was dissolved in TBE buffer (Tris-borate-EDTA, 89 mM Tris-borate and 2 mM EDTA, pH 8.3). Agarose gel electrophoresis was conducted/ran at constant voltage 5-10 V/cm.

Table 8. Double digestion: reaction components.

Three tables for double digestion of the plasmid or IF_1 fragment. 10x or 1x means dilution. The 'U' stands for unit.

DOUBLE DIGESTION

	Total volume 30 µl		
SAMPLE	**Initial conc/amount**	**Volume, µl**	**Final conc./amount**
pET28b(+)	854.9 ng/µl	1.2	1026 ng
NEB3.1 10x buffer	10x	3	1x
NcoI	10U/µl	1.5	15U
XhoI	20U/µl	0.75	15U
PCR H_2O		23.6	

DOUBLE DIGESTION

	Total volume 30 µl

SAMPLE	Initial conc/amount	Volume, µl	Final conc./amount
rat IF_1	18 ng/µl	13.9	250 ng
NEB3.1 10 buffer	10x	3	1x
NcoI	10U/µl	1	10U
XhoI	20U/µl	0.5	10U
PCR H_2O		11.6	

3.2.2.4 Cultivation and recombinant protein expression

The IF_1 fragment and pET28b(+) plasmid after restriction were subjected to ligation with T4 DNA Ligase (New England Biolabs, USA). All the components were calculated/added according to the table 9. Mixture containing all the components was incubated at 16 °C over night. The reaction was stopped by the heat inactivation at 65 °C for 10 minutes.

Table 9. Components of the ligation reaction.

Molar ratio of 1:3 plasmid to insert was applied in the reaction. 50 ng of the plasmid and 26 ng of fragment were used for the ligation.

	Rat IF_1 (894 bp)
COMPONENT	**Volume, µL**
T4 DNA LIGASE BUFFER 10X	2
pET28b(+) plasmid (5227 bp)	2.94
Insert DNA (IF_1 fragment)	4.25
Nuclease-free water	9.81
T4 DNA ligase	1

The mixture was then transformed into the *E.coli* DH5α competent cells (Thermo Fisher Scientific, USA) for the amplification of the plasmid. The procedure was performed on ice. An aliquot of 50 µL DH5α cells was thawed, 2 µL of the ligated DNA (30 ng) was pipetted into the cell mixture with following incubation on ice for 30 min. After the incubation, the cells were subjected to heat shock at 42 °C for 10 sec and placed on ice for 5 min. SOC medium (Thermo Fisher Scientific, USA) in the volume of 400 µL was added into the tubes, that were then placed in incubator shaker at 350 rpm, 37 °C for 60 min. In the next step, bacterial cultures were spread onto selection plates (LB medium

with 1.5% agarose) containing kanamycin (30 µg/mL, Merck Millipore, USA) and incubated overnight at 37 °C.

Chosen colonies were pinned from the plates and transferred into the 14 mL falcons with 3 mL LB medium containing kanamycin (50 µg/mL). These starter cultures were placed in incubator shaker at 250 rpm and cultivated/growing overnight at 37 °C. In the morning starters were stored at 4 °C until evening, when 50 µL of starter was inoculated into 50 mL LB medium (with kanamycin, 50 µg/mL). The overnight cultivation/growth was performed under identical conditions. The next morning plasmid was isolated from DH5α bacterial cultures via NucleoBond Xtra kit (Macherey-Nagel, Germany). Concentration of the DNA was then measured using Nanodrop.

Plasmid isolated from DH5α bacterial cultures was transformed into the *E.coli* BL21(DE3) (Thermo Fisher Scientific, USA) competent cells for the expression of IF_1 recombinant protein. The procedure was performed on ice. An aliquot of 20 µL BL21(DE3) cells was thawed, 2 µL of the ligated DNA (40 ng) was pipetted into the cell mixture with following incubation on ice for 30 min. After the incubation, the cells were subjected to heat shock at 42°C for 10 sec and placed on ice for 5 min. SOC medium (Thermo Fisher Scientific, USA) in the volume of 200 µL was added into the tubes, that were then placed in incubator shaker at 350 rpm, 37 °C for 60 min. In the next step, bacterial cultures were spread onto selection plates (LB medium with 1.5% agarose) containing kanamycin (30 µg/mL) and incubated overnight at 37 °C. Growing/culturing of starter cultures from the colonies was perform under(with) the same protocol as it has been described for DH5α cells.

3.2.2.5 IF_1 recombinant protein purification

Starter cultures from the BL21(DE3) cells were prepared according to the above-mentioned protocol for DH5α cells. In order to choose clone that produce the high amount of the expressed protein, plus/minus IPTG induction experiment was performed. Four starter cultures (3 mL volume each) were cultivated overnight. From each starter 500 µL were stored at 4 °C, next 500 µL were stored at -80 °C as glycerol stocks (1:1 (v/v) ratio 80% (v/v) glycerol to bacterial culture) and 2 mL were used for +/- experiment. One mL from each starter was cultivated 3 hours at 37 °C without addition of IPTG and one mL from each starter was cultivated with addition of 1.2 mM IPTG. After that bacterial cultures were centrifuged 10 min at 4 °C, 3000 g speed, supernatant was removed and pellets were resuspended in 50 µL PBS (with 10 mM $MgCl_2$ and 10U Benzonase nuclease, Merck Millipore, USA). The samples were sonicated in water bath for 5 min at RT and lysed with SLB 4. The samples were analysed on SDS-page electrophoresis,

one gel was subjected to staining. Incubation for 1 hour in staining solution (50% methanol, 10% acetic acid, 0.1% Coomassie Brilliant Blue R-250, dH_2O) with following overnight incubation in destaining solution (40% methanol, 10% acetic acid, dH_2O). The second identical gel was subjected to WB and immunodetection (6x-His Epitope Tag Antibody, cat.# MA1-135, Mo/M, 1:500 dilution). One clone expressing high amount of the recombinant protein was selected from the 4 starter cultures for following cultivation and purification.

When the optimal starter culture was selected (S5), the next step was the optimization of the IPTG concentration for induction of protein expression. Following concentrations were tested: 0.75; 1.0; 1.2 and 1.5 mM. The samples were analysed on SDS-page electrophoresis as was described in previous paragraph. I have also performed optimization of the expression duration time and temperature: combinations of 3, 4, 6 hours or overnight (16-18 hrs) induction times at 18, 25, 30 or 37 °C were tested. The samples were analysed on SDS-page electrophoresis as was described in previous paragraph. When the optimal conditions were selected, batch purification method was performed.

The culture of selected starter (S6) for the batch purification was cultivated in either 50 or 100 mL of LB medium. Bacterial culture was centrifuged 10 min at 4 °C, 3000 g speed, supernatant was removed and pellet was washed in the buffer A (0.1 M NaCl, 20 mM Tris-HCl, 25 mM imidazole, 10% (v/v) glycerol, pH 7.4) with following cycle of centrifugation. After the second centrifugation, the pellet was incubated for 10 min in 2.5 mL buffer A^s supplemented with Benzonase (518U) and protease inhibitor cocktail, PIC (Merck Millipore, USA), then the pellet was resuspended, transferred into the 5 mL tube and subjected to sonication to break the bacterial cells and extract the proteins. In order to follow the processing of the expressed protein during purification and preparational steps, 50 µL of sample was transferred into new tube at each step for following SDS-page analysis. To receive advanced cell lysis, sample was frizzed for 10 min at -20 °C and thawed at RT, the process was repeated three times before the sonication procedure. After cycles of freezing, sample was sonicated with microsond K76 for 1 min with pulsation (1 sec on, 1 sec off) at 60 % amplitude in the ultrasonic homogenizer BANDELIN SONOPULS (BANDELIN electronic GmbH, Germany). This cycle was repeated 5 times with 1 min pause between sonication cycles. All the sonication steps were repeated three times (15 cycles of sonication in total). Sonicated sample was centrifugated for 20 min at 4 °C, 5000 g speed, supernatant was transferred into new tube and subjected to the next cycle of centrifugation for 20 min at 4 °C, 30000 g speed, whereas the pellet was resuspended with 2.5 mL of buffer A^s. After the second

cycle of centrifugation, supernatant was again transferred into new tube, pellet was resuspended in 2.5 mL of buffer A^s and all the samples were stored at -80 °C until assayed.

Batch purification was performed in 1.5 mL tubes. Ni-NTA Agarose/ HisPur™ Ni-NTA Resin (Thermo Fisher Scientific, USA) was applied in the purification. Resin slurry in the volume of 200 µL was transferred into the tube and centrifuged for 1 min at 2700 RPM, supernatant was removed and the resin was washed 2 times with 200 µL of Binding buffer A (0.1 M NaCl, 20 mM Tris-HCl, 25 mM imidazole, 10% (v/v) glycerol, pH 7.4). Cell lysate in the volume of 500 µL was pipetted into the 1.5 mL tube containing washed resin. The tube was incubated for 15 min at 4 °C on rotating platform. Then the mixture was centrifuged for 1 min at 2700 RPM, supernatant was stored as flow-through (FT) fraction. The resin was washed 3 times with 300 µL of Binding buffer A. In the next step the protein was eluted in three steps with increasing concentration of imidazole in the elution buffers (up to 500 mM). After each elution, the supernatant was transferred into new 1.5 mL tube. Different imidazole concentrations were applied during the optimization: 50, 75, 100, 300 or 500 mM. After elution process, the resin remaining in the tube was incubated with SLB, centrifuged and supernatant together with all the SDS-samples collected from every step were subjected to SDS-PAGE electrophoresis, separated proteins were either Coomassie-Blue stained or transferred onto PVDF membrane to perform immunodetection.

3.2.2.6 Large-scale purifiction of IF_1 by FPLC chromatography on column

Purification of rat IF_1 construct was performed on FPLC system with 5 mL HisTrap HP column (GE Healthcare, USA). Selected starter S6 was cultivated in 7 L of LB medium. Bacterial culture was centrifuged 10 min at 4°C, 3000 g speed, supernatant was removed and pellet was resuspended with Buffer A (0.1 M NaCl, 20 mM Tris-HCl, 25 mM imidazole, 10% (v/v) glycerol, pH 7.4), resuspended pellets were pooled and conducted to second cycle of centrifugation (washing step). Then the pellet was resuspended in 60 mL of buffer A supplemented with Benzonase, Lysozyme (100 µg/mL), and protease inhibitor cocktail, PIC (Merck Millipore, USA). Suspension was sonicated for 15 min with 3 sec on/17 sec off pulsation (overall duration is approximately 100 min), amplitude 55, power 50-55 Wt at 4°C. Sonicated sample was filtered through the sterile filter, 0.22 µm (Millipore, Germany). During the sonication, FPLC system together with the HisTrap column were prepared for the purification. FPLC buffer inlets, pumps, HisTrap column and injection loop were washed with filtered distilled water to remove 20% ethanol used as preservative for the FPLC system when not in use, then the FPLC system was washed with Buffer A (0.1 M NaCl, 20 mM Tris-HCl, 25 mM

imidazole, 10% (v/v) glycerol, pH 7.4) at the flow rate of 2 mL/min. When the record of Absorbance showed to constant (at approximately 20-25 mL of buffer flow), filtered sample was injected into the loop at the 0,5 mL/min flow rate. In the next step, Buffer B (0.1 M NaCl, 20 mM Tris-HCl, 500 mM imidazole, 10% (v/v) glycerol, pH 7.4) was introduced into the system and gradient of 0-100% of Buffer B was applied. Flow rate changed to 1 mL/min and collecting of fractions (1.5 mL volume each) had started. After 20 min, when concentration of Buffer B in the system attained 100%, purification was finished.

Eluted fractions were then subjected to concentrating with following dialysis. Optimal fractions, containing (higher) quantities of purified rat IF_1 protein, were pooled and concentrated in Centrifugal Filter Units 4 mL, 3 kDa MWCO (Millipore, Germany) (by the manufacturer's instruction: 45 min centrifugation at 10°C, 3000 g). Then concentrated fractions were dialyzed with Spectra/Por, 1 mL, 3.5-5 kDa MWCO (Repligen, USA) into 20 mM Tris-HCl, pH 7.4, 10% glycerol: 3 hours in 500 mL and then overnight in 1000 mL, at 4°C.

3.2.2.7 ATPase hydrolytic activity

The hydrolytic activity was measured with or without complex V inhibitor, oligomycin to detect the sensible fraction of ATP synthase (figure 13). The Pullman assay was performed on isolated liver mitochondria from spontaneously hypertensive rat (SHR) rat strain. The mitochondria were isolated by differential centrifugation as described in (Pecinová *et al.*, 2011). In brief, minced liver tissue was homogenized with teflon-glass homogenizer Heidolph RZR 2041 (Heidolph Instruments, Germany), the entire process was carried out on ice or at 4 °C. 10% homogenate was filtered through a polyamide screen and centrifuged at low speed, 600 g for 10 min. Pellet containing nuclei was discarded, supernatant was collected and then centrifuged at high speed, 10000 g for 10 min. Postmitochondrial supernatant was disposed and pellet of crude mitochondria was resuspended in STE medium (0.32M sucrose, 10 mM Tris–HCl, 1 mM EDTA, pH 7.4) and again centrifuged at high speed. The final pellet was resuspended in STE medium, aliquoted and stored at -80 °C.

An aliquot of pellet of isolated liver mitochondria was resuspended at protein concentration of 9-11 mg/ml in 10 mL of 20 mM Tris-HCl, pH 8.0, 10% (v/v) glycerol and 500x diluted PIC. The resuspended mitochondria were then solubilized with 1% (w/v) DDM on ice for 30 min. The sample was then centrifuged for 20 min at 4 °C, 10000 rpm speed. Supernatant was collected and prepared for the measurement of ATPase hydrolytic activity. 5 µL of sample were mixed in the cuvette with 495 µL of 5 mM Tris-

HCl, pH 8.0. The reaction was started with addition of 500 µL of mixture (75 mM Tris-HCl, 10 mM MgCl2, 20 mM KCl, 0.2 mM NADH, 0.4 mM 2-phosphoenolpyruvate, 0.5 mM ATP, 0.2 % BSA, 1 mM FCCP, 2 µM antimycin A, 1 µM rotenone, 8 U/ml lactate dehydrogenase + 8 U/ml pyruvate kinase (Merck Millipore, USA)]. Each measurement was performed for 3 min at 37 °C. To measure the inhibitor-sensitive part of ATPase activity, 3 µM of oligomycin was added to the cuvette with all described constituents. The IF_1 construct purified with His-tag in previous step was then applied in the Pullman ATPase assay to determine the amount of protein required for the inhibition of the complex V in the sample of isolated liver mitochondria. 2.8 mg of the IF_1 construct was mixed with the 10 mL of the sample and 40 µL of MgATP (200 mM ATP, 400 mM $MgSO_4$, pH 8.0) was added twice in 5 min interval. The ATPase hydrolytic activity was determined 10-15 min after the addition of the IF_1 construct. When the ATP synthase was inhibited by IF_1 to approximately the same level as with oligomycin, the sample containing mixture of ATP synthase and IF_1 construct was then purified using GST-tag.

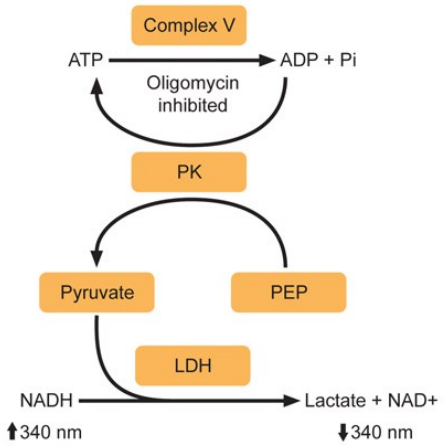

Figure 13. Scheme of the ATPase hydrolytic activity coupled assay.

During the assay decrease of A_{340} representing an oxidation of NADH is measured. PK – pyruvate kinase, PEP – 2-phosphoenolpyruvate, LDH – lactate dehydrogenase. Adapted and adjusted from manual to Mitochondrial Complex V Activity Assay Kit (Merck Millipore, USA).

3.2.2.8 Small-scale affinity purification of ATP synthase

Batch purification was performed in 5 mL tube. Glutathione Sepharose 4B (GE Healthcare, USA) was applied in the purification. Resin slurry in the volume of 1000 µL was transferred into the tube and centrifuged for 5 min at 500 g, supernatant was removed and the resin was washed 3 times with 4 mL of Equilibration buffer (20 mM Tris–HCl, pH 7.3, 0.1% DDM, 10% glycerol, 0.15 M NaCl and 5 mM dithiothreitol). Solubilized rat liver mitochondria mixed with purified IF1 construct in the volume of 2 mL was pipetted into the 5 mL tube containing washed resin. The tube with mixture was incubated for 1 hour at RT on rotating platform. Then the mixture was centrifuged for 5

min at 500 g, supernatant was stored as flow-through (FT) fraction. The resin was washed 2 times with 4 mL of Equilibration buffer and once with 1 mL of Wash and Elution buffer (20 mM Tris– HCl pH 7.3, 0.1% DDM, 10% glycerol and 10 mM EDTA). Supernatants ("wash" fractions) were stored for SDS-PAGE analysis. Both Equilibration and Wash and Elution buffers contained mixture of phospholipids: 50 µg/mL of POPC, 25 µg/mL of POPE, 20 µg/mL of CL and 5 µg/mL of POPG (POPC - 1-palmitoyl-2-oleoyl-sn-glycero-3-phosphocholine, POPE - 1-palmitoyl-2-oleoyl-sn-glycero-3-phosphoethanolamine, POPG - 1-palmitoyl-2-oleoyl-sn-glycero-3-[phospho-rac-(1-glycerol)], CL – cardiolipin, Merck Millipore, USA). In the next step the protein was eluted in three steps. The first elution was performed by addition of 1 mL of Wash and Elution buffer and incubating the mixture 2 hours at RT with following centrifugation for 5 min at 500 g. The second elution was performed with overnight incubation with Wash and Elution buffer. After each elution step, the supernatant was transferred into new 1,5 mL tube. For the third elution step 1 mL of Elution buffer (50 mM Tris-HCl, 10 mM reduced glutathione, pH 8.0) was added to resin, after 5 minutes the mixture was centrifuged for 5 min at 500 g. After elution process, the resin remaining in the tube was incubated with SLB, centrifuged and supernatant together with all the SDS-samples collected from every step were subjected to SDS-PAGE electrophoresis with following WB and immunodetection and Coomassie Blue R-250 staining.

4 Results

4.1.1 Functional consequences of ATP synthase deficiencies

In the first part of my master thesis, I focussed on the characterisation of the range of clones with knockdowns of the ATP synthase central stalk subunits. This work was part of the larger project, now submitted for publication (Nuskova *et al.*, 2018), looking into thresholds of various biochemical parameter required for pathological presentation of the defect. Control and knockdown (KD) lines were generated on HEK293 cell line by short hairpin RNA (shRNA) according to the article (Nuskova *et al.*, 2018). C 2-1, C 2-3, C 2-4 and C 2-7 are knockdown clones with decreased expression of γ subunit; D 4-1 and D 25-11 – δ subunit and E 2-5, E 4-2, E 5-4 – ε subunit.

4.1.1.1 ATP synthase subunits content

To characterize Content of ATP synthase in the HEK293 knockdown and control cell lines the electrophoretic analysis under denaturating conditions (SDS-PAGE) was performed. Sodium Dodecyl Sulphate (SDS) is an anionic detergent, that covers the intrinsic charges of proteins, and in the result, migrating proteins have the same charge and, therefore, are separated by their molecular mass (Reynolds and Tanford, 1970; Smith, 1984). SDS-PAGE based on Tricine-Tris buffer system is suitable for separating proteins in the mass range of 1-100 kDa (Schägger, 2006), which is optimal range to cover mass spectrum of ATP synthase subunits (5-55 kDa). Subunits of the Complex V have been visualized by Western Blot with immunodetection on PVDF membrane (figure 14 and 15).

As can be seen from the figure 14, content of the individual ATP synthase subunits was decreased in the KD clones comparing with control. Quantification of immunodetection showed that clone D 25-11 has the lowest relative subunits content showing 6.7 % of F_1-ε and 7.9 % of F_1-δ subunit relative to control (figure 14b). Clones D 4-1 and E 2-5, for example, represent slightly increased content of studied subunits when compared to controls (figure 14b). In contrast with other complex V subunits, the content of F_o-c subunit persists at control levels or is even mildly increased level in KD clones (figure 14c).

4.1.1.2 Respiratory chain complexes content

To quantify content of respiratory chain complexes (CI-CIV) and representative subunits for each RC complex in the set of clones, Tricine SDS-PAGE electrophoresis was used. RC complexes content varied among KD clones (figure 15). There was significantly increased content of subunit core2 of cIII in C 2-7, E 4-2 and both D clones.

Variability in the content of proteins NDUFA9, cI (C 2-1, C 2-3, C 2-4, D 25-11), Cox4, cIV (C 2-3, D 25-11, E 5-4) and F_1-α, cV (all clones except D 4-1 and E 2-5) between individual clones and control was in some cases significant.

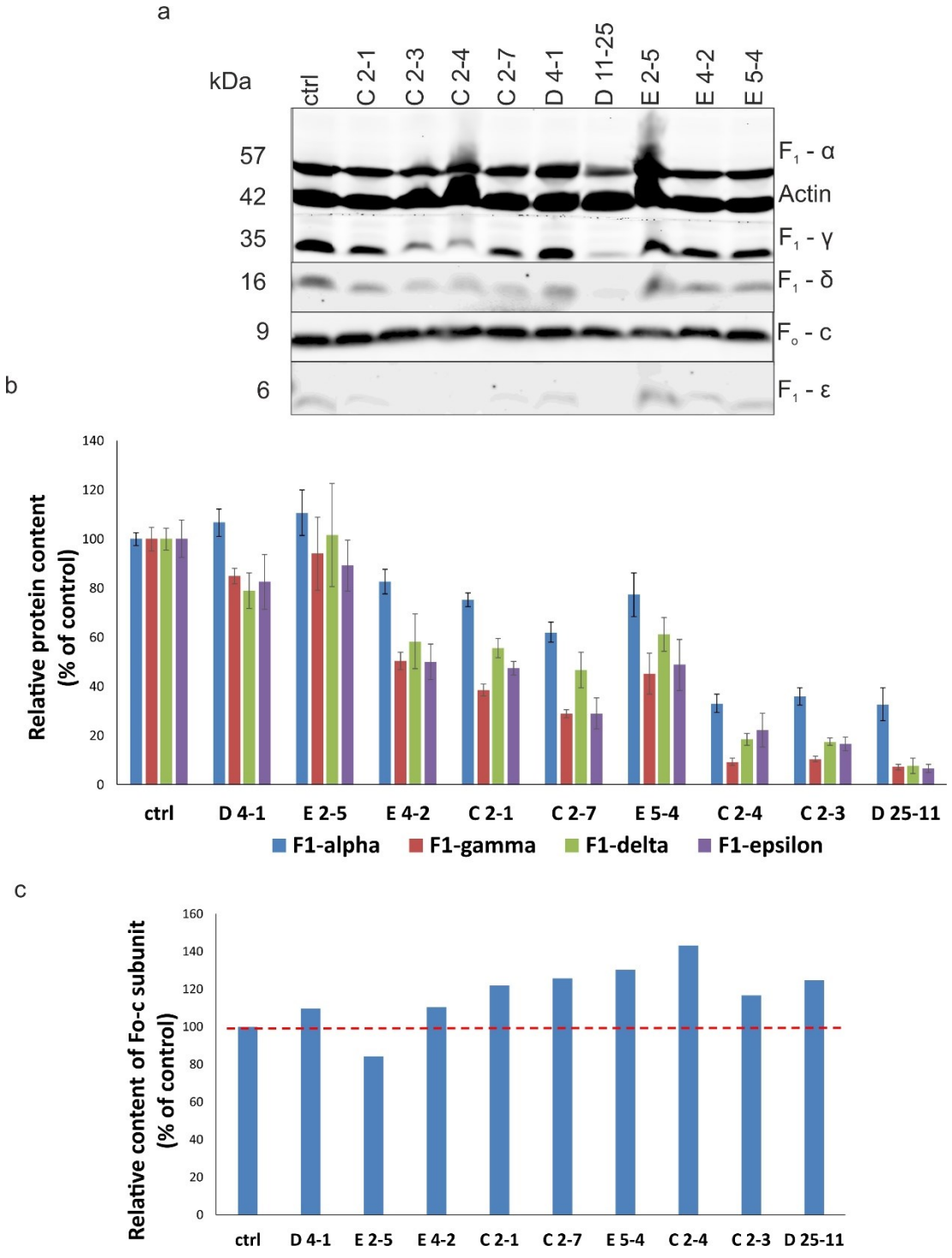

Figure 14. Representative immunodetection of ATP synthase subunits in KD and control cell lines.

Samples prepared from cell lysates, separated on SDS-PAGE electrophoresis (50 μg of protein per well) followed by Western Blot analysis. (a) Representation of the ATP synthase subunits. Actin served as loading control. (b, c) Relative protein content of individual ATP synthase subunits. (c) Red dash line marks the F_o-c subunit level in control (100 %). (a, b) Error bars represent SEM (n=4).

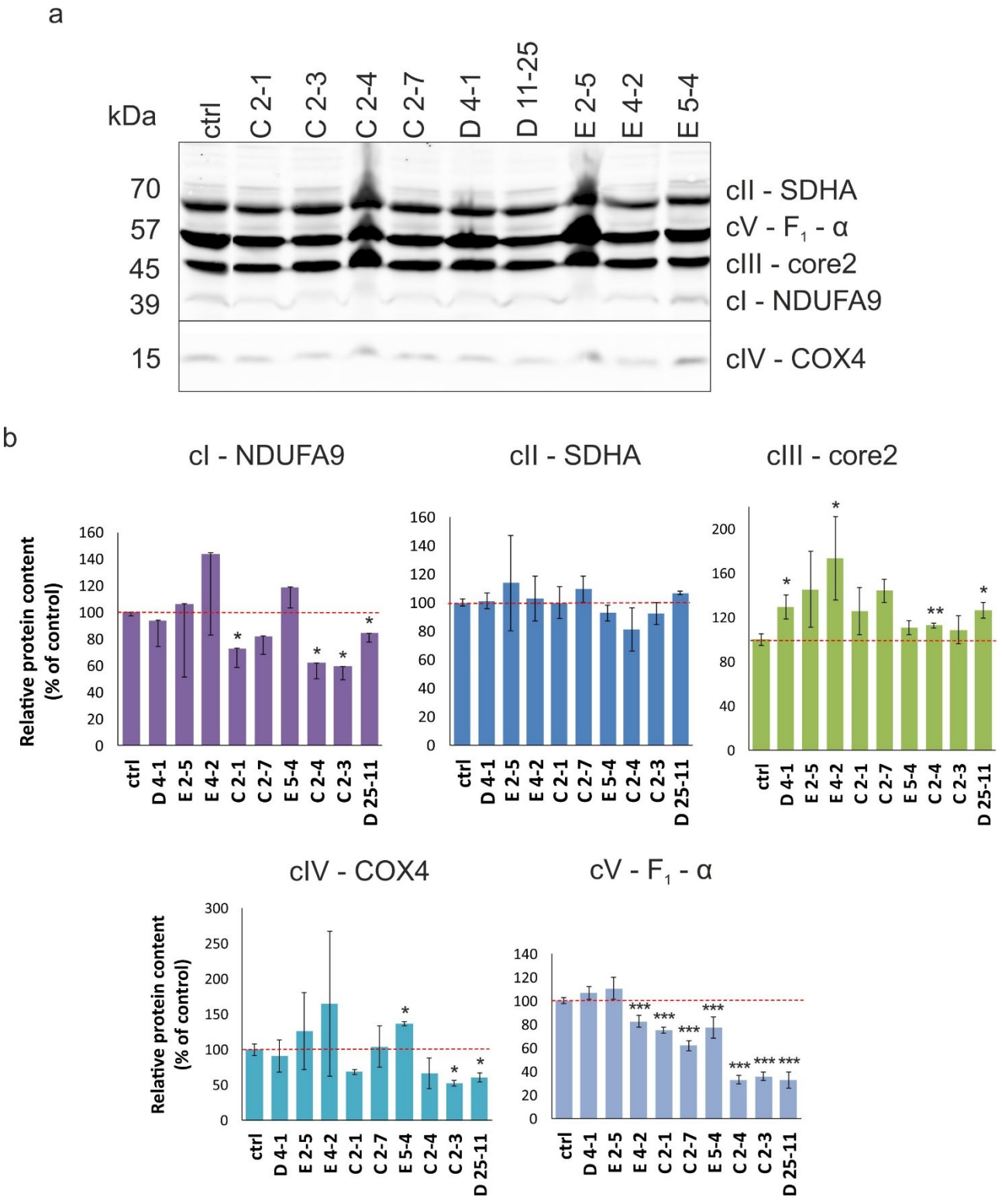

Figure 15. Representative immunodetection of subunits of OXPHOS complexes in KD and control cell lines.

Samples prepared from cell lysates, conducted to SDS-PAGE electrophoresis (50 μg of protein per well) with following Western Blot analysis. (a) Representation of selected subunits of OXPHOS complexes. (b) Relative protein content of selected subunits of OXPHOS complexes. Red dash line marks the individual subunit level in control (100 %) Error bars represent SEM (n=4 or n=2). Asterisks (*) represent p-value related to control: * for <0.05; ** for <0.01; *** for <0.001.

4.1.1.3 Assembled ATP synthase content

Blue-native PAGE electrophoresis was employed to determine the content of fully assembled ATP synthase. Using such electrophoresis, native conformation of particular proteins as well as protein complexes could be determined. The mobility of individual proteins thus depends on their charge to mass ratio and physical shape. The proteins also retain their enzymatic activity that could be measured in-gel after the electrophoresis. Samples are solubilized with non-ionic detergents, e.g. digitonin, dodecylmaltoside (DDM) or triton X-100. Dodecylmaltoside used in this case is a mild detergent that separates individual protein complexes, membranous hydrophobic proteins and oligomers into holoenzymes or monomers. (Wittig, Braun and Schägger, 2006).

To estimate the content and assembly state of ATP synthase in KD clones, BN-PAGE analysis and Western Blot were applied. Results on figure 3a demonstrate appearance of different assembly forms of complex V, with most prevalent form being monomers. In the control cells, however, we can still see remaining portion to ATP synthase to be present in dimers, even when DDM was used for solubilisation. Moreover, it is noticeable that content of assembled ATP synthase varies in KD clones (figure 16a, b) ranging from 15 % in case of D 25-11 to 90 % in case of E 2-5. In some clones there was also apparent a band with M_w of approximately 330-380 kDa, representing F_1 sub-complex (α subunit containing subcomplexes).

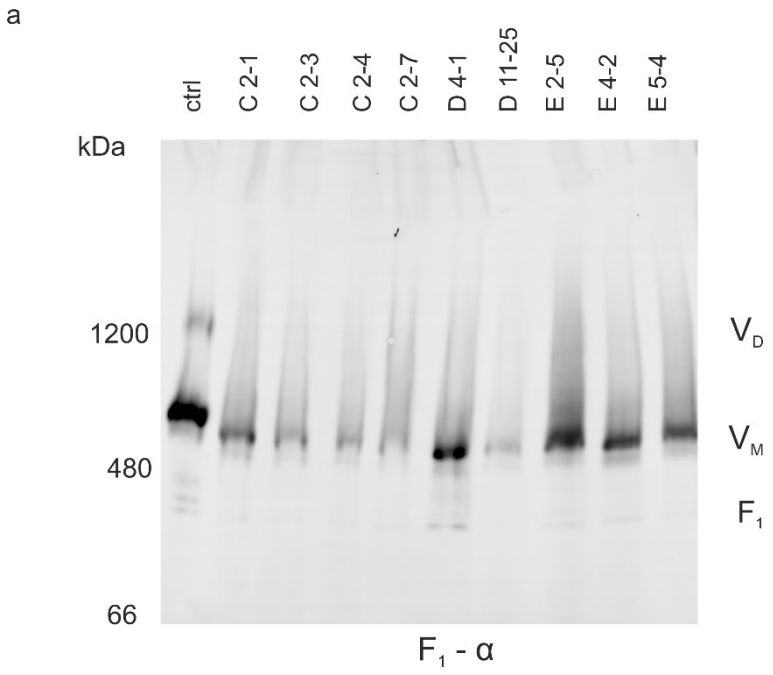

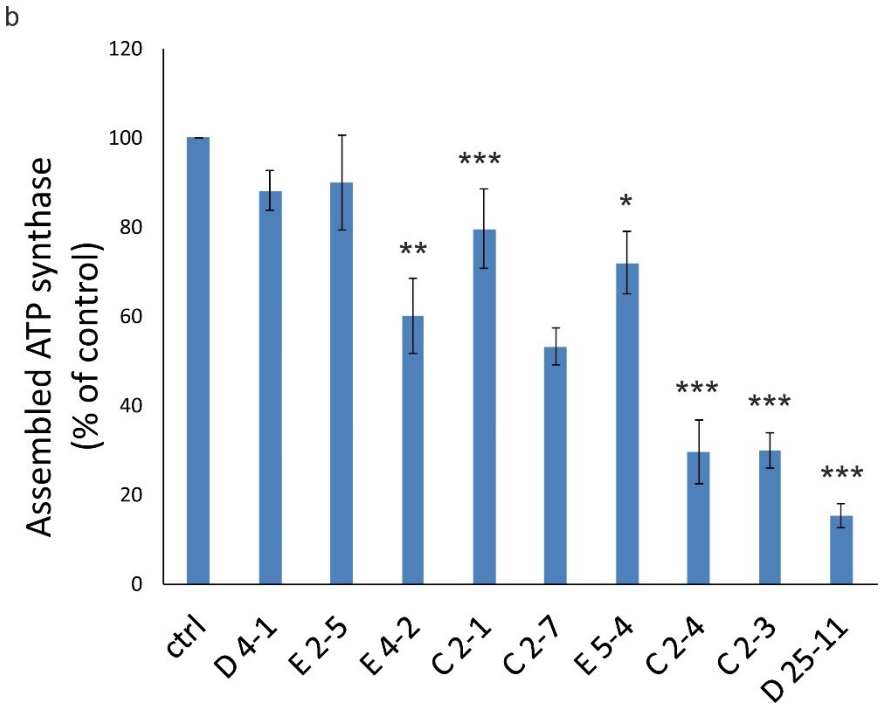

Figure 16. Immunodetection of ATP synthase assembly state in KD clones and control cell lines.

Samples prepared from isolated mitochondria, conducted to BN-PAGE electrophoresis (solubilisation with DDM, 50 μg of protein per well) with following Western Blot analysis. (a) Representative image of ATP synthase assembly forms detected with antibody against F_1-α subunit. V_D – dimer of complex V, V_M – monomer of complex V, F_1 – soluble portion of complex V. (b) Quantification of assembled ATP synthase (in form of monomer). Error bars represent SEM (n=4). Asterisks (*) represent p-value related to control: * for <0.05; ** for <0.01; *** for <0.001.

4.1.1.4 Biochemical characterization of knockdown clones

To perform analysis of OXPHOS function and explore capacities of individual OXPHOS complexes, we focused on comparison between control cell line and the most extreme, e.g. with lowest ATP synthase content clone D 25-11 (see section 4.1.1.3). Respiration was measured on permeabilized cells (figure 17) with the high resolution respirometry instrument, OROBOROS Oxygraph-2k (OROBOROS INSTRUMENTS, Innsbruck, Austria). The Oxygraph is highly precise and requires small amount of a sample. During the experiment, the sample is placed in a glass chamber filled with medium and the oxygen concentration is determined via polarographic oxygen sensor (POS) under continual stirring of sample. Clark-type POS possesses a platinum or golden cathode and an Ag/AgCl electrode.

As it can be seen, routine respiration (in intact cells) was decreased in D 25-11 compared to control (figure 17 and 18a). Then the system was saturated with pyruvate and malate

to observe complex I capacity. Addition of ADP stimulates complex V, facilitates utilization of $\Delta\psi_m$ and activates respiration. Glutamate works as an extra substrate for complex I. After that succinate and glycerol phosphate were added into the systems, introducing additional electron input into respiratory chain through their respective dehydrogenases (respiratory state 3, OXPHOS capacity). Higher rates of oxygen consumption in control are noticeable. When ETC was saturated with substrates, oligomycin was used to inhibit the ATP synthase and disable the proton translocation through the enzyme (state 4). Following titration with the FCCP uncoupler served to achieve maximal respiratory rate. After observation of ETC capacity, the individual complexes were inhibited by injection of rotenone (cI), rmalonate (cII) and antimycin A (cIII). To evaluate maximal capacity of complex IV addition of ascorbate and TMPD, artificial substrates feeding the electrons directly to cytochrome c/COX, was performed. Rates of respiration between control and D 25-11 clone are comparable. KCN introduces inhibition of cIV and KCN insensitive oxygen consumption subtracted as ascorbate and TMPD autooxidation.

Quantification of selected parameters indicated lower rate of Routine respiration in D 25-11 clone comparing with the control (figure 18a). OXPHOS capacity was found to be also decreased in selected clone. Leak state characterizes OXPHOS system coupling and indicates potential leakage of protons, but no difference was found between the samples. No significant dissimilarity was detected also for both ETC and COX capacities.

Data from the measurements were used to calculate respiratory control ratios (figure 5b). UCR - uncoupling control ratio - characterizes relation between OXPHOS and ETC capacities, the UCR is always greater than 1, higher values indicate presence of ATP synthase defect, this parameter was increased in D 25-11 from 1.8 to 2.7 RCI (ADP) - respiration control index after addition of ADP – describing the ration between saturated complex I and complex V activity after ADP injection. RCI (ADP) was significantly decreased in clone with ATP synthase deficiency from 2.4 to 1.8. The other one, RCI (oligo) index is ratio between OXPHOS capacity and Leak state, was also significantly decreased from 3.71 to 2.53 in D 25-11.

Ctrl

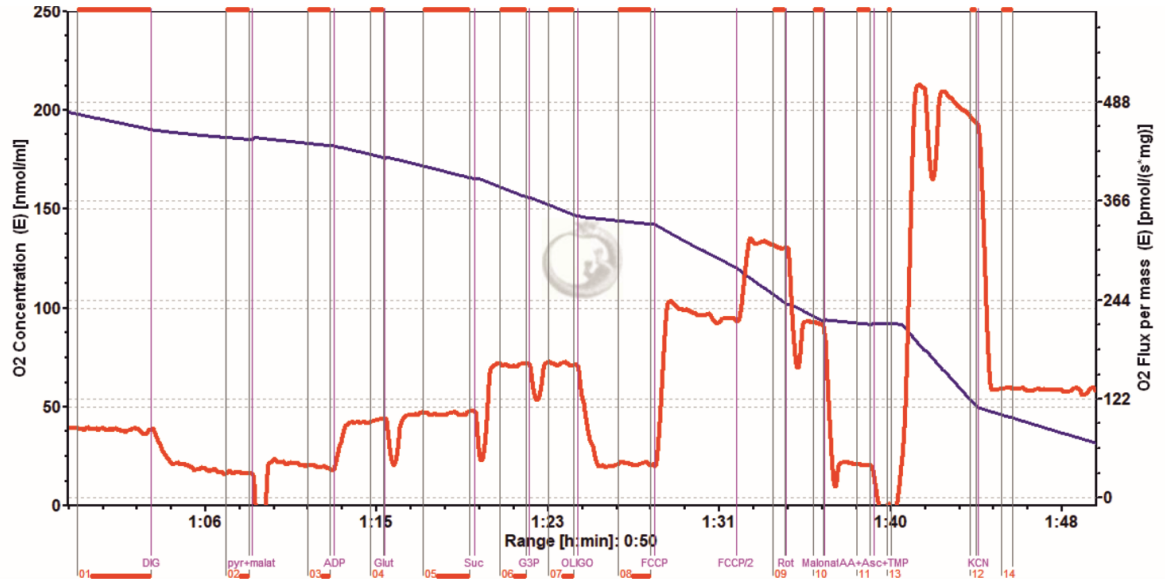

D 25-11

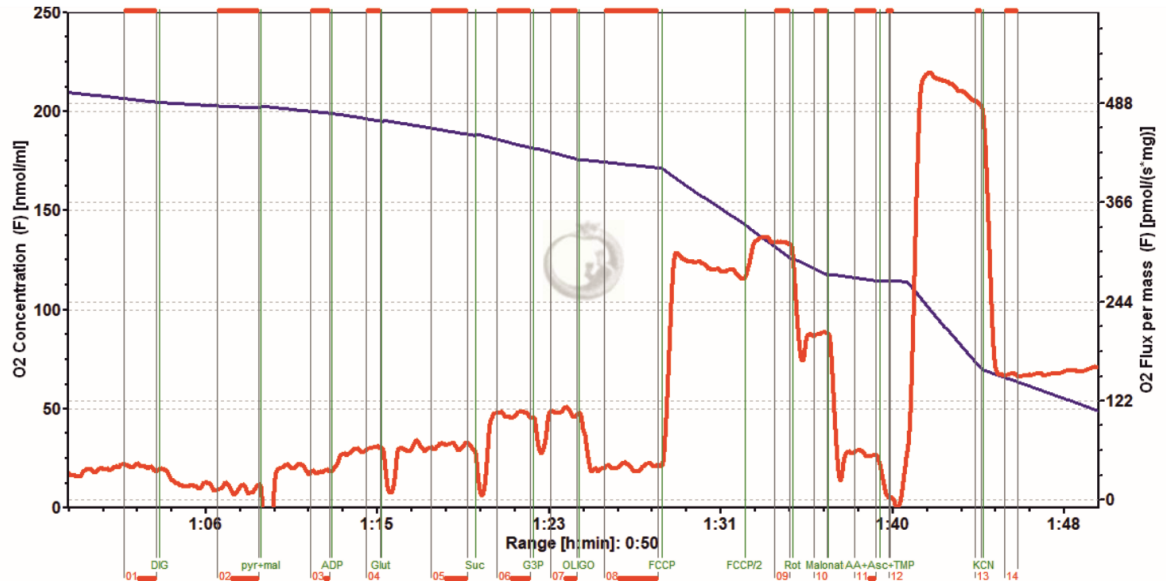

Figure 17. Representative record of measurement of respiration in D 25-11 KD clone and control cell line.

Respiration was measured on permeabilized cells, concentration of the sample inside the chamber was always 0.3 mg/mL. X axis – time range, left Y axis represent oxygen concentration inside chamber, right Y axis – respiration rate. Red line signifies respiration rate (right Y), blue line – oxygen consumption (left Y).

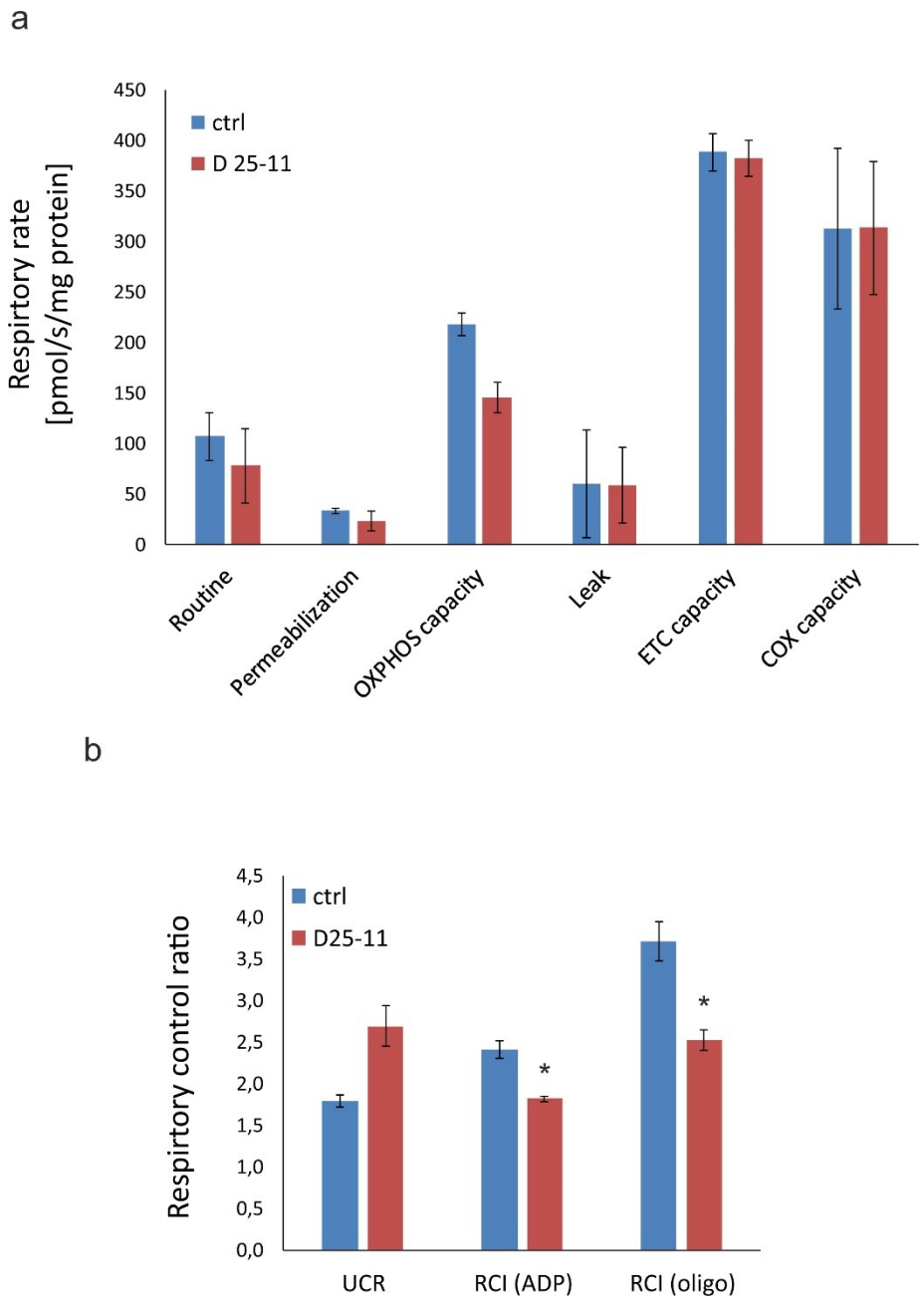

Figure 18. Quantification of respiration measurement and respiratory control ratios.

Representative parameters (a) and respiratory control ratios (b), values are mean of two measurements. Error bars represent SEM (n=2). Asterisks (*) represent p-value related to control: * for <0.05.

4.1.1.5 Cell viability

Given the observed differences in ATP synthase content and apparent dysfunction at the biochemical level, in the next experiment we asked, whether we can observe threshold for the cell viability connected with increasing ATP synthase deficiency. Measurement of cell viability was conducted using CellTiter-Blue® assay kit in all respective clones.

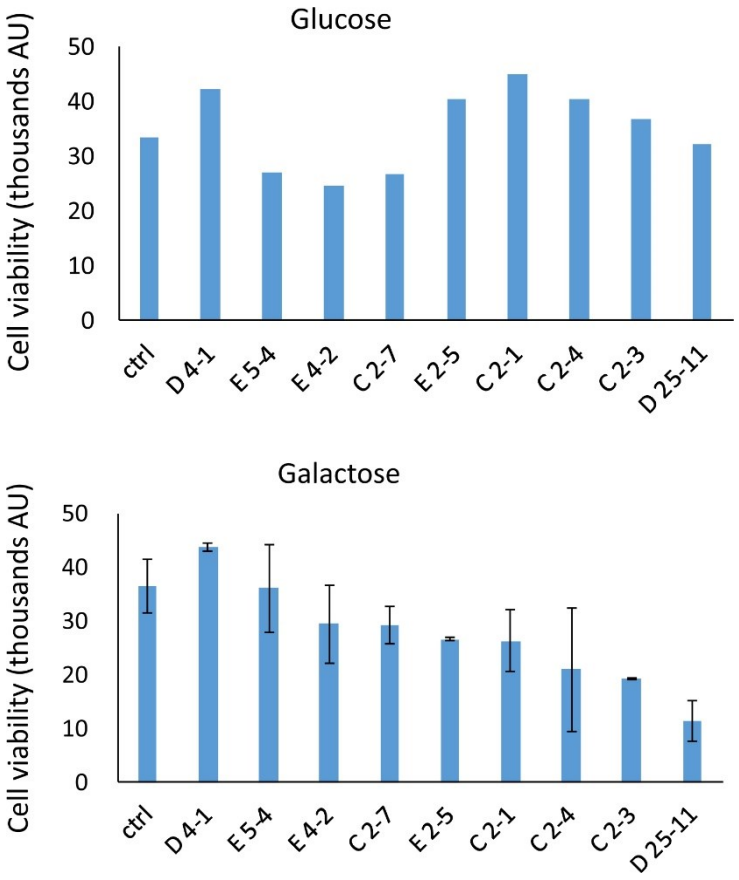

Figure 19. Cell viability measured in glucose rich or glucose free medium.

Error bars indicate the standard error of the mean (n=2). AU – Arbitrary Units, here fluorescence measured at 560/590 nm.

Measurement of cell viability in glucose-rich medium, used for routine cell culture, displayed inter individual differences among individual clones but no obvious trend related to ATP synthase content. However, this changed substantially once we started to cultivate individual clones in glucose-free medium supplemented with galactose and pyruvate. Individual clones responded differently to stress conditions of the experiment, with clone D 25-11 showing the lowest viability and clone D 4-1 exceeding the control (figure 19). When plotted against residual ATP synthase content, a logarithmic dependence is can be observed (figure 20). Calculated threshold for the cell viability

occurred at 52 % of residual ATP synthase content. The results suggest that cells with enzyme content reduced below 50 % are incapable of growth on galactose and, therefore, utilization of oxidative phosphorylation for energy production.

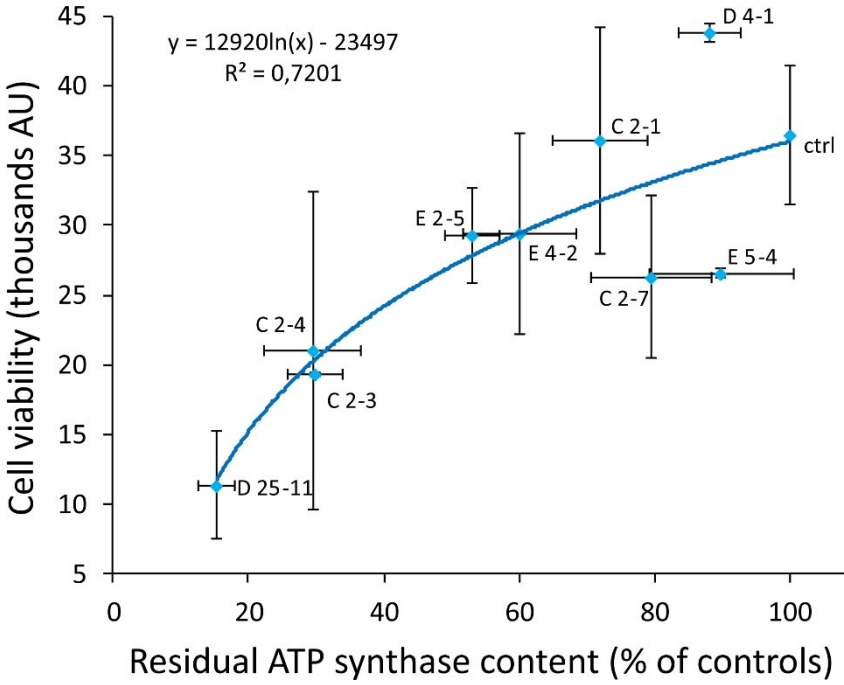

Figure 20. Cell viability in glucose free medium plotted against ATP synthase content.

Each dot in the plot represents one KD clone or control HEK293 cells. Error bars indicate the standard error of the mean (n=2 for the cell viability and n=4 for the enzyme content).
AU – Arbitrary Units, here fluorescence measured at 560/590 nm.

4.1.2 ATP synthase purification

In the second part of my thesis, I focused on development of method for affinity purification of mammalian F1Fo-ATP synthase, which would allow purifying both fully assembled enzyme as well as individual subcomplexes. Using this approach, one will be able to characterize in detail various ATP synthase subassemblies (as observed e.g. in clone D 4-1 in Fig 16a) and define individual steps of the holoenzyme assembly. For this purpose I decided to take advantage of the reversible binding of IF1 protein to the ATP synthase and use this feature for affinity enrichment of the enzyme. This approach was originally developed for the purification of bovine ATP synthase by Bason *et al.*, 2011 and my aim was to adapt it for the use in human and rodent models.

4.1.2.1 Molecular cloning

In order to apply the IF_1 protein for ATP-synthase purification, first it has to be cloned into the plasmid and expressed in bacteria as recombinant protein. The bacterial

system provides large enough quantity of expressed protein for the following application or analysis.

Construct containing sequence of rat IF_1 protein inhibitory domain (AAs 1-60 of the full length IF1), 14 AA linker, GST-tag and His-tag (figure 21) was cloned into expression plasmid pET28b(+) through the *NcoI* and *XhoI* cloning sites. Presence of two tags was dictated by the preffered buffer systems and purification conditions preffered either for (i) recombinant IF_1 construct purification from bacteria through His-tag or (ii) intact ATP synthase elution without release of purified IF_1 construct bound on sepharose GST beads though the GST-tag. Before molecular cloning, pET28b(+) plasmid was subjected to restriction digest with *NcoI* and *XhoI* restriction enzymes (figure 22), fragment of plasmid digested with both enzymes (double digest) was then applied to ligation with IF_1 construct/fragment and transformation into DH5α competent cells.

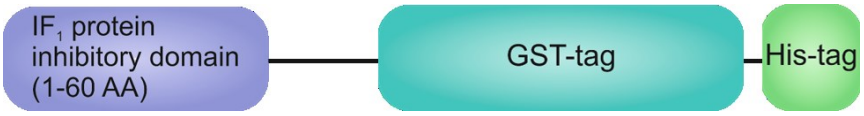

Figure 21. Scheme of recombinant IF1 protein construct.

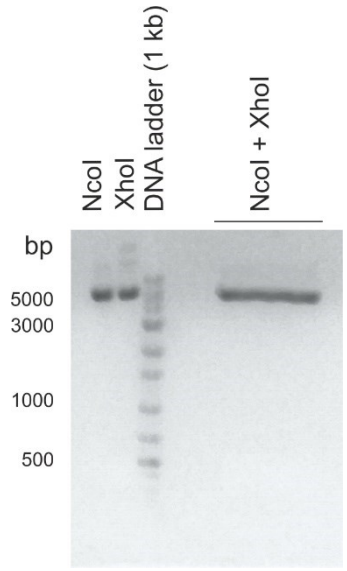

Figure 22. Agarose gel electrophoresis of pET28b(+) plasmid restriction digest with NcoI and XhoI RE.
NcoI + XhoI double digest generated a fragment for the following molecular cloning.

To verify efficacy of the cloning and transformation, DNA from *E.coli* DH5α cells was purified and subjected to restriction digest (figure 23). Not only single and double digest with *NcoI* and *XhoI* RE was performed, but also digest with different RE, *XbaI*. Plasmid without IF_1 construct has shorter length, which means that in case of a single

restriction, product would also have shorter length. This difference is noticeable when comparing pET28b(+) plasmid, plasmid with rat IF_1 construct after digestion with *XbaI*. Yet, double digestion with *NcoI* and *XhoI* should result in fragments with identical length in both samples (plasmid with and without rat construct), which is also apparent.

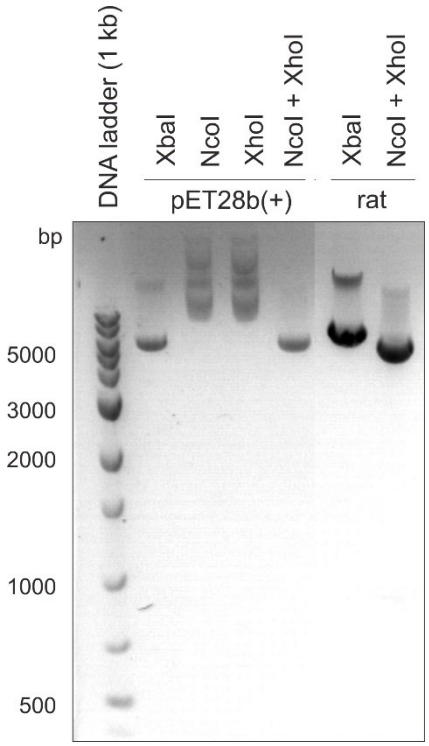

Figure 23. Control restriction digest of plasmid DNA purified from DH5α bacterial lysates.

Rat states isolated DNA containing cloned construct with rat IF_1 sequence. pET28b(+) denotes plasmid without insert.

After molecular cloning and transformation into DH5α bacterial cells, colonies carrying plasmid with rat IF_1 construct were subjected to DNA isolation and restriction analysis with *NcoI* and *XhoI* RE. DNA sequencing revealed no mutations (figure 24). DNA concentration of sample was high and also the purity was sufficient (ideal value for DNA is ~1.8).

Sample	ng/µL	260/280
rat IF1	505.85	1.89

Figure 24. Results of molecular cloning.

Representative fragment of sequenced DNA of sample with rat IF_1 and measurement of DNA concentration of samples. T7 terminator and pETup2 are names of primers for sequencing. Asterisk (*) marks positions which have a single, fully conserved residue, Concentration is expressed in ng/µL, 260/280 absorbance assess the purity of a sample.

4.1.2.2 Cultivation and protein expression

For the purpose of protein expression, plasmid DNA isolated form the DH5α bacterial cultures was transformed into the BL21(DE3) competent bacterial strain. As a first optimization step, +/- experiment on bacterial cultures testing the ability of IPTG to induce recombinant protein expression from the plasmid was performed (described in methods, section 3.2.2.4). Clone S6 showing high protein expression level was selected for further experiments (figure 25).

4.1.2.3 Finding optimal conditions for recombinant IF1 expression

When IF1 expressing sample was selected, work followed with optimization of cultivating conditions for protein expression. Three parameters were optimized: cultivating temperature, time of induction, and concentration of IPTG (figure 26). Results of this experiment demonstrated that higher amount of protein were expressed under conditions of induction at 37°C for 6 and 4 hours. Overnight induction at lower temperature (25°C) showed to be the least effective (figure 26a, b). Different

concentrations of IPTG displayed no distinct changes in the amount of expressed protein, though 1.5 mM IPTG appeared to be less efficient (figure 26c).

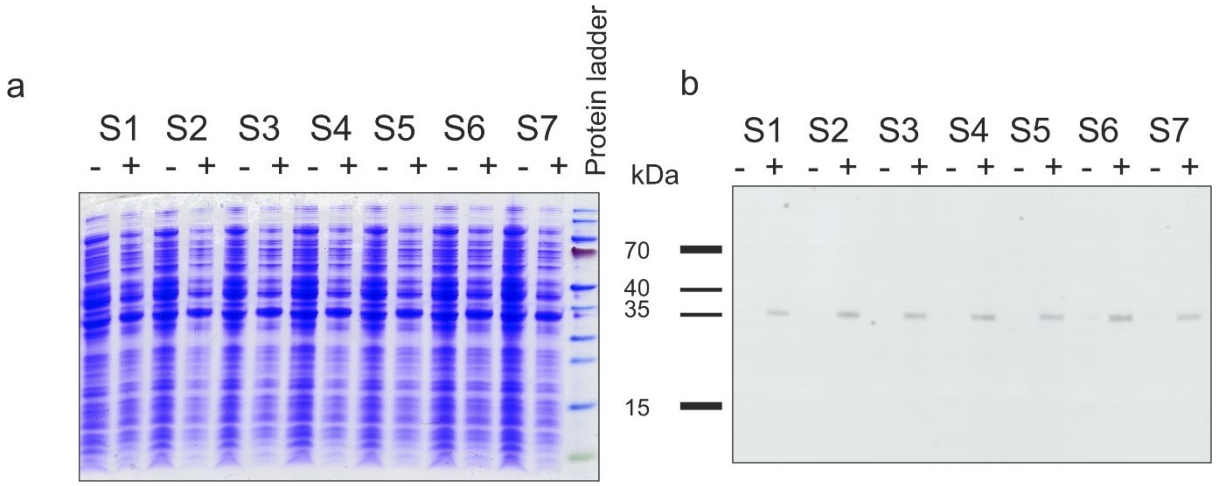

Figure 25. Results of +/- protein expression experiment in bacterial cultures.

(a) SDS-PAGE electrophoresis gel dyed with Comassie Blue. (b) Western Blot and immunodetection with antibody against His-tag. S1-S7 are samples; mark + or - means cultures induced or not induced with 1 mM IPTG. Samples were prepared from bacterial lysate and loaded in amount of 2 μL per well.

To prepare sample for the following purification, fractionation analysis was performed (figure 27). Cultivation at 37°C again proved optimal protein expression compared with 30°C. Sequence of IF_1 used for molecular cloning is expressed as soluble protein and neither the sequence itself nor His- or GST-tags should form aggregates, therefore expressed rat IF_1 construct should be present in a soluble fraction after centrifugation. However, it is apparent that even at high-speed centrifugation large amount of expressed protein remained as precipitate. The possible explanation can be long time of induction at 37°C, which forced bacterial culture to store higher amounts of expressed protein in inclusion bodies, as shorter induction time proved to be better and recombinant protein remained in sufficient quantity in supernatant (figure 27b).

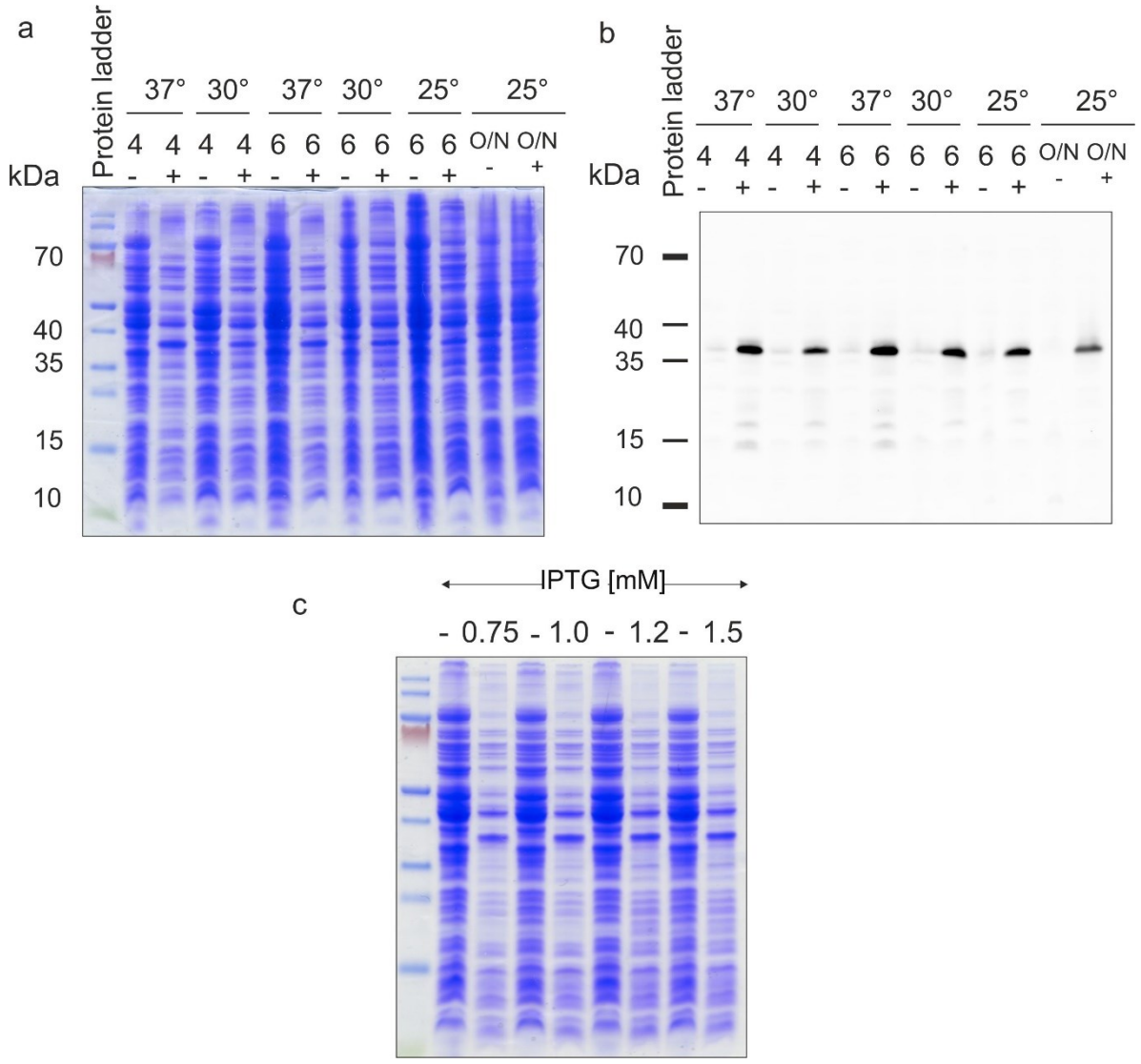

Figure 26. Optimization of protein expression in bacterial culture.

(a, c) SDS-PAGE electrophoresis gel dyed with Comassie Blue. (b) Western Blot and immunodetection with antibody against His-tag. (a, b) Samples marked + or - mean starter culture to be induced or not induced with 1 mM IPTG, (c) numbers mean induction with IPTG,"-" means no IPTG was added. (a, b) Numbers mean time of induction (in hours), O/N – overnight (16 hours). Samples were prepared from bacterial lysate and loaded in amount of 2 μL per well.

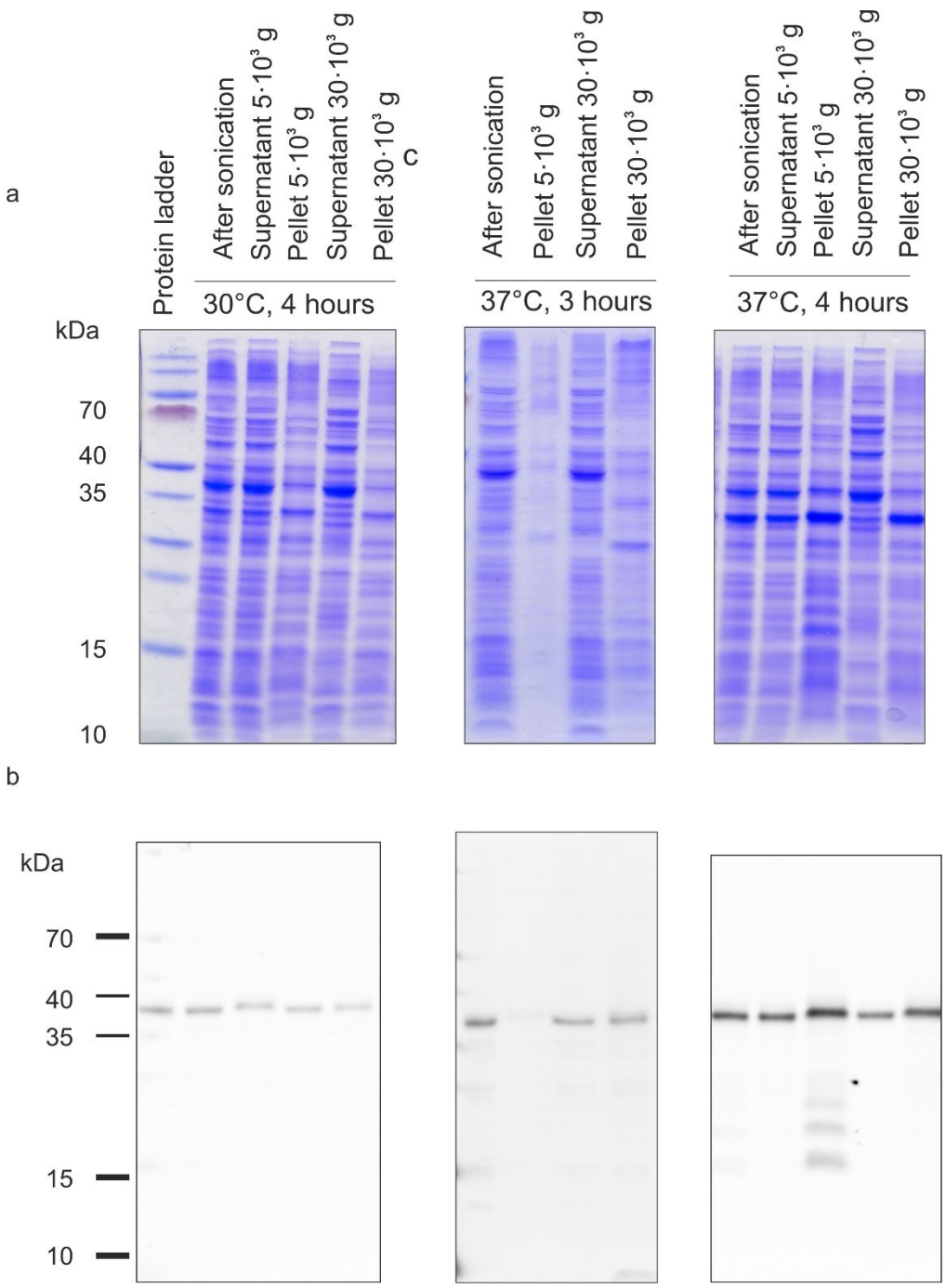

Figure 27. Fractionation analysis of bacterial lysate.

(a) SDS-PAGE electrophoresis gel dyed with Comassie Blue. (b) Western Blot and immunodetection with antibody against His-tag. Cultivation was performed at 30 or 37°C with induction for 4 or 3 hours. After sonication bacterial culture was centrifuged at $5 \cdot 10^3$ g, supernatant was then centrifuged at $30 \cdot 10^3$ g, this supernatant was then applied for purification. Samples were loaded in amount of 10 µg per well.

4.1.2.4 Small-scale IF_1 purification

Prior to purification on column (as described in methods section 3.2.2.5), I applied a small-scale batch purification (figure 28). It is apparent, that Flow through fraction contained extremely small amount of expressed protein. As long as this fraction is rinsed with washing buffer that has the same composition (primarily 25 mM imidazole) as resuspending buffer, rat IF_1 construct should be tightly bound to His-bind resin. Various concentrations of imidazole were utilized to identify an optimal range. The batch method does not allow to apply concentration gradient, as utilized on FPLC when using a column affinity chromatography. During the optimization of elution step in batch method both gradual and discontinuous elution was performed. The results form discontinuous elution are shown in figure 15a, b: sample was divided into the equal amounts; each of them was purified in one-step elution with respect to different imidazole concentration. It is noticeable that only 300 mM imidazole is able to elute expressed protein, though large amount of protein still remained bound to resin beads. In case of the gradual elution (figure 28c, b) one sample was eluted in three steps with increasing imidazole concentration. This type of elution is closer to the column purification. Here, rat IF_1 construct was eluted with higher efficiency compared with the discontinuous elution. In addition, there was a smaller amount of protein remaining on resin beads.

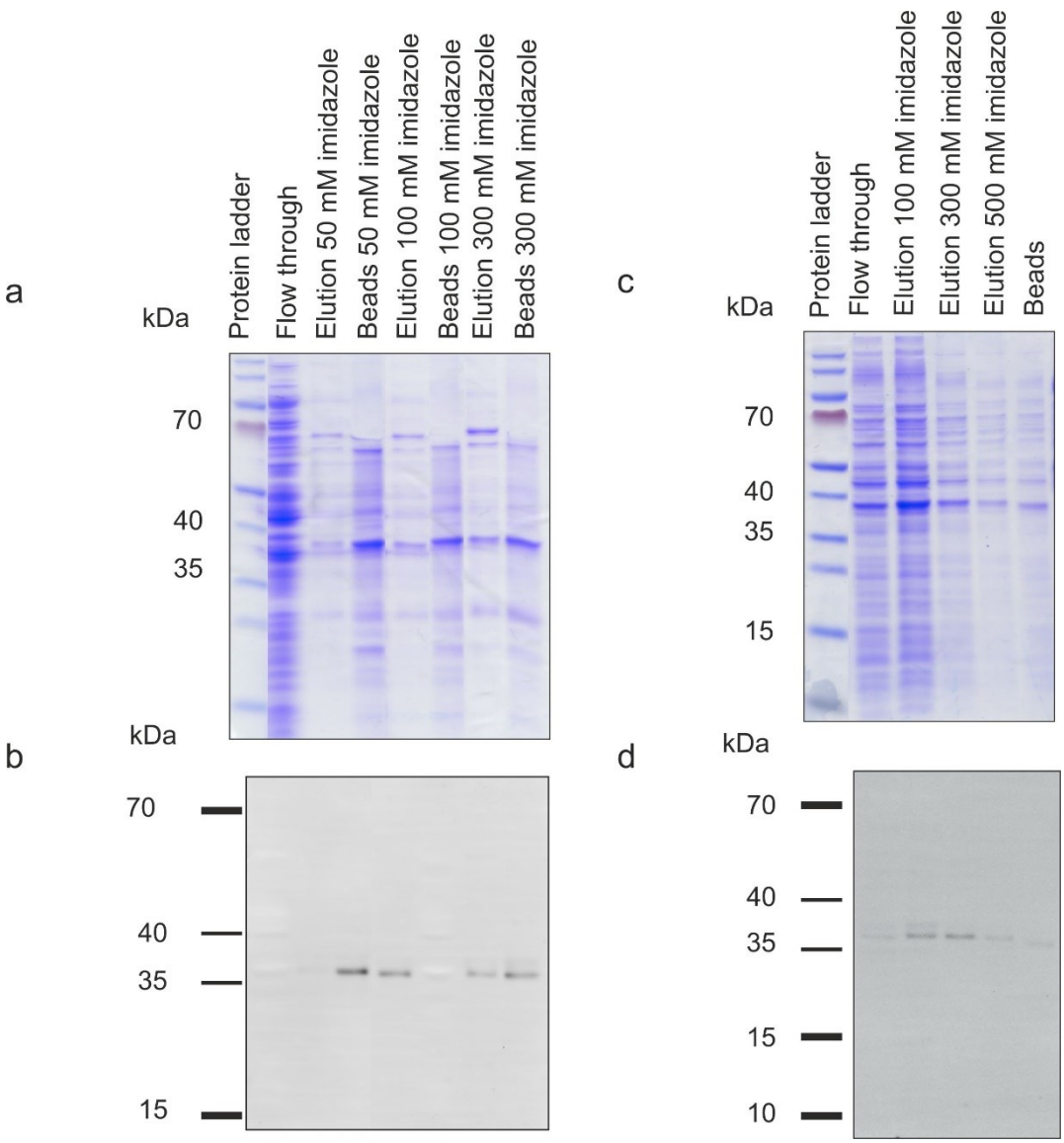

Figure28. Small-scale purification of rat IF_1 construct: optimization of elution step.

(a, c) SDS-PAGE electrophoresis gel dyed with Comassie Blue. (b, d) Western Blot and immunodetection with antibody against His-tag. Flow through – fraction rinsed after incubation of sample with the His-bind resin. Beads – fraction remained on His-bind resin beads after the last elution step. All samples except for the Flow through were loaded in amount of 10 µL per well, Flow through – 10 µg.

4.1.2.5 Large-scale IF_1 purification

When rat IF_1 construct purification through the His-tag was optimized at small-scale, I switched to column purification on FPLC (figure 29). The process of column purification is described in section 3.2.2.6. The chromatogram and SDS-PAGE electrophoresis indicated successful elution of expressed protein with 25 – 500 mM imidazole gradient. Peak of absorbance occurred at approximately 200-250 mM imidazole (figure 29a), which corresponds to rat IF_1 construct. Due to presence of

imidazole in the buffers and purified protein, eluted fractions were concentrated and desalted by dialysis (figure 29c). When comparing pattern of proteins in input and after dialysis it is apparent, that dialysis cleared sample from some proteins, but still even after dialysis concentrated eluted fractions contain unspecific proteins. By approximal calculation 5.6 mg of eluted protein was obtained from 7 L of bacterial culture.

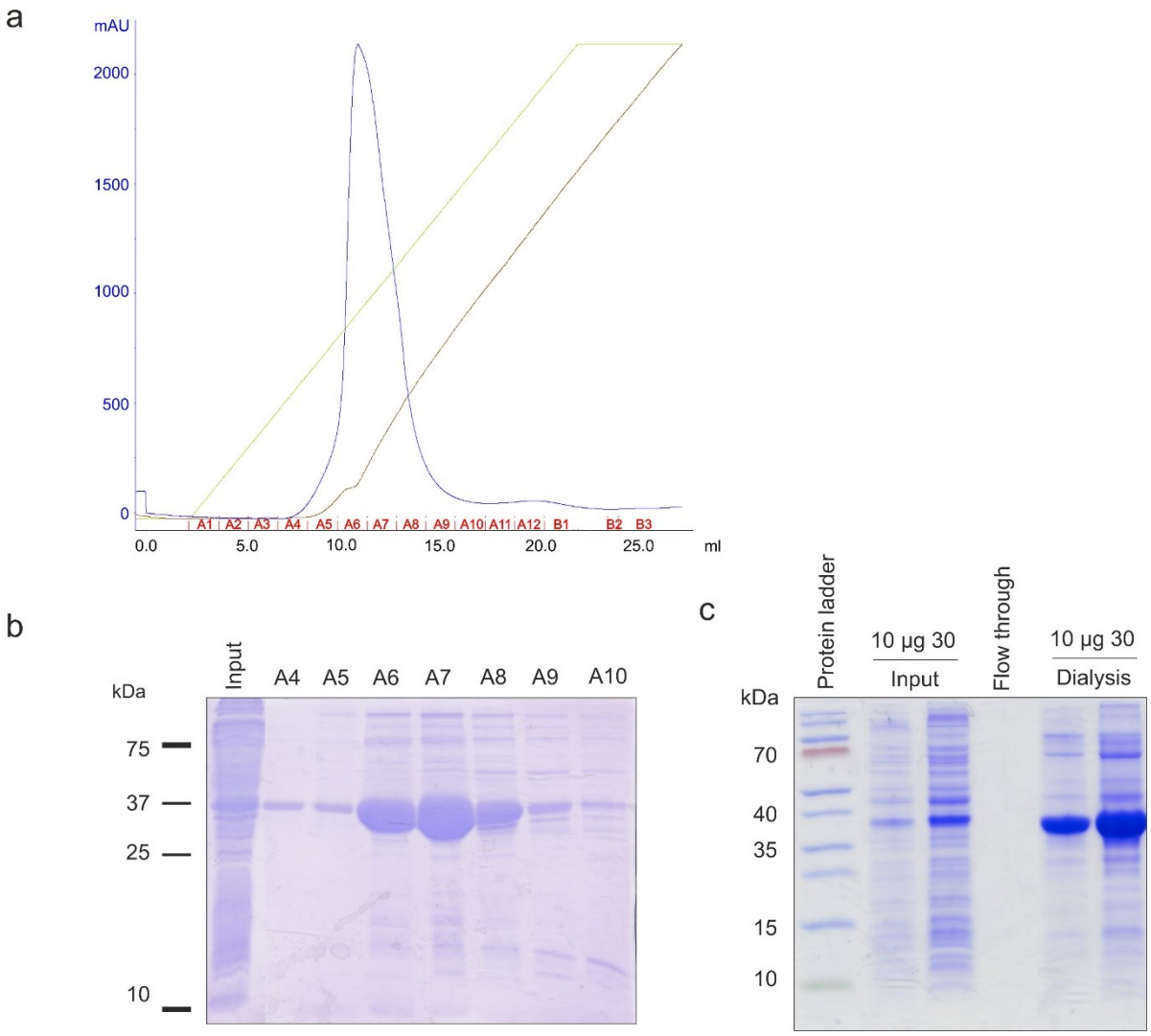

Figure29. Purification of rat IF construct with HisTrap column on FPLC.

(a) Chromatogram of the purification process. X-axis represents flow of buffer in mL. Y-axis represents absorbance at 280 nm, mAU or milli Absorbance Units. Peak in blue is showed for Absorbance. Brown line is Conductivity; green – Concentration of the flow. A1-B4 mean fractions. (b, c) SDS-PAGE electrophoresis gel dyed with Comassie Blue. Input is filtrated sample introduced to the column, A4-A10 – fractions with respect to the chromatogram. Flow through – fraction of sample after concentrating with ViVa Spin Concentrator. Dialysis – fraction of sample after dialysis. Samples were loaded in amount of 5 µL per well (b), 25 µL (c, Flow through), 10 and 30 µg (c, Input and Dialysis).

4.1.2.6 ATP-synthase binding

Inhibitory activity of IF_1 on ATP synthase depends on ability to bind the enzyme: binding is a prerequisite for inhibition. To confirm the inhibitory activity of purified recombinant IF_1 I tested its ability to inhibit ATP hydrolytic activity in rat liver mitochondria (figure 30). During the enzymatic test decrease of A_{340} (coupled oxidation of NADH) is monitored. By addition of various substrates and inhibitors differences in absorbance rate can be tracked. Inhibitory effect of purified IF_1 protein was compared with oligomycin under two different pH, 8.0 and 7.0. Results indicated that IF_1 inhibited hydrolytic activity of ATP synthase under both pH conditions. When compared to oligomycin, it is noticeable that under pH 7.0 inhibitory activity of IF_1 was higher than that of oligomycin, but initial ATPase enzymatic activity was lower at pH 7.0 than at pH 8.0.

4.1.2.7 ATP synthase purification

For IF_1 based affinity purification of ATP synthase, batch method with Glutathione Sepharose 4B binding beads was used. Mitochondrial preparation was solubilised by 0.1% DDM, IF_1 was added to the preparation at the molar ratio of 10x excess to F_1 in the mitochondrial preparation and efficient binding and full inhibition was verified through ATP hydrolytic activity measurement (as in sections 3.2.2.7 and 3.3.2.8). This preparation was bound to GST beads, washed and subsequently purified ATP synthase was eluted by chelatation of Mg^{2+} ions by EDTA. As can be seen from electrophoretic and WB analysis (figure 31), yield of the purification appeared to be relatively low, but we achieved to purify clear preparation of ATP synthase. Anti IF_1 antibody revealed the presence of recombinant protein in both eluted fractions. Two ATP synthase subunits, F_1-α and F_1-γ, were monitored by WB. In case of F_1-α, its content was constant in both input and eluates, while signal of F_1-γ was lower in eluates than in input fraction. We used SDHA, a subunit of cII, as a marker of cross-contamination of the eluted fraction by other OXPHOS proteins and as can be seen, SDHA signal cannot be observed in the eluates, indicating sufficiently clean ATP synthase preparation (figure 31b).

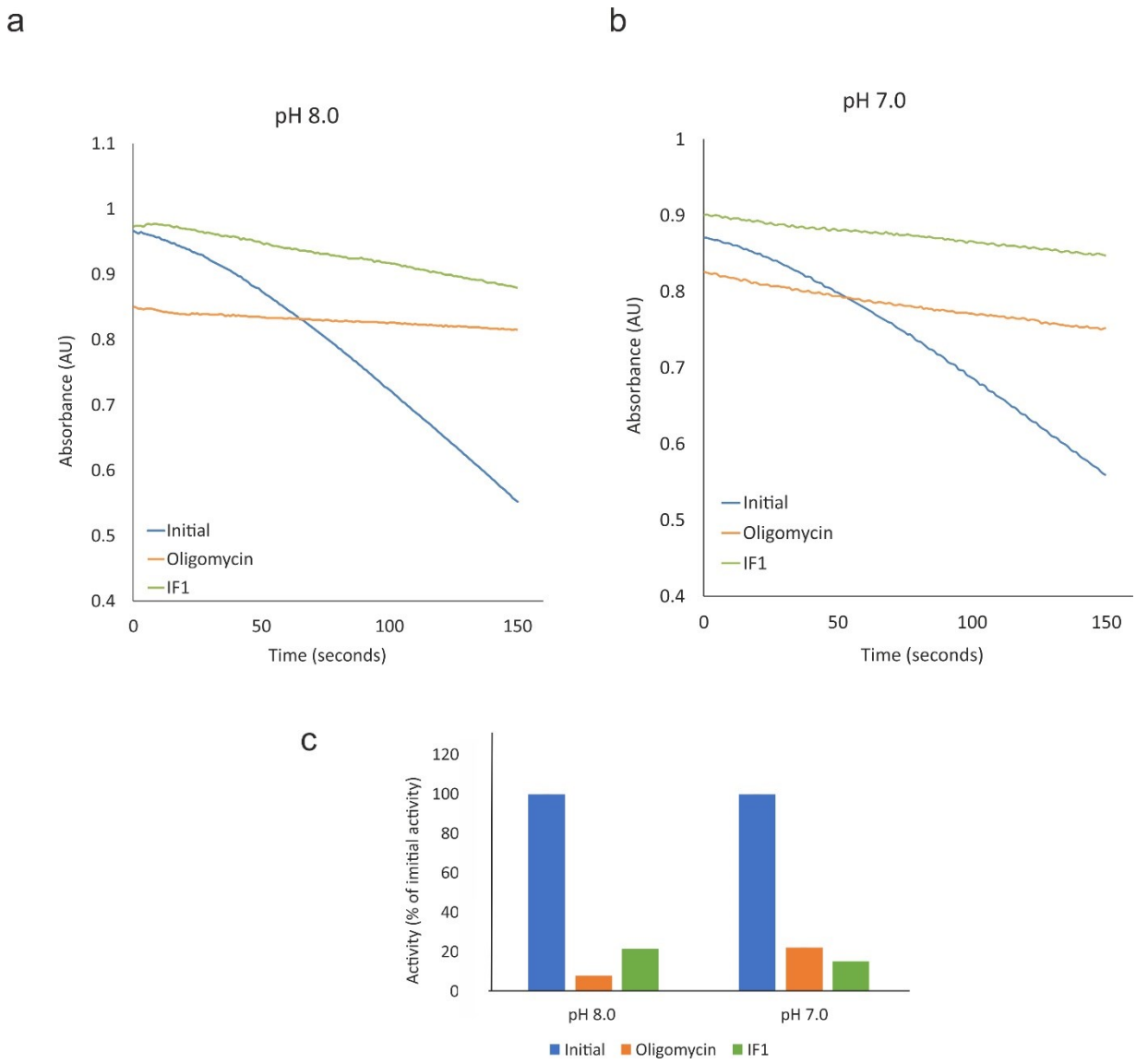

Figure 30. Measurement of ATP synthase hydrolytic activity isolated from rat liver mitochondria.

(a, b) Representative records from measurement of ATP synthase hydrolytic activity under different pH. Absorbance was measured at 340 nm. Initial – enzymatic activity without any additives, Oligomycin – after addition of oligomycin, IF_1 – after addition of purified rat IF_1. (c) Comparison of hydrolytic ATP synthase activity without/after additives under different pH.

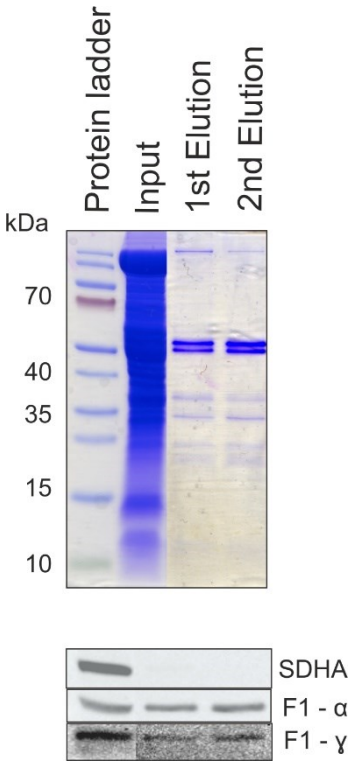

Figure 31. Representative image of batch purification of ATP synthase from rat liver mitochondria.

(a) SDS-PAGE electrophoresis gel dyed with Comassie Blue. (b) Western Blot and immunodetection with antibodies against IF_1, SDHA, F_1-α and F_1-γ. Input is filtrated sample introduced to the Sepharose 4B beads. Samples were loaded in amount of 20 µL per well.

5 Discussion

Mitochondrial ATP synthase is the last complex of OXPHOS apparatus that utilizes the proton-motive force build by tle complexes I-IV and produces ATP. Thorough studies on structure, function and biogenesis of the enzyme have been performed to gain knowledge about ATP synthase itself and its relationship with other components of OXPHOS system. Most of our knowledge arises from the studies on *S. cerevisiae* yeast model, including current model of ATP synthase assembly (Rak, Gokova and Tzagoloff, 2011), dimer and oligomers structures of the enzyme (Arnold *et al.*, 1998; Davies *et al.*, 2012). Even though the undisputed advantages of the yeast models arising form easy genetic manipulation, short time and plethora of available mutant strains, many of the gained observations are not directly applicable to mammalian species and, especially, to complex V-associated pathologies in humans. Over the last decade, the research has reoriented towards understanding of human complex pathologies. Structure of the enzyme has been elucidated in several mammalian species (Runswick *et al.*, 2013) and human cell lines (He *et al.*, 2018). Studies on patients and cell lines with complex V deficiencies revealed the role of individual subunits in function, biogenesis of ATP synthase and impact of subunit deficiencies on OXPHOS system, oxidative damage and mitochondrial physiology (Kucharczyk *et al.*, 2009; Hejzlarová *et al.*, 2014). However, the question of contribution of ATP synthase central stalk subunits to cV biogenesis remained unclear, as well as biochemical thresholds for the pathologic presentation of ATP synthase deficiencies, where defects of central stalk (γ, δ, and ε subunits) can serve as very good model.

Structural and functional characterization of ATP synthase central stalk defects represents large project at the department of Bioenergetics and within this project I focussed on the characterization of structural composition and functional properties of ATP synthase on HEK293 models of γ, δ and ε subunits deficiencies.

5.1.1 Different residual content of ATP synthase in KD clones

Expression of genes encoding γ, δ, and ε subunits of ATP synthase central stalk was silenced by shRNAs in HEK293 cell line to produce knockdown clones. We found out decreased content of individual subunits of ATP synthase in each of nine clones with exception of F_o-c subunit which not even did not follow this decrease of other ATP synthase subunits, but showen even accumulation to approximately 120% in some of the clones. Furthermore, we revealed reduced amount of fully assembled monomeric cV in KD clones that contained 15-90 % compared to control, with D 25-11 clone harbouring the lowest content of active ATP synthase. Amount of other OXPHOS subunits in KD clones was variable, significant change in quantity of core2 subunit (cIII) and NDUFA9

(cI) was observed in four clones. This is not the first case when the mild accumulation of RC subunits was detected. For example, in a patient with a mutation in gene *ATP5E* encoding for ε subunit, patient's fibroblasts and mitochondria display unchanged or increased content of ETC enzymes, whereas content of cV was decreased (Mayr *et al.*, 2010). Data from patients with mutation in gene *ATP5D* encoding for subunit δ show similar behaviour as well (Oláhová *et al.*, 2018). Not only ATP synthase deficiencies with primary defects in enzyme's subunits represent this phenotype, but also mutations in cV assembly factors can exhibit the same trend, for instance, mutation in *TMEM70* gene encoding for the self-titled ancillary factor of ATP synthase (Havlíčková Karbanová *et al.*, 2012).

Decreased content of cV subunits in KD clones is in accordance with the previous studies from our laboratory (Havlícková *et al.*, 2010; Mayr *et al.*, 2010; Pecina *et al.*, 2018) and other works aimed at F_1 subunits deficiencies. For example, mutation in gene *ATP5A1* coding for α subunit in patient fibroblasts showed reduced content of fully assembled cV together with diminished quantity of individual ATP synthase subunits (Jonckheere *et al.*, 2013); similar phenotype was observed in HeLa cells deficient in β subunit (De Meirleir *et al.*, 2004). Diminished content of complex V subunits can be interpreted as degradation of subunits' excess that was not incorporated into monomers of ATP synthase.

Preservation of the F_o-c subunit content in KD clones was also in agreement with previous studies (Havlícková *et al.*, 2010; Mayr *et al.*, 2010; Pecina *et al.*, 2018). There was a difference among KD clones: some of them represented unaltered content of F_o-c subunit, when others showed rather mildly elevated level. This phenotype occurs in only some types of ATP synthase deficiencies, as for example deficiency of any of supernumerary subunit leads to reduced content of F_o-c subunit (He *et al.*, 2018). One of possible explanations is different degradation mechanisms individual subunits (reviewed in Stiburek and Zeman, 2010). It has been demonstrated that Oxa1l, protein responsible for biogenesis of mitochondrial membrane proteins, is required for the proper biogenesis of ATP synthase (Stiburek *et al.*, 2007). Knockdown of Oxa1l in HEK293 cell line had decreased content of ATP synthase and its activity was lower in contrast to control. Yeast homolog, Oxa1 was shown to interact with the newly synthesized Atp9 subunit (mammalian F_o-c subunit) and regulate assembly of the Atp9 oligomer (Jia, Dienhart and Stuart, 2007).

5.1.2 KD clone with the lowest residual content of ATP synthase – biochemical characterization

Data from patients with cV deficiencies indicate residual ATP synthase content ranging from 10 to 30 % of normal enzyme content (reviewed in Houštěk *et al.*, 2006). Among nine KD clones, D 25-11 contained the lowest amount of ATP synthase, 15 % compared to control. This clone was chosen for the further characterization to analyse the impact of this low content of enzyme on cellular respiration and ATP production by oxidative phosphorylation.

Results obtained from the measurements on Oxygraph showed non-significant decrease in rate of endogenous respiration in D 25-11 clone. The OXPHOS capacity, or ADP-stimulated respiration, was also non-significantly reduced in D 25-11 comparably to control, however respiration rate after inhibition of ATP synthase and the ETC capacity were similar to control. In addition, UCR parameter indicating respiration capacity of uncoupled mitochondria was calculated to be higher in D 25-11 clone than in control which is indeed suggestive for the presence of ATP synthase defect. Together with that, RCI index was significantly reduced both with respiratory substrates for cI, RCI(ADP), and with combined substrates for cI, cII and GPDH, RCI(oligo), from 2.41 to 1.82 and from 3.71 to 2.53, respectively. RCI(oligo) can be decreased either by lowered OXPHOS capacity or by higher Leak state that implicates damaged IMM. Values for Leak state were nearly equal in both KD clone and control, thus diminished RCI(oligo) in D 25-11 is a result of decreased capacity for ATP synthesis by oxidative phosphorylation. These results implied that the activity of none of ETC complexes was impaired, whereas utilization of $\Delta\psi_m$ by complex V was affected in the selected clone. Impaired ADP phosphorylation capacity and absence of proton leak in the KD clone was in accordance with studies on central stalk subunits deficiencies in human cell lines and patients. The UCR ratio was previously indicated to be significantly increased in KD of γ and δ subunits (Pecina *et al.*, 2018). Higher value of UCR and reduced ADP phosphorylation capacity were measured also in lymphocytes with ATP synthase defect due to mutation in *TMEM70* gene (Pecina *et al.*, 2014). Furthermore, in both cases, oligomycin titration revealed diminished quantity of functional ATP synthase in mitochondria of affected cells that demonstrated decrease in coupled respiration already at low concentrations/titer of inhibitor.

5.1.3 Cell viability

To assess how deficiency of central stalk subunits affected cell viability, proliferation assay was performed. First measurement in glucose-rich DMEM medium

showed no difference in rates of proliferation of individual KD clones compared to controls. To force the cells towards mitochondrial ATP production, in further experiments the cultivation conditions were modified and glucose was replaced by galactose. This approach has been use repeatedly to stress cells with defects of mitochondrial energy provision (Rossignol *et al.*, 2004). Induced stress condition led to the lethality of KD clones with lowest residual ATP synthase content (C 2-3, C 2-4 and D 25-11). Various combinations of supplements were tested to overcome lethality (not shown), the definitive composition besides galactose, included dialyzed FBS and pyruvate. Results of cell viability measurement displayed diminished rates of proliferation of KD clones with ATP synthase content less than 50 % compared to control, with lowest rate indicated in D 25-11 clone.

5.1.4 Relation to $\Delta\psi_m$ and ROS production

Due to ATP synthase deficiency, KD clones displayed metabolic shift when cultivated in glucose-rich medium and exhibit diminished cell viability under cultivation in nutrient-poor/glucose-free medium. Apart from impaired ATP synthesis by oxidative phosphorylation, one more possible explanation can be suggested regarding defective cell viability: high reactive ROS production and oxidative damage. In our recent study on KD of γ and δ subunits, TPP^+-selective electrode was used to follow real-time changes in mitochondrial membrane potential ($\Delta\psi_m$) in digitonin-permeabilized cells (Pecina *et al.*, 2018). Affected cells/mitochondria represent elevated values of mitochondrial membrane potential and reduced dissipation of $\Delta\psi_m$ under ADP stimulation, the situation that was also established for various ATP synthase defects (Mráček *et al.*, 2006; Hejzlarová *et al.*, 2015).

Hyperpolarization of IMM was demonstrated to provoke generation of reactive oxygen species by the respiratory chain (Korshunov, Skulachev and Starkov, 1997). Analysis of ROS production performed in cells of patients suffering from the ATP synthase defects showed raised production of ROS (Mráček *et al.*, 2006; reviewed in Houštěk *et al.*, 2004). In addition, studies on NARP cells carrying mutation in *MT-ATP6* gene encoding F_o-a subunit of ATP synthase showed the advantageous effect of antioxidants by decreasing ROS level in these cells (Mattiazzi *et al.*, 2004; Baracca *et al.*, 2007).

Neither $\Delta\psi_m$, no ROS generation was directly measured in this work. Based on the previous studies, it would be interesting to perform these experiments, which can contribute to characterisation of functional consequences of central stalk subunits' deficiencies.

5.1.5 Purification of ATP synthase

Typical method of choice for studying of native comformation and assembly of OXPHOS complexes are various native electrophoretic techniques, such as BN-, CN- or hrCN-PAGE. Native electrophoresis together with pulse-case labelling was particularly helpful, when it was applied to respiratory chain complexes cI-cIV. Assembly intermediates were observed here and throughoutly analyzed (For example, cI and cIV, respectively, Lazarou *et al.*, 2007, 2009). These approaches, however, were not efficient in case of cV, as they can reveal only a few subassemblies including canonical F_1-part, F_1-c ring and fully assembled holoenzyme (Wittig *et al.*, 2010; Hejzlarová *et al.*, 2015).

Immunocapture techniques present another method that was successfully employed for ATP synthase purification (Aggeler *et al.*, 2002) or for subsequent analyses - for instance immunoprecipitation and cross-linking analysis of ATP synthase and TMEM70 protein (Kratochvílová *et al.*, 2014) or ATP synthase isolation and MS characterization from mitochondria of HAP1 cells with deficiencies of individual cV subunits (He, Carroll, *et al.*, 2017; He, Ford, *et al.*, 2017; He *et al.*, 2018). Still, this method has a disadvantage in its inability to purify native forms of subassemblies, presence of which was proved by BN-PAGE and ATPase in-gel activity. Additional limitation of immunoprecipitation (IP) is that IP eluate contains total subunit content including components of the all intermediates. Therefore, individual subassemblies cannot be separated and their subunit composition cannot be analyzed.

Yet another possibility to purify enzymatically active ATP synthase in its native form is chromatography purification on column. The pioneers of this method developed different protocols for ATP synthase chromatography purification. First procedures of this technique required multi-level column purification due to impurity of eluted fractions (Lutter *et al.*, 1993; Buchanan and Walker, 1996). Purified ATP synthase was primarily used for crystallography, thus, large amount of input material was required for the chromatography purification which makes this procedure inappropriate for cell cultures.

Recent findings on the structure and function of IF_1 inhibitory factor of ATP synthase enabled the protein to be employed on the ATP synthase affinity purification (Bason *et al.*, 2011; Runswick *et al.*, 2013). In contrast to earlier purifications, current procedure requires IF_1 to be engineered to facilitate affinity purification of ATP synthase. This approach have been successfully applied on yeasts and several mammalian species (Runswick *et al.*, 2013; Liu *et al.*, 2015). Purified ATP synthase is catalytically active and appears to be in its native form. Affinity purification performed on column and

followed by size exclusion chromatography allows separation of individual cV intermediates and subassemblies by their molecular weight.

Described method of ATP synthase purification was initially applied to bovine enzyme with IF_1 construct containing 1-60 AA sequence of bovine inhibitory protein (Bason *et al.*, 2011). Later, sequence of bovine IF_1 was used for purification of ATP synthase from other mammalian species including ovine and porcine enzymes (Runswick *et al.*, 2013), employment of bovine IF_1 sequence construct in all three species led to successful ATP synthase purification. Based on this experience and high 1-60 AA sequence similarity between rat and human inhibitory proteins, we decided to use rat 1-60 AA sequence to design IF_1 construct for ATP synthase purification from HEK293 cells. There are several projects at the Department of Bioenergetics focused on cV deficiencies with rodents as an experimental model: rat knockout of DAPIT ATP synthase subunit and inducible TMEM70 mouse knockout. Thus, the technique of ATP synthase purification using rat IF_1 construct would be applicable both for rodent models and human cell lines.

As first step, IF_1 construct engineering and its expression in BL21(DE3) strain of *E.coli* was accomplished. Bacterial cells carried pET28(+) plasmids with the sequence of IF_1 construct. Even though the BL21(DE3) strain of *E.coli* and pET28b(+) plasmid are adapted for high protein expression, yields of IF_1 construct expression were rather low. In the original protocol, C41(DE3) *E.coli* strain and pRun expression plasmid were applied. C41(DE3) competent cells proved to produce higher yields of expressed proteins (Miroux and Walker, 1996); hence, the IF_1 construct was transformed into the C41(DE3) to test over-production efficiency. Surprisingly, results of this transformation were negative; none of the pinned colonies displayed IF_1 construct expression. Despite the poor over-production of the recombinant IF_1 protein in BL21(DE3) strain, following work was performed on this *E.coli* strain.

Optimization of cultivation and protein expression was focused on several parameters: concentration of inducing agent (IPTG), time and temperature during bacterial cultivation and induction of protein expression. Although in the primary protocol long-time induction of protein expression (18 hours) at low temperature (25°C) was used (Bason *et al.*, 2011), these conditions displayed to be of less efficient in our expression system. Instead, short-time (3 and 4 hours) expression at higher temperature (37°C) appeared to be prefferential for our expression of IF_1 construct protein. There was no apparent difference in yield of protein expression under various concentrations of IPTG,

thence final concentration of 1 mM IPTG was selected, the concentration similar to that reported in the original paper (0.286 mg/ml).

When membranous protein are expressed in bacterial expression systems, they can often be aggregated or/and stored into inclusion bodies (for example, Montigny *et al.*, 2004; Zhang *et al.*, 2015). In most cases these aggregated proteins can be purified and refolded, but the procedure implies additional steps during purification. Besides membranous proteins inclusion bodies contain proteins that can represent danger/toxicity for bacteria; higher amounts of expressed proteins (over-production) can also be toxic for bacteria and can push produced protein into inclusion bodies or maintain them as micellar-like or proteo-lipidic aggregates. Over-production of ATP synthase membranous proteins in BL21(DE3) strain was reported to fail or exhibit low expression (Miroux and Walker, 1996). Despite the IF_1 construct consisting of proteins soluble in their native form (His-tag, GST-tag and 1-60 AA of IF_1), it was important to determine if the construct is not stored into inclusion bodies or aggregates in BL21(DE3). Comassie Blue staining of the gels and WB analysis displayed presence of the IF_1 construct both in soluble supernatant and in pellet, latter represented by inclusion bodies, membrane debris and/or aggregated/damaged proteins. It is possible that BL21(DE3) expression system was partly incapable of the IF_1 construct over-production and stored portion of the protein into inclusion bodies. For further work, only fraction containing soluble IF_1 construct (supernatant) was used.

As it is described in result section 4.1.2.4, small-scale (batch) His-tag purification of the IF_1 construct was performed prior to column purification. Batch method does not allow generating a gradient of buffer as it is enabled in case of column purification. Different concentrations of imidazole were applied to select a concentration range for the later column purification. SDS-PAGE analysis revealed appearance of the IF_1 construct even at 500 mM imidazole. Thus, 25-500 mM range of imidazole concentration was selected instead of 25-300 mM stated in the original protocol (Bason *et al.*, 2011). Nickel affinity purification with HisTrap column resulted in successful elution of the recombinant protein, its purity (both before and after dialysis and concentration) seemed lower comparing with the results reported in literatur (Bason *et al.*, 2011; supplementary data). From 7 L of bacterial culture approximately 5.6 mg of recombinant protein were obtained, individual fractions were concentrated with final concentration of 26.3 mg/mL which was similar to one noted in the original paper (Bason *et al.*, 2011; 24 mg/mL).

To verify inhibitory activity of purified IF_1 construct ATPase hydrolytic activity on rat liver mitochondria was measured in both absence and presence of oligomycin

inhibitor and recombinant IF_1 construct. The IF_1 construct showed to be catalytically active, it inhibited ATP hydrolytic activity under both 8.0 and 7.0 pH, however, efficiency of recombinant protein appeared to be higher at pH 7.0 (16 % of remaining ATPase activity in contrast to oligomycin, 22 %).

Finally, I managed to perform beads based purification of ATP synthase using IF_1 affinity approach from solubilized mitochondria from rat liver was performed (results, section 4.2.1.6 and 4.2.1.7). By this approach I managed to obtain pure fraction of TAP synthase without contamination of other OXPHOS complexes. The only drawback was, that flow-through fractions appeared to still contain high quantity of ATP synthase, i.e. there was poor efficiency of the capture. There are several possible explanations: it can be due to low binding capacity of the sepharose beads, insufficient amount of recombinant IF_1 added to solubilized mitochondria, inappropriate pH or/and composition of buffers. Therefore, while the technique of ATP synthase affinity purification clearly showed its utility in our hands, further optimization will be required to optimize yields and make this methor suitable for preparations based on cell culture models.

6 Conclusions

First part of my work focussed on the functional consequences of ATP synthase deficiencies on HEK293 cell models with silenced expression of γ, δ and ε central stalk subunits. This was studied on a range of clones with variable knockdown efficiency. Knockdown clones represent decreased content of fully assembled ATP synthase in range of 15 – 90 % of control. Content of individual enzyme subunits showed to be decreased with exception of F_o-c subunit retaining unaltered levels in KD clones. Characterization of respiration and oxidative phosphorylation in the clone with lowest quantity of ATP synthase, D 25-11, indicated diminished capacity for ATP synthesis and inability to dissipate $\Delta\psi_m$ under stimulation of ADP. Measurement of cell viability under nutrient-poor cultivation demonstrated inability of cells to proliferate when residual ATP synthase content is less than 50 % of control. This was in line with other biochemical thresholds determined by co-workers in this experimental system and represents foundation work for thorough characterisation of threshold values for presentation of ATP synthase deficiencies in patients. All these data are part of the currently submitted manuscript (Nuskova *et al.*, 2018).

Second part of the thesis was devoted to adaptation of technique of ATP synthase purification through the IF_1 inhibitory protein to isolate and study individual subassemblies of cV in abovementioned models of ATP synthase deficiency. Engineering, expression and purification of recombinant rat IF_1 construct was optimized and efficient purification of ATP synthase from rat liver was achieved. While efficiency of IF1 binding to the GST beads will still require additional optimisations, this method represents valuable addition to the sprectrum of tools available at the department of Bioenergetics and will be used for future characterisations of subunit composition in various vestigial ATP synthases.

7 Bibliography

Abrahams, J. P., Leslie, A. G., Lutter, R. and Walker, J. E. (1994) 'Structure at 2.8 A resolution of F1-ATPase from bovine heart mitochondria.', *Nature*, 370(6491), pp. 621–8. doi: 10.1038/370621a0.

Aggeler, R., Coons, J., Taylor, S. W., Ghosh, S. S., Garcia, J. J., Capaldi, R. A. and Marusich, M. F. (2002) 'A functionally active human F1F0 ATPase can be purified by immunocapture from heart tissue and fibroblast cell lines. Subunit structure and activity studies.', *The Journal of biological chemistry*. American Society for Biochemistry and Molecular Biology, 277(37), pp. 33906–12. doi: 10.1074/jbc.M204538200.

Alberts Bruce, Johnson Alexander, Lewis Julian, Morgan David, Raff Martin, Roberts Keith, and W. P. (2015) *Molecular Biology of the Cell*. 6th edn. Edited by Z. E. Lewis Sherry Granum. New York: Garland Science, Taylor & Francis Group, LCC.

Allegretti, M., Klusch, N., Mills, D. J., Vonck, J., Kühlbrandt, W. and Davies, K. M. (2015) 'Horizontal membrane-intrinsic α-helices in the stator a-subunit of an F-type ATP synthase', *Nature*, 521(7551), pp. 237–240. doi: 10.1038/nature14185.

Anderson, S., Bankier, A. T., Barrell, B. G., de Bruijn, M. H., Coulson, A. R., Drouin, J., Eperon, I. C., Nierlich, D. P., Roe, B. A., Sanger, F., Schreier, P. H., Smith, A. J., Staden, R. and Young, I. G. (1981) 'Sequence and organization of the human mitochondrial genome.', *Nature*, 290(5806), pp. 457–65.

Andersson, S. G. E., Zomorodipour, A., Andersson, J. O., Sicheritz-Pontén, T., Alsmark, U. C. M., Podowski, R. M., Näslund, A. K., Eriksson, A.-S., Winkler, H. H. and Kurland, C. G. (1998) 'The genome sequence of Rickettsia prowazekii and the origin ofmitochondria', *Nature*. Nature Publishing Group, 396(6707), pp. 133–140. doi: 10.1038/24094.

Andrews, R. M., Kubacka, I., Chinnery, P. F., Lightowlers, R. N., Turnbull, D. M. and Howell, N. (1999) 'Reanalysis and revision of the Cambridge reference sequence for human mitochondrial DNA.', *Nature genetics*, 23(2), p. 147. doi: 10.1038/13779.

Arnold, I., Pfeiffer, K., Neupert, W., Stuart, R. A. and Schägger, H. (1998) 'Yeast mitochondrial F1F0-ATP synthase exists as a dimer: identification of three dimer-specific subunits.', *The EMBO journal*, 17(24), pp. 7170–8. doi: 10.1093/emboj/17.24.7170.

Baker, L. A., Watt, I. N., Runswick, M. J., Walker, J. E. and Rubinstein, J. L. (2012)

‘Arrangement of subunits in intact mammalian mitochondrial ATP synthase determined by cryo-EM.’, *Proceedings of the National Academy of Sciences of the United States of America*, 109(29), pp. 11675–80. doi: 10.1073/pnas.1204935109.

Baracca, A., Sgarbi, G., Mattiazzi, M., Casalena, G., Pagnotta, E., Valentino, M. L., Moggio, M., Lenaz, G., Carelli, V. and Solaini, G. (2007) ‘Biochemical phenotypes associated with the mitochondrial ATP6 gene mutations at nt8993’, *Biochimica et Biophysica Acta (BBA) - Bioenergetics*. Elsevier, 1767(7), pp. 913–919. doi: 10.1016/J.BBABIO.2007.05.005.

Bason, J. V, Montgomery, M. G., Leslie, A. G. W. and Walker, J. E. (2014) ‘Pathway of binding of the intrinsically disordered mitochondrial inhibitor protein to F1-ATPase.’, *Proceedings of the National Academy of Sciences of the United States of America*, 111(31), pp. 11305–11310. doi: 10.1073/pnas.1411560111.

Bason, J. V, Runswick, M. J., Fearnley, I. M. and Walker, J. E. (2011) ‘Binding of the inhibitor protein IF(1) to bovine F(1)-ATPase.’, *Journal of molecular biology*. Elsevier, 406(3), pp. 443–53. doi: 10.1016/j.jmb.2010.12.025.

Belogrudov, G. I. (2008) ‘The proximal N-terminal amino acid residues are required for the coupling activity of the bovine heart mitochondrial factor B’, *Archives of Biochemistry and Biophysics*, 473(1), pp. 76–87. doi: 10.1016/j.abb.2008.02.022.

Belogrudov, G. I. (2009) ‘Recent advances in structure-functional studies of mitochondrial factor B.’, *Journal of bioenergetics and biomembranes*, 41(2), pp. 137–43. doi: 10.1007/s10863-009-9210-1.

Belogrudov, G. I. and Hatefi, Y. (2002) ‘Factor B and the mitochondrial ATP synthase complex’, *Journal of Biological Chemistry*, 277(8), pp. 6097–6103. doi: 10.1074/jbc.M111256200.

Bezawork-Geleta, A., Rohlena, J., Dong, L., Pacak, K. and Neuzil, J. (2017) ‘Mitochondrial Complex II: At the Crossroads’, *Trends in Biochemical Sciences*. Elsevier Current Trends, 42(4), pp. 312–325. doi: 10.1016/J.TIBS.2017.01.003.

Blaza, J. N., Vinothkumar, K. R. and Hirst, J. (2018) ‘Structure of the Deactive State of Mammalian Respiratory Complex I’, *Structure*, 26(2), p. 312–319.e3. doi: 10.1016/j.str.2017.12.014.

Buchanan, S. K. and Walker, J. E. (1996) *Large-scale chromatographic purification of F 1 F o-ATPase and complex I from bovine heart mitochondria*, *Biochem. J*.

Buzhynskyy, N., Sens, P., Prima, V., Sturgis, J. N. and Scheuring, S. (2007) ‘Rows of

ATP Synthase Dimers in Native Mitochondrial Inner Membranes', *Biophysical Journal*. Elsevier, 93(8), pp. 2870–2876. doi: 10.1529/biophysj.107.109728.

Cabezon, E., Butler, P. J., Runswick, M. J. and Walker, J. E. (2000) 'Modulation of the oligomerization state of the bovine F1-ATPase inhibitor protein, IF1, by pH.', *The Journal of biological chemistry*, 275(33), pp. 25460–4. doi: 10.1074/jbc.M003859200.

Cabezón, E., Runswick, M. J., Leslie, A. G. and Walker, J. E. (2001) 'The structure of bovine IF(1), the regulatory subunit of mitochondrial F-ATPase.', *The EMBO journal*. EMBO Press, 20(24), pp. 6990–6. doi: 10.1093/emboj/20.24.6990.

Campanella, M., Casswell, E., Chong, S., Farah, Z., Wieckowski, M. R., Abramov, A. Y., Tinker, A. and Duchen, M. R. (2008) 'Regulation of Mitochondrial Structure and Function by the F1Fo-ATPase Inhibitor Protein, IF1', *Cell Metabolism*. Cell Press, 8(1), pp. 13–25. doi: 10.1016/J.CMET.2008.06.001.

Carroll, J., Fearnley, I. M., Skehel, J. M., Shannon, R. J., Hirst, J. and Walker, J. E. (2006) 'Bovine complex I is a complex of 45 different subunits.', *The Journal of biological chemistry*. American Society for Biochemistry and Molecular Biology, 281(43), pp. 32724–7. doi: 10.1074/jbc.M607135200.

Cízková, A., Stránecký, V., Mayr, J. A., Tesarová, M., Havlícková, V., Paul, J., Ivánek, R., Kuss, A. W., Hansíková, H., Kaplanová, V., Vrbacký, M., Hartmannová, H., Nosková, L., Honzík, T., Drahota, Z., Magner, M., Hejzlarová, K., Sperl, W., Zeman, J., Houstek, J. and Kmoch, S. (2008) 'TMEM70 mutations cause isolated ATP synthase deficiency and neonatal mitochondrial encephalocardiomyopathy.', *Nature genetics*, 40(11), pp. 1288–90. doi: 10.1038/ng.246.

Collinson, I. R., Runswick, M. J., Fearnley, I. M., Skehel, J. M., van Raaij, M. J., Walker, J. E., Buchanan, S. K. and Griffiths, D. E. (1994) 'FoMembrane Domain of ATP Synthase from Bovine Heart Mitochondria: Purification, Subunit Composition, and Reconstitution with F1-ATPase', *Biochemistry*, 33(25), pp. 7971–7978. doi: 10.1021/bi00191a026.

Davies, K. M., Anselmi, C., Wittig, I., Faraldo-Gomez, J. D. and Kuhlbrandt, W. (2012) 'Structure of the yeast F1Fo-ATP synthase dimer and its role in shaping the mitochondrial cristae', *Proceedings of the National Academy of Sciences*, 109(34), pp. 13602–13607. doi: 10.1073/pnas.1204593109.

Davies, K. M., Strauss, M., Daum, B., Kief, J. H., Osiewacz, H. D., Rycovska, A., Zickermann, V. and Kühlbrandt, W. (2011) 'Macromolecular organization of ATP

synthase and complex I in whole mitochondria.', *Proceedings of the National Academy of Sciences of the United States of America*, 108(34), pp. 14121–6. doi: 10.1073/pnas.1103621108.

DiMauro, S. (2013) 'Mitochondrial DNA Mutation Load', *JAMA Neurology*, 70(12), pp. 1484–1485. doi: 10.1001/jamaneurol.2013.4401.

Dubendorf, J. W. and Studier, F. W. (1991) 'Controlling basal expression in an inducible T7 expression system by blocking the target T7 promoter with lac repressor', *Journal of Molecular Biology*. Academic Press, 219(1), pp. 45–59. doi: 10.1016/0022-2836(91)90856-2.

Duvezin-Caubet, S., Caron, M., Giraud, M.-F., Velours, J. and di Rago, J.-P. (2003) 'The two rotor components of yeast mitochondrial ATP synthase are mechanically coupled by subunit delta.', *Proceedings of the National Academy of Sciences of the United States of America*, 100(23), pp. 13235–40. doi: 10.1073/pnas.2135169100.

Duvezin-Caubet, S., Rak, M., Lefebvre-Legendre, L., Tetaud, E., Bonnefoy, N. and Di Rago, J. P. (2006) 'A "petite obligate" mutant of Saccharomyces cerevisiae. Functional mtDNA is lethal in cells lacking the δ subunit of mitochondrial F1-ATPase', *Journal of Biological Chemistry*, 281(24), pp. 16305–16313. doi: 10.1074/jbc.M513805200.

Ernster, L. and Schatz, G. (1981) 'Mitochondria: a historical review.', *The Journal of cell biology*, 91(3 Pt 2), p. 227s–255s.

Faccenda, D. and Campanella, M. (2012) 'Molecular Regulation of the Mitochondrial F_1F_o-ATPsynthase: Physiological and Pathological Significance of the Inhibitory Factor 1 (IF_1)', *International Journal of Cell Biology*, 2012, pp. 1–12. doi: 10.1155/2012/367934.

Fearnley, I. M. and Walker, J. E. (1986) 'Two overlapping genes in bovine mitochondrial DNA encode membrane components of ATP synthase.', *The EMBO Journal*, 5(8), pp. 2003–2008.

Ferguson, S. J. (2000) 'ATP synthase: What dictates the size of a ring?', *Current Biology*, 10(21), pp. 804–808. doi: 10.1016/S0960-9822(00)00765-X.

Fernández-Vizarra, E., Tiranti, V. and Zeviani, M. (2009) 'Assembly of the oxidative phosphorylation system in humans: What we have learned by studying its defects', *Biochimica et Biophysica Acta - Molecular Cell Research*. Elsevier B.V., 1793(1), pp. 200–211. doi: 10.1016/j.bbamcr.2008.05.028.

Formentini, L., Pereira, M. P., Sánchez-Cenizo, L., Santacatterina, F., Lucas, J. J.,

Navarro, C., Martínez-Serrano, A. and Cuezva, J. M. (2014) 'In vivo inhibition of the mitochondrial H^+-ATP synthase in neurons promotes metabolic preconditioning', *EMBO Journal*, 33(7), pp. 762–778. doi: 10.1002/embj.201386392.

Formentini, L., Sánchez-Aragó, M., Sánchez-Cenizo, L. and Cuezva, J. M. (2012) 'The Mitochondrial ATPase Inhibitory Factor 1 Triggers a ROS-Mediated Retrograde Prosurvival and Proliferative Response', *Molecular Cell*. Cell Press, 45(6), pp. 731–742. doi: 10.1016/J.MOLCEL.2012.01.008.

Galkin, A., Dröse, S. and Brandt, U. (2006) 'The proton pumping stoichiometry of purified mitochondrial complex I reconstituted into proteoliposomes', *Biochimica et Biophysica Acta (BBA) - Bioenergetics*. Elsevier, 1757(12), pp. 1575–1581. doi: 10.1016/J.BBABIO.2006.10.001.

García, J. J., Morales-Ríos, E., Cortés-Hernandez, P. and Rodríguez-Zavala, J. S. (2006) 'The inhibitor protein (IF1) promotes dimerization of the mitochondrial F1F0-ATP synthase.', *Biochemistry*, 45(42), pp. 12695–703. doi: 10.1021/bi060339j.

García-Bermúdez, J. and Cuezva, J. M. (2016) 'The ATPase Inhibitory Factor 1 (IF1): A master regulator of energy metabolism and of cell survival', *Biochimica et Biophysica Acta (BBA) - Bioenergetics*. Elsevier B.V., 1. doi: 10.1016/j.bbabio.2016.02.004.

García-Bermúdez, J., Sánchez-Aragó, M., Soldevilla, B., del Arco, A., Nuevo-Tapioles, C. and Cuezva, J. M. (2015) 'PKA Phosphorylates the ATPase Inhibitory Factor 1 and Inactivates Its Capacity to Bind and Inhibit the Mitochondrial H+-ATP Synthase', *Cell Reports*. Cell Press, 12(12), pp. 2143–2155. doi: 10.1016/J.CELREP.2015.08.052.

Gibbons, C., Montgomery, M. G., Leslie, A. G. and Walker, J. E. (2000) 'The structure of the central stalk in bovine F(1)-ATPase at 2.4 A resolution.', *Nature structural biology*, 7(11), pp. 1055–61. doi: 10.1038/80981.

Gilkerson, R. W., Selker, J. M. L. and Capaldi, R. A. (2003) 'The cristal membrane of mitochondria is the principal site of oxidative phosphorylation', *FEBS Letters*, 546(2–3), pp. 355–358. doi: 10.1016/S0014-5793(03)00633-1.

Gnaiger, E. (2008) 'Polarographic Oxygen Sensors, the Oxygraph, and High-Resolution Respirometry to Assess Mitochondrial Function', in *Drug-Induced Mitochondrial Dysfunction*. Hoboken, NJ, USA: John Wiley & Sons, Inc., pp. 325–352. doi: 10.1002/9780470372531.ch12.

Gnaiger, E. (2014) *Mitochondrial Pathways and Respiratory Control An Introduction to OXPHOS Analysis*, *Mitochondrial Physiology Network*.

Gorman, G. S., Chinnery, P. F., DiMauro, S., Hirano, M., Koga, Y., McFarland, R., Suomalainen, A., Thorburn, D. R., Zeviani, M. and Turnbull, D. M. (2016) 'Mitochondrial diseases', *Nature Reviews Disease Primers*. Nature Publishing Group, 2, p. 16080. doi: 10.1038/nrdp.2016.80.

Greaves, L. C., Reeve, A. K., Taylor, R. W. and Turnbull, D. M. (2012) 'Mitochondrial DNA and disease', *The Journal of Pathology*, 226(2), pp. 274–286. doi: 10.1002/path.3028.

Guélin, E., Chevallier, J., Rigoulet, M., Guérin, B. and Velours, J. (1993) 'ATP synthase of yeast mitochondria. Isolation and disruption of the ATP epsilon gene.', *The Journal of biological chemistry*, 268(1), pp. 161–7. doi: 10.1371/JOURNAL.PONE.0050644.

Habersetzer, J., Larrieu, I., Priault, M., Salin, B., Rossignol, R., Brèthes, D. and Paumard, P. (2013) 'Human F1F0 ATP synthase, mitochondrial ultrastructure and OXPHOS impairment: a (super-)complex matter?', *PloS one*. Public Library of Science, 8(10), p. e75429. doi: 10.1371/journal.pone.0075429.

Hardonnière, K., Fernier, M., Gallais, I., Mograbi, B., Podechard, N., Le Ferrec, E., Grova, N., Appenzeller, B., Burel, A., Chevanne, M., Sergent, O., Huc, L., Bortoli, S. and Lagadic-Gossmann, D. (2017) 'Role for the ATPase inhibitory factor 1 in the environmental carcinogen-induced Warburg phenotype', *Scientific Reports*. Nature Publishing Group, 7(1), p. 195. doi: 10.1038/s41598-017-00269-7.

Havlícková, V., Kaplanová, V., Nůsková, H., Drahota, Z. and Houstek, J. (2010) 'Knockdown of F1 epsilon subunit decreases mitochondrial content of ATP synthase and leads to accumulation of subunit c.', *Biochimica et biophysica acta*, 1797(6–7), pp. 1124–9. doi: 10.1016/j.bbabio.2009.12.009.

Havlíčková Karbanová, V., Čížková Vrbacká, A., Hejzlarová, K., Nůsková, H., Stránecký, V., Potocká, A., Kmoch, S. and Houštěk, J. (2012) 'Compensatory upregulation of respiratory chain complexes III and IV in isolated deficiency of ATP synthase due to TMEM70 mutation', *Biochimica et Biophysica Acta (BBA) - Bioenergetics*. Elsevier, 1817(7), pp. 1037–1043. doi: 10.1016/J.BBABIO.2012.03.004.

He, J., Carroll, J., Ding, S., Fearnley, I. M. and Walker, J. E. (2017) 'Permeability transition in human mitochondria persists in the absence of peripheral stalk subunits of ATP synthase', *Proceedings of the National Academy of Sciences*. National Academy of Sciences, p. 201711201. doi: 10.1073/pnas.1711201114.

He, J., Ford, H. C., Carroll, J., Ding, S., Fearnley, I. M. and Walker, J. E. (2017)

‘Persistence of the mitochondrial permeability transition in the absence of subunit c of human ATP synthase.’, *Proceedings of the National Academy of Sciences of the United States of America*. National Academy of Sciences, 114(13), pp. 3409–3414. doi: 10.1073/pnas.1702357114.

He, J., Ford, H. C., Carroll, J., Douglas, C., Gonzales, E., Ding, S., Fearnley, I. M. and Walker, J. E. (2018) ‘Assembly of the membrane domain of ATP synthase in human mitochondria.’, *Proceedings of the National Academy of Sciences of the United States of America*, p. 201722086. doi: 10.1073/pnas.1722086115.

Hejzlarová, K., Kaplanová, V., Nůsková, H., Kovářová, N., Ješina, P., Drahota, Z., Mráček, T., Seneca, S. and Houštěk, J. (2015) ‘Alteration of structure and function of ATP synthase and cytochrome c oxidase by lack of Fo-a and Cox3 subunits caused by mitochondrial DNA 9205delTA mutation.’, *The Biochemical journal*, 466(3), pp. 601–11. doi: 10.1042/BJ20141462.

Hejzlarová, K., Mráček, T., Vrbacký, M., Kaplanová, V., Karbanová, V., Nůsková, H., Pecina, P. and Houštěk, J. (2014) ‘Nuclear genetic defects of mitochondrial ATP synthase.’, *Physiological research / Academia Scientiarum Bohemoslovaca*, 63 Suppl 1(1995), pp. S57-71.

Holt, I. J., Harding, A. E., Petty, R. K. and Morgan-Hughes, J. A. (1990) ‘A new mitochondrial disease associated with mitochondrial DNA heteroplasmy.’, *American journal of human genetics*, 46(3), pp. 428–33.

Houštěk, J., Kmoch, S. and Zeman, J. (2009) ‘TMEM70 protein - A novel ancillary factor of mammalian ATP synthase’, *Biochimica et Biophysica Acta - Bioenergetics*, 1787(5), pp. 529–532. doi: 10.1016/j.bbabio.2008.11.013.

Houštěk, J., Mráček, T., Vojtíšková, A. and Zeman, J. (2004) ‘Mitochondrial diseases and ATPase defects of nuclear origin’, *Biochimica et Biophysica Acta (BBA) - Bioenergetics*. Elsevier, 1658(1–2), pp. 115–121. doi: 10.1016/J.BBABIO.2004.04.012.

Houštěk, J., Pícková, A., Vojtíšková, A., Mráček, T., Pecina, P. and Ješina, P. (2006) ‘Mitochondrial diseases and genetic defects of ATP synthase’, *Biochimica et Biophysica Acta - Bioenergetics*, 1757(9–10), pp. 1400–1405. doi: 10.1016/j.bbabio.2006.04.006.

Chinnery, P. F., Taylor, D. J., Manners, D., Styles, P. and Lodi, R. (2001) ‘No correlation between muscle A3243G mutation load and mitochondrial function in vivo’, *Neurology*, 56(8), pp. 1101–1104. doi: 10.1212/WNL.56.8.1101.

Iwata, S., Lee, J. W., Okada, K., Lee, J. K., Iwata, M., Rasmussen, B., Link, T. A., Ramaswamy, S. and Jap, B. K. (1998) 'Complete Structure of the 11-Subunit Bovine Mitochondrial Cytochrome bc 1 Complex', 281(July), pp. 64–72.

Jesina, P., Tesarová, M., Fornůsková, D., Vojtísková, A., Pecina, P., Kaplanová, V., Hansíková, H., Zeman, J. and Houstek, J. (2004) 'Diminished synthesis of subunit a (ATP6) and altered function of ATP synthase and cytochrome c oxidase due to the mtDNA 2 bp microdeletion of TA at positions 9205 and 9206.', *The Biochemical journal*. Portland Press Ltd, 383(Pt. 3), pp. 561–71. doi: 10.1042/BJ20040407.

Jia, L., Dienhart, M. K. and Stuart, R. A. (2007) 'Oxa1 directly interacts with Atp9 and mediates its assembly into the mitochondrial F1Fo-ATP synthase complex.', *Molecular biology of the cell*. American Society for Cell Biology, 18(5), pp. 1897–908. doi: 10.1091/mbc.e06-10-0925.

Jiko, C., Davies, K. M., Shinzawa-Itoh, K., Tani, K., Maeda, S., Mills, D. J., Tsukihara, T., Fujiyoshi, Y., Kühlbrandt, W. and Gerle, C. (2015) 'Bovine F1Fo ATP synthase monomers bend the lipid bilayer in 2D membrane crystals', *eLife*, 4, p. e06119. doi: 10.7554/eLife.06119.

Jonckheere, A. I., Herma Renkema, G., Bras, M., Van Den Heuvel, L. P., Hoischen, A., Gilissen, C., Nabuurs, S. B., Huynen, M. A., De Vries, M. C., Smeitink, J. A. M. and Rodenburg, R. J. T. (2013) 'A complex v ATP5A1 defect causes fatal neonatal mitochondrial encephalopathy', *Brain*, 136(5), pp. 1544–1554. doi: 10.1093/brain/awt086.

Jonckheere, A. I., Hogeveen, M., Nijtmans, L., van den Brand, M., Janssen, A., Diepstra, H., van den Brandt, F., van den Heuvel, B., Hol, F., Hofste, T., Kapusta, L., Dillmann, U., Shamdeen, M., Smeitink, J., Smeitink, J. and Rodenburg, R. (2009) 'A novel mitochondrial ATP8 gene mutation in a patient with apical hypertrophic cardiomyopathy and neuropathy.', *BMJ case reports*. BMJ Publishing Group, 2009. doi: 10.1136/bcr.07.2008.0504.

Joshi, S., Hughes, J. B., Shaikh, F. and Sanadi, D. R. (1979) 'On the role of coupling factor B in the mitochondrial Pi-ATP exchange reaction.', *The Journal of biological chemistry*, 254(20), pp. 10145–52.

Joshi, S., Kantham, L., Kaplay, S. and Sanadi, D. R. (1985) 'Monoclonal antibodies to mitochondrial', *FEBS Journal*, 179(1), pp. 144–147.

Junge, W., Lill, H. and Engelbrecht, S. (1997) 'ATP synthase: an electrochemical

ransducer with rotatory mechanics', *Trends in Biochemical Sciences*. Elsevier Current Trends, 22(11), pp. 420–423. doi: 10.1016/S0968-0004(97)01129-8.

Kadenbach, B. and Hüttemann, M. (2015) 'The subunit composition and function of mammalian cytochrome c oxidase', *Mitochondrion*. Elsevier, 24, pp. 64–76. doi: 10.1016/J.MITO.2015.07.002.

Korshunov, S. S., Skulachev, V. P. and Starkov, A. A. (1997) 'High protonic potential actuates a mechanism of production of reactive oxygen species in mitochondria.', *FEBS letters*, 416(1), pp. 15–8.

Kratochvílová, H., Hejzlarová, K., Vrbacký, M., Mráček, T., Karbanová, V., Tesařová, M., Gombitová, A., Cmarko, D., Wittig, I., Zeman, J. and Houštěk, J. (2014) 'Mitochondrial membrane assembly of TMEM70 protein', *Mitochondrion*, 15, pp. 1–9. doi: 10.1016/j.mito.2014.02.010.

Kühlbrandt, W. (2015) 'Structure and function of mitochondrial membrane protein complexes', *BMC Biology*, 13(1), p. 89. doi: 10.1186/s12915-015-0201-x.

Kucharczyk, R., Zick, M., Bietenhader, M., Rak, M., Couplan, E., Blondel, M., Caubet, S. D. and di Rago, J. P. (2009) 'Mitochondrial ATP synthase disorders: Molecular mechanisms and the quest for curative therapeutic approaches', *Biochimica et Biophysica Acta - Molecular Cell Research*. Elsevier B.V., 1793(1), pp. 186–199. doi: 10.1016/j.bbamcr.2008.06.012.

Ladoukakis, E. D. and Zouros, E. (2017) 'Evolution and inheritance of animal mitochondrial DNA: rules and exceptions.', *Journal of biological research (Thessalonike, Greece)*. BioMed Central, 24, p. 2. doi: 10.1186/s40709-017-0060-4.

Lai-Zhang, J., Xiao, Y. and Mueller, D. M. (1999) 'Epistatic interactions of deletion mutants in the genes encoding the F1-ATPase in yeast Saccharomyces cerevisiae.', *The EMBO journal*. EMBO Press, 18(1), pp. 58–64. doi: 10.1093/emboj/18.1.58.

Lam, K. W., Warshaw, J. B. and Sanadi, D. R. (1967) 'The mechanism of oxidative phosphorylation: XIV. Purification and properties of a second energy-transfer factor', *Archives of Biochemistry and Biophysics*. Academic Press, 119, pp. 477–484. doi: 10.1016/0003-9861(67)90479-1.

Lazarou, M., McKenzie, M., Ohtake, A., Thorburn, D. R. and Ryan, M. T. (2007) 'Analysis of the assembly profiles for mitochondrial- and nuclear-DNA-encoded subunits into complex I.', *Molecular and cellular biology*, 27(12), pp. 4228–4237. doi: 10.1128/MCB.00074-07.

Lazarou, M., Smith, S. M., Thorburn, D. R., Ryan, M. T. and McKenzie, M. (2009) 'Assembly of nuclear DNA-encoded subunits into mitochondrial complex IV, and their preferential integration into supercomplex forms in patient mitochondria', *FEBS Journal*, 276(22), pp. 6701–6713. doi: 10.1111/j.1742-4658.2009.07384.x.

Lee, J. K., Belogrudov, G. I. and Stroud, R. M. (2008) 'Crystal structure of bovine mitochondrial factor B at 0.96-A resolution.', *Proceedings of the National Academy of Sciences of the United States of America*, 105(36), pp. 13379–84. doi: 10.1073/pnas.0805689105.

Lippe, G., Sorgato, M. C. and Harris, D. A. (1988) 'Kinetics of the release of the mitochondrial inhibitor protein. Correlation with synthesis and hydrolysis of ATP', *Biochimica et Biophysica Acta (BBA) - Bioenergetics*, 933(1), pp. 1–11. doi: 10.1016/0005-2728(88)90050-3.

Liu, S., Charlesworth, T. J., Bason, J. V, Montgomery, M. G., Harbour, M. E., Fearnley, I. M. and Walker, J. E. (2015) 'The purification and characterization of ATP synthase complexes from the mitochondria of four fungal species.', *The Biochemical journal*. Portland Press Ltd, 468(1), pp. 167–75. doi: 10.1042/BJ20150197.

Lutter, R., Saraste, M., van Walraven, H. S., Runswick, M. J., Finel, M., Deatherage, J. F. and Walker, J. E. (1993) 'F1F0-ATP synthase from bovine heart mitochondria: development of the purification of a monodisperse oligomycin-sensitive ATPase.', *The Biochemical journal*, 295 (Pt 3), pp. 799–806.

Martin, J., Mahlke, K. and Pfanner, N. (1991) 'Role of an energized inner membrane in mitochondrial protein import: ΔΨ drives the movement of presequences', *Journal of Biological Chemistry*, 266(27), pp. 18051–18057.

Martin, W. F., Garg, S. and Zimorski, V. (2015) 'Endosymbiotic theories for eukaryote origin.', *Philosophical transactions of the Royal Society of London. Series B, Biological sciences*. The Royal Society, 370(1678), p. 20140330. doi: 10.1098/rstb.2014.0330.

Matthies, D., Preiss, L., Klyszejko, A. L., Muller, D. J., Cook, G. M., Vonck, J. and Meier, T. (2009) 'The c13 Ring from a Thermoalkaliphilic ATP Synthase Reveals an Extended Diameter Due to a Special Structural Region', *Journal of Molecular Biology*. Academic Press, 388(3), pp. 611–618. doi: 10.1016/J.JMB.2009.03.052.

Mattiazzi, M., Vijayvergiya, C., Gajewski, C. D., DeVivo, D. C., Lenaz, G., Wiedmann, M. and Manfredi, G. (2004) 'The mtDNA T8993G (NARP) mutation results in an impairment of oxidative phosphorylation that can be improved by antioxidants', *Human*

Molecular Genetics. Oxford University Press, 13(8), pp. 869–879. doi: 10.1093/hmg/ddh103.

Mayr, J. A., Havlíčková, V., Zimmermann, F., Magler, I., Kaplanová, V., Ješina, P., Pecinová, A., Nůsková, H., Koch, J., Sperl, W. and Houštěk, J. (2010) 'Mitochondrial ATP synthase deficiency due to a mutation in the ATP5E gene for the F1 ε subunit', *Human Molecular Genetics*, 19(17), pp. 3430–3439. doi: 10.1093/hmg/ddq254.

De Meirleir, L., Seneca, S., Lissens, W., De Clercq, I., Eyskens, F., Gerlo, E., Smet, J. and Van Coster, R. (2004) 'Respiratory chain complex V deficiency due to a mutation in the assembly gene ATP12.', *Journal of medical genetics*, 41(2), pp. 120–4. doi: 10.1136/jmg.2003.012047.

Meunier, B., Fisher, N., Ransac, S., Mazat, J.-P. and Brasseur, G. (2013) 'Respiratory complex III dysfunction in humans and the use of yeast as a model organism to study mitochondrial myopathy and associated diseases', *Biochimica et Biophysica Acta (BBA) - Bioenergetics*. Elsevier, 1827(11–12), pp. 1346–1361. doi: 10.1016/J.BBABIO.2012.11.015.

Miroux, B. and Walker, J. E. (1996) 'Over-production of Proteins in Escherichia coli: Mutant Hosts that Allow Synthesis of some Membrane Proteins and Globular Proteins at High Levels', *J. Mol. Biol*, 260, pp. 289–298.

MITCHELL, P. (1961) 'Coupling of phosphorylation to electron and hydrogen transfer by a chemi-osmotic type of mechanism.', *Nature*. Nature Publishing Group, 191(4784), pp. 144–8. doi: 10.1038/191144a0.

Miyabayashi, S., Hanamizu, H., Nakamura, R., Endo, H. and Tada, K. (1992) 'Defects of mitochondrial respiratory enzymes in cloned cells from MELAS fibroblasts', *Journal of Inherited Metabolic Disease*, 15(5), pp. 797–802. doi: 10.1007/BF01800024.

Montigny, C., Penin, F., Lethias, C. and Falson, P. (2004) 'Overcoming the toxicity of membrane peptide expression in bacteria by upstream insertion of Asp-Pro sequence', *Biochimica et Biophysica Acta (BBA) - Biomembranes*. Elsevier, 1660(1–2), pp. 53–65. doi: 10.1016/J.BBAMEM.2003.10.013.

Moradi-Ameli, M. and Godinot, C. (1983) 'Characterization of monoclonal antibodies against mitochondrial F1-ATPase.', *Proceedings of the National Academy of Sciences of the United States of America*. National Academy of Sciences, 80(20), pp. 6167–71.

Mráček, T., Pecina, P., Vojtíšková, A., Kalous, M., Šebesta, O. and Houštěk, J. (2006) 'Two components in pathogenic mechanism of mitochondrial ATPase deficiency:

Energy deprivation and ROS production', *Experimental Gerontology*, 41(7), pp. 683–687. doi: 10.1016/j.exger.2006.02.009.

Mueller, D. M. (2000a) 'Partial assembly of the yeast mitochondrial ATP synthase.', *Journal of bioenergetics and biomembranes*, 32(4), pp. 391–400. doi: 10.1023/A:1005532104617.

Mueller, D. M. (2000b) 'Partial assembly of the yeast mitochondrial ATP synthase.', *Journal of bioenergetics and biomembranes*, 32(4), pp. 391–400. doi: 10.1023/A:1005532104617.

Nicholls, D. G., Ferguson, S. J., Nicholls, D. G. and Ferguson, S. J. (2013a) '1 – Chemiosmotic Energy Transduction', in *Bioenergetics*, pp. 3–12. doi: 10.1016/B978-0-12-388425-1.00001-4.

Nicholls, D. G., Ferguson, S. J., Nicholls, D. G. and Ferguson, S. J. (2013b) '5 – Respiratory Chains', in *Bioenergetics*, pp. 91–157. doi: 10.1016/B978-0-12-388425-1.00005-1.

Noji, H., Yasuda, R., Yoshida, M. and Kinosita, K. (1997) 'Direct observation of the rotation of F1-ATPase', *Nature*, pp. 299–302. doi: 10.1038/386299a0.

Nuskova, H., Kovalcikova, J., Efimova, I., Pecinova, A., Pecina, P., Houstek, J. and Mracek, T. (2018) 'Biochemical thresholds for pathological presentation of ATP synthase deficiencies', *BBA Bioenergetics*, submitted.

Oláhová, M., Yoon, W. H., Thompson, K., Jangam, S., Fernandez, L., Davidson, J. M., Kyle, J. E., Grove, M. E., Fisk, D. G., Kohler, J. N., Holmes, M., Dries, A. M., Huang, Y., Zhao, C., Contrepois, K., Zappala, Z., Frésard, L., Waggott, D., Zink, E. M., Kim, Y.-M., Heyman, H. M., Stratton, K. G., Webb-Robertson, B.-J. M., Adams, D. R., Alejandro, M. E., Allard, P., Azamian, M. S., Bacino, C. A., Balasubramanyam, A., Barseghyan, H., Batzli, G. F., Beggs, A. H., Behnam, B., Bican, A., Bick, D. P., Birch, C. L., Bonner, D., Boone, B. E., Bostwick, B. L., Briere, L. C., Brown, D. M., Brush, M., Burke, E. A., Burrage, L. C., Chen, S., Clark, G. D., Coakley, T. R., Cogan, J. D., Cooper, C. M., Cope, H., Craigen, W. J., D'Souza, P., Davids, M., Dayal, J. G., Dell'Angelica, E. C., Dhar, S. U., Dillon, A., Dipple, K. M., Donnell-Fink, L. A., Dorrani, N., Dorset, D. C., Douine, E. D., Draper, D. D., Eckstein, D. J., Emrick, L. T., Eng, C. M., Eskin, A., Esteves, C., Estwick, T., Ferreira, C., Fogel, B. L., Friedman, N. D., Gahl, W. A., Glanton, E., Godfrey, R. A., Goldstein, D. B., Gould, S. E., Gourdine, J.-P. F., Groden, C. A., Gropman, A. L., Haendel, M., Hamid, R., Hanchard, N. A., Handley, L. H., Herzog, M. R., Holm, I. A., Hom, J., Howerton, E. M., Huang, Y., Jacob, H. J., Jain,

M., Jiang, Y., Johnston, J. M., Jones, A. L., Kohane, I. S., Krasnewich, D. M., Krieg, E. L., Krier, J. B., Lalani, S. R., Lau, C. C., Lazar, J., Lee, B. H., Lee, H., Levy, S. E., Lewis, R. A., Lincoln, S. A., Lipson, A., Loo, S. K., Loscalzo, J., Maas, R. L., Macnamara, E. F., MacRae, C. A., Maduro, V. V., Majcherska, M. M., Malicdan, M. C. V., Mamounas, L. A., Manolio, T. A., Markello, T. C., Marom, R., Martínez-Agosto, J. A., Marwaha, S., May, T., McConkie-Rosell, A., McCormack, C. E., McCray, A. T., Might, M., Moretti, P. M., Morimoto, M., Mulvihill, J. J., Murphy, J. L., Muzny, D. M., Nehrebecky, M. E., Nelson, S. F., Newberry, J. S., Newman, J. H., Nicholas, S. K., Novacic, D., Orange, J. S., Pallais, J. C., Palmer, C. G. S., Papp, J. C., Parker, N. H., Pena, L. D. M., Phillips, J. A., Posey, J. E., Postlethwait, J. H., Potocki, L., Pusey, B. N., Reuter, C. M., Robertson, A. K., Rodan, L. H., Rosenfeld, J. A., Sampson, J. B., Samson, S. L., Schoch, K., Schroeder, M. C., Scott, D. A., Sharma, P., Shashi, V., Silverman, E. K., Sinsheimer, J. S., Smith, K. S., Spillmann, R. C., Splinter, K., Stoler, J. M., Stong, N., Sullivan, J. A., Sweetser, D. A., Tifft, C. J., Toro, C., Tran, A. A., Urv, T. K., Valivullah, Z. M., Vilain, E., Vogel, T. P., Wahl, C. E., Walley, N. M., Walsh, C. A., Ward, P. A., Waters, K. M., Westerfield, M., Wise, A. L., Wolfe, L. A., Worthey, E. A., Yamamoto, S., Yang, Y., Yu, G., Zastrow, D. B., Zheng, A., Snyder, M., Merker, J. D., Montgomery, S. B., Fisher, P. G., Feichtinger, R. G., Mayr, J. A., Hall, J., Barbosa, I. A., Simpson, M. A., Deshpande, C., Waters, K. M., Koeller, D. M., Metz, T. O., Morris, A. A., Schelley, S., Cowan, T., Friederich, M. W., McFarland, R., Van Hove, J. L. K., Enns, G. M., Yamamoto, S., Ashley, E. A., Wangler, M. F., Taylor, R. W., Bellen, H. J., Bernstein, J. A. and Wheeler, M. T. (2018) 'Biallelic Mutations in ATP5F1D, which Encodes a Subunit of ATP Synthase, Cause a Metabolic Disorder', *The American Journal of Human Genetics*. Cell Press, 102(3), pp. 494–504. doi: 10.1016/J.AJHG.2018.01.020.

Orriss, G. L., Runswick, M. J., Collinson, I. R., Miroux, B., Fearnley, I. M., Skehel, J. M. and Walker, J. E. (1996) 'The delta- and epsilon-subunits of bovine F1-ATPase interact to form a heterodimeric subcomplex.', *The Biochemical journal*, 314, pp. 695–700.

Osman, C., Wilmes, C., Tatsuta, T. and Langer, T. (2007) 'Prohibitins interact genetically with Atp23, a novel processing peptidase and chaperone for the F1Fo-ATP synthase.', *Molecular biology of the cell*, 18(2), pp. 627–35. doi: 10.1091/mbc.E06-09-0839.

Paumard, P., Vaillier, J., Coulary, B., Schaeffer, J., Soubannier, V., Mueller, D. M., Brèthes, D., di Rago, J.-P. and Velours, J. (2002) 'The ATP synthase is involved in generating mitochondrial cristae morphology.', *The EMBO journal*, 21(3), pp. 221–30.

doi: 10.1093/emboj/21.3.221.

Pecina, P., Houšťková, H., Mráček, T., Pecinová, A., Nůsková, H., Tesařová, M., Hansíková, H., Janota, J., Zeman, J. and Houštěk, J. (2014) 'Noninvasive diagnostics of mitochondrial disorders in isolated lymphocytes with high resolution respirometry', *BBA Clinical*, 2, pp. 62–71. doi: 10.1016/j.bbacli.2014.09.003.

Pecina, P., Nůsková, H., Karbanová, V., Kaplanová, V., Mráček, T. and Houštěk, J. (2018) 'Role of the mitochondrial ATP synthase central stalk subunits γ and δ in the activity and assembly of the mammalian enzyme.', *Biochimica et biophysica acta*. Elsevier B.V, 1859(5), pp. 374–381. doi: 10.1016/j.bbabio.2018.02.007.

Pecinová, A., Drahota, Z., Nůsková, H., Pecina, P. and Houštěk, J. (2011) 'Evaluation of basic mitochondrial functions using rat tissue homogenates', *Mitochondrion*, 11(5), pp. 722–728. doi: 10.1016/j.mito.2011.05.006.

Pullman, M. E. and Monroy, G. C. (1963) 'A Naturally Occurring Inhibitor of Mitochondrial Adenosine Triphosphatase Occurring Adenosine Inhibitor of Mitochondrial Triphosphatase *', *Journal of Biological Chemistry*, 238(11), pp. 3762–3769.

Rak, M., Gokova, S. and Tzagoloff, A. (2011) 'Modular assembly of yeast mitochondrial ATP synthase', *The EMBO Journal*, 30(5), pp. 920–930. doi: 10.1038/emboj.2010.364.

Rao Sanadi, D. (1982) 'Mitochondrial coupling factor B: Properties and role in ATP synthesis', *Biochimica et Biophysica Acta (BBA) - Reviews on Bioenergetics*. Elsevier, 683(1), pp. 39–56. doi: 10.1016/0304-4173(82)90012-X.

Reynolds, J. A. and Tanford, C. (1970) 'Binding of Dodecyl Sulfate to Proteins at High Binding Ratios. Possible Implications for the State of Proteins in Biological Membranes', *Proceedings of the National Academy of Sciences*, 66(3), pp. 1002–1007. doi: 10.1073/pnas.66.3.1002.

Rossignol, R., Faustin, B., Rocher, C., Malgat, M., Mazat, J.-P. and Letellier, T. (2003) 'Mitochondrial threshold effects.', *The Biochemical journal*. Portland Press Ltd, 370(Pt 3), pp. 751–62. doi: 10.1042/BJ20021594.

Rossignol, R., Gilkerson, R., Aggeler, R., Yamagata, K., Remington, S. J. and Capaldi, R. A. (2004) 'Energy substrate modulates mitochondrial structure and oxidative capacity in cancer cells.', *Cancer research*. American Association for Cancer Research, 64(3), pp. 985–93. doi: 10.1158/0008-5472.CAN-03-1101.

Rossignol, R., Malgat, M., Mazat, J. P. and Letellier, T. (1999) 'Threshold effect and

tissue specificity. Implication for mitochondrial cytopathies.', *The Journal of biological chemistry*. American Society for Biochemistry and Molecular Biology, 274(47), pp. 33426–32. doi: 10.1074/JBC.274.47.33426.

Runswick, M. J., Bason, J. V, Montgomery, M. G., Robinson, G. C., Fearnley, I. M. and Walker, J. E. (2013) 'The affinity purification and characterization of ATP synthase complexes from mitochondria.', *Open biology*, 3(2), p. 120160. doi: 10.1098/rsob.120160.

Sagan, L. (1967) 'On the origin of mitosing cells', *Journal of Theoretical Biology*, 14(3), p. 225–IN6. doi: 10.1016/0022-5193(67)90079-3.

Sánchez-Aragó, M., Formentini, L., Martínez-Reyes, I., García-Bermudez, J., Santacatterina, F., Sánchez-Cenizo, L., Willers, I. M., Aldea, M., Nájera, L., Juarránz, Á., López, E. C., Clofent, J., Navarro, C., Espinosa, E. and Cuezva, J. M. (2013) 'Expression, regulation and clinical relevance of the ATPase inhibitory factor 1 in human cancers', *Oncogenesis*. Nature Publishing Group, 2(4), pp. e46–e46. doi: 10.1038/oncsis.2013.9.

Sánchez-Cenizo, L., Formentini, L., Aldea, M., Ortega, A. D., García-Huerta, P., Sánchez-Aragó, M. and Cuezva, J. M. (2010) 'Up-regulation of the ATPase inhibitory factor 1 (IF1) of the mitochondrial H+-ATP synthase in human tumors mediates the metabolic shift of cancer cells to a Warburg phenotype.', *The Journal of biological chemistry*. American Society for Biochemistry and Molecular Biology, 285(33), pp. 25308–13. doi: 10.1074/jbc.M110.146480.

Santacatterina, F., Sánchez-Cenizo, L., Formentini, L., Mobasher, M. A., Casas, E., Rueda, C. B., Martínez-Reyes, I., Núñez de Arenas, C., García-Bermúdez, J., Zapata, J. M., Sánchez-Aragó, M., Satrústegui, J., Valverde, Á. M. and Cuezva, J. M. (2016) 'Down-regulation of oxidative phosphorylation in the liver by expression of the ATPase inhibitory factor 1 induces a tumor-promoter metabolic state.', *Oncotarget*, 7(1), pp. 490–508. doi: 10.18632/oncotarget.6357.

Sazanov, L. A. (2015) 'A giant molecular proton pump: structure and mechanism of respiratory complex I', *Nature Reviews Molecular Cell Biology*. Nature Publishing Group, 16(6), pp. 375–388. doi: 10.1038/nrm3997.

Scorrano, L., Ashiya, M., Buttle, K., Weiler, S., Oakes, S. A., Mannella, C. A. and Korsmeyer, S. J. (2002) 'A distinct pathway remodels mitochondrial cristae and mobilizes cytochrome c during apoptosis', *Developmental Cell*, 2(1), pp. 55–67. doi: 10.1016/S1534-5807(01)00116-2.

Schägger, H. (2006) ‘Tricine-SDS-PAGE.’, *Nature protocols*. Nature Publishing Group, 1(1), pp. 16–22. doi: 10.1038/nprot.2006.4.

Schägger, H., Link, T. A., Engel, W. D. and von Jagow, G. (1986) ‘Isolation of the eleven protein subunits of the bc1 complex from beef heart.’, *Methods in enzymology*, 126(1983), pp. 224–37. doi: 10.1016/S0076-6879(86)26024-3.

Smith, B. J. (1984) ‘SDS Polyacrylamide Gel Electrophoresis of Proteins’, *Proteins*, 1, pp. 41–56. doi: 10.1385/0-89603-062-8:41.

Stiburek, L., Fornuskova, D., Wenchich, L., Pejznochova, M., Hansikova, H. and Zeman, J. (2007) ‘Knockdown of Human Oxa1l Impairs the Biogenesis of F1Fo-ATP Synthase and NADH:Ubiquinone Oxidoreductase’, *Journal of Molecular Biology*. Academic Press, 374(2), pp. 506–516. doi: 10.1016/J.JMB.2007.09.044.

Stiburek, L. and Zeman, J. (2010) ‘Assembly factors and ATP-dependent proteases in cytochrome c oxidase biogenesis’, *Biochimica et Biophysica Acta (BBA) - Bioenergetics*. Elsevier, 1797(6–7), pp. 1149–1158. doi: 10.1016/J.BBABIO.2010.04.006.

Stock, D., Leslie, A. G. W. and Walker, J. E. (1999) ‘Molecular Architcture of the Rotary Motor in ATP Synthase’, *Science*, 286(November), pp. 1700–1705..

Stock, D., Leslie, A. G. and Walker, J. E. (1999) ‘Molecular architecture of the rotary motor in ATP synthase.’, *Science (New York, N.Y.)*. American Association for the Advancement of Science, 286(5445), pp. 1700–5. doi: 10.1126/SCIENCE.286.5445.1700.

Strauss, M., Hofhaus, G., Schröder, R. R. and Kühlbrandt, W. (2008) ‘Dimer ribbons of ATP synthase shape the inner mitochondrial membrane.’, *The EMBO journal*, 27(7), pp. 1154–60. doi: 10.1038/emboj.2008.35.

Sun, F., Huo, X., Zhai, Y., Wang, A., Xu, J., Su, D., Bartlam, M. and Rao, Z. (2005) ‘Crystal Structure of Mitochondrial Respiratory Membrane Protein Complex II’, *Cell*. Cell Press, 121(7), pp. 1043–1057. doi: 10.1016/J.CELL.2005.05.025.

Tetaud, E., Godard, F., Giraud, M.-F., Ackerman, S. H. and di Rago, J.-P. (2014) ‘The depletion of F□ subunit ε in yeast leads to an uncoupled respiratory phenotype that is rescued by mutations in the proton-translocating subunits of F□.’, *Molecular biology of the cell*. American Society for Cell Biology, 25(6), pp. 791–9. doi: 10.1091/mbc.E13-02-0112.

Tsukihara, T., Aoyama, H., Yamashita, E., Tomizaki, T., Yamaguchi, H., Shinzawa-

Itoh, K., Nakashima, R., Yaono, R. and Yoshikawa, S. (1996) 'The whole structure of the 13-subunit oxidized cytochrome c oxidase at 2.8 A.', *Science (New York, N.Y.)*, 272(5265), pp. 1136–44.

Tzagoloff, A., Barrientos, A., Neupert, W. and Herrmann, J. M. (2004) 'Atp10p Assists Assembly of Atp6p into the F 0 Unit of the Yeast Mitochondrial ATPase*'. in Press. doi: 10.1074/jbc.M401506200.

VERNHAM, G. A., REID, F. M., RUNDLE, P. A. and JACOBS, H. T. (1994) 'Bilateral sensorineural hearing loss in members of a maternal lineage with a mitochondrial point mutation', *Clinical Otolaryngology*. Wiley/Blackwell (10.1111), 19(4), pp. 314–319. doi: 10.1111/j.1365-2273.1994.tb01238.x.

Vollmar, M., Schlieper, D., Winn, M., Büchner, C. and Groth, G. (2009) 'Structure of the c14rotor ring of the proton translocating chloroplast ATP synthase', *Journal of Biological Chemistry*, 284(27), pp. 18228–18235. doi: 10.1074/jbc.M109.006916.

Walker, J. E. (2013) 'The ATP synthase: the understood, the uncertain and the unknown.', *Biochemical Society transactions*. Portland Press Limited, 41(1), pp. 1–16. doi: 10.1042/BST20110773.

Walker, J. E., Lutter, R., Dupuis, A. and Runswick, M. J. (1991) 'Identification of the subunits of F1F0-ATPase from bovine heart mitochondria', *Biochemistry*, 30(22), pp. 5369–5378. doi: 10.1021/bi00236a007.

Wang, Z. G. and Ackerman, S. H. (2000) 'The assembly factor Atp11p binds to the beta-subunit of the mitochondrial F(1)-ATPase.', *The Journal of biological chemistry*, 275(8), pp. 5767–72. doi: 10.1074/jbc.275.8.5767.

Wang, Z. G., Sheluho, D., Gatti, D. L. and Ackerman, S. H. (2000) 'The alpha-subunit of the mitochondrial F(1) ATPase interacts directly with the assembly factor Atp12p.', *The EMBO journal*, 19(7), pp. 1486–93. doi: 10.1093/emboj/19.7.1486.

Wang, Z. G., White, P. S. and Ackerman, S. H. (2001) 'Atp11p and Atp12p are Assembly Factors for the F1-ATPase in Human Mitochondria', *Journal of Biological Chemistry*, 276(33), pp. 30773–30778. doi: 10.1074/jbc.M104133200.

Watt, I. N., Montgomery, M. G., Runswick, M. J., Leslie, A. G. W. and Walker, J. E. (2010) 'Bioenergetic cost of making an adenosine triphosphate molecule in animal mitochondria.', *Proceedings of the National Academy of Sciences of the United States of America*. National Academy of Sciences, 107(39), pp. 16823–7. doi: 10.1073/pnas.1011099107.

Wei, S., Fukuhara, H., Kawada, C., Kurabayashi, A., Furihata, M., Ogura, S.-I., Inoue, K. and Shuin, T. (2015) 'Silencing of ATPase Inhibitory Factor 1 Inhibits Cell Growth via Cell Cycle Arrest in Bladder Cancer.', *Pathobiology : journal of immunopathology, molecular and cellular biology*. Karger Publishers, 82(5), pp. 224–32. doi: 10.1159/000439027.

Wikström, M. (1984) 'Two protons are pumped from the mitochondrial matrix per electron transferred between NADH and ubiquinone', *FEBS Letters*, 169(2), pp. 300–304. doi: 10.1016/0014-5793(84)80338-5.

Wilkens, V., Kohl, W. and Busch, K. (2013) 'Restricted diffusion of OXPHOS complexes in dynamic mitochondria delays their exchange between cristae and engenders a transitory mosaic distribution.', *Journal of cell science*, 126(Pt 1), pp. 103–16. doi: 10.1242/jcs.108852.

Wirth, C., Brandt, U. and Hunte, C. (2016) 'Structure and function of mitochondrial complex I', *Biochimica et Biophysica Acta (BBA) - Bioenergetics*. Elsevier, 1857(7), pp. 902–914. doi: 10.1016/J.BBABIO.2016.02.013.

Wittig, I., Braun, H. P. and Schägger, H. (2006) 'Blue native PAGE', *Nature Protocols*, 1(1), pp. 418–428. doi: 10.1038/nprot.2006.62.

Wittig, I., Karas, M. and Schägger, H. (2007) 'High resolution clear native electrophoresis for in-gel functional assays and fluorescence studies of membrane protein complexes.', *Molecular & cellular proteomics : MCP*. American Society for Biochemistry and Molecular Biology, 6(7), pp. 1215–25. doi: 10.1074/mcp.M700076-MCP200.

Wittig, I., Meyer, B., Heide, H., Steger, M., Bleier, L., Wumaier, Z., Karas, M. and Schägger, H. (2010) 'Assembly and oligomerization of human ATP synthase lacking mitochondrial subunits a and A6L', *Biochimica et Biophysica Acta (BBA) - Bioenergetics*, 1797(6–7), pp. 1004–1011. doi: 10.1016/j.bbabio.2010.02.021.

Wittig, I. and Schägger, H. (2005) 'Advantages and limitations of clear-native PAGE', *Proteomics*, 5(17), pp. 4338–4346. doi: 10.1002/pmic.200500081.

Wittig, I. and Schägger, H. (2009) 'Supramolecular organization of ATP synthase and respiratory chain in mitochondrial membranes.', *Biochimica et biophysica acta*. Elsevier B.V., 1787(6), pp. 672–80. doi: 10.1016/j.bbabio.2008.12.016.

Xiao, Y., Metzl, M. and Mueller, D. M. (2000) 'Partial uncoupling of the mitochondrial membrane by a heterozygous null mutation in the gene encoding the gamma- or delta-

subunit of the yeast mitochondrial ATPase.', *The Journal of biological chemistry*. American Society for Biochemistry and Molecular Biology, 275(10), pp. 6963–8. doi: 10.1074/JBC.275.10.6963.

Yin, T., Lu, L., Xiong, Z., Wei, S. and Cui, D. (2015) 'ATPase inhibitory factor 1 is a prognostic marker and contributes to proliferation and invasion of human gastric cancer cells', *Biomedicine and Pharmacotherapy*, 70(C), pp. 90–96. doi: 10.1016/j.biopha.2014.12.036.

Zeng, X., Neupert, W. and Tzagoloff, A. (2007) 'The metalloprotease encoded by ATP23 has a dual function in processing and assembly of subunit 6 of mitochondrial ATPase.', *Molecular biology of the cell*, 18(2), pp. 617–26. doi: 10.1091/mbc.E06-09-0801.

Zhang, Z., Kuipers, G., Niemiec, Ł., Baumgarten, T., Slotboom, D. J., de Gier, J.-W. and Hjelm, A. (2015) 'High-level production of membrane proteins in E. coli BL21(DE3) by omitting the inducer IPTG', *Microbial Cell Factories*. BioMed Central, 14(1), p. 142. doi: 10.1186/s12934-015-0328-z.

Zhou, L., Chomyn, A., Attardi, G. and Miller, C. A. (1997) '"Mito mutations in single cells: MERRF in neurons"Myoclonic epilepsy and ragged red fibers (MERRF) syndrome: selective vulnerability of CNS neurons does not correlate with the level of mitochondrial tRNAlys mutation in individual neuronal isolates', *J Neurosci*, 17(20), pp. 7746–7753.

Zhu, J., Vinothkumar, K. R. and Hirst, J. (2016) 'Structure of mammalian respiratory complex I.', *Nature*. Europe PMC Funders, 536(7616), pp. 354–358. doi: 10.1038/nature19095.